11-6-2009

Investigation of the Factors Influencing Skid Resistance and the International Friction Index

Luis G. Fuentes
University of South Florida

Investigation of the Factors Influencing Skid Resistance and the International Friction Index

by

Luis G. Fuentes

A thesis submitted in partial fulfillment
of the requirements for the degree of
Doctor of Philosophy
Department of Civil and Environmental Engineering
College of Engineering
University of South Florida

Co-Major Professor: Manjriker Gunaratne, Ph.D.
Co-Major Professor: Daniel Hess, Ph.D.
Gray Mullins, Ph.D.
Jian John Lu, Ph.D.
George Yanev, Ph.D.

Date of Approval:
November 6, 2009

Keywords: Skid resistance, IFI, Roughness, Speed constant, Macrotexture

DEDICATION

To my parents, Luis Guillermo and Maria Lourdes who supported me all these years, and to Mercy who stood by my side the whole way.

ACNOWLEDGMENTS

I wish to thank my mayor advisor, Dr. G, for his constructive advice, and patience throughout my graduate study. I would also like to express my most sincere appreciation to Dr. Gray Mullins who was always there for me when I needed advice. I also wish to extend my gratitude to Dr. Daniel Hess, whose guidance helped me go thru many problems I encounter during my studies.

During my graduate study, financial support provided by the National Aeronautics and Space Administration (NASA) is gratefully acknowledged.

I feel indebted to my parents for their continuous support. Special appreciation and love go to my fiancé, Mercy Gomez, who has been supportive during these past years. Without their help, patience, and encouragement, I could not complete my doctoral studies.

TABLE OF CONTENTS

LIST OF TABLES

LIST OF FIGURES

Investigation of the Factors Influencing Skid Resistance and the International Friction Index

by

Luis G. Fuentes

ABSTRACT

This dissertation is compiled of the findings of several phases of a detailed research study that was aimed at investigating the Skid Resistance phenomenon.

In the first phase of the dissertation research a study was performed to evaluate the different factors that influence frictional measurements obtained using the Dynamic Friction Tester (DFT). A temperature calibration factor that would account for temperature effects on DFT readings and IFI computations was developed. In addition, other variables that also affect the friction measurements obtained using the DFT are identified.

In the next phase of the dissertation research the effect of pavement roughness on the Skid Resistance was investigated. The variation of the normal load and its nonlinear relation to SN was used to explain lower SN values measured on relatively rougher surfaces. The feasibility of using the International Roughness Index (IRI) and the Dynamic Load Coefficient (DLC) as predictors of the reduction in SN due to pavement roughness was also investigated.

In the final phase of the dissertation research an in-depth investigation was carried out to better understand the principles underlying the concept of the International Friction Index (IFI), and specifically the role played by the Speed Constant (S_p) parameter in the IFI computations. The parameter S_p dictates the speed variation of the wet friction measurements taken on a given pavement surface. The results of the current investigation suggest the revision of the procedure for computation of the S_p parameter to incorporate device specific properties.

Furthermore, the incorporation of vehicle characteristics in the S_p parameter computations would help address a well known deficiency of the IFI, which is the inconsistent *FR60* (predicted friction at 60 km/h) obtained from the friction values measured at two different slip speeds on the same surface. This study also showed that the modification of the S_p parameter reduces significantly the slip speed dependency of the device calibration parameters *A* and *B*.

Finally, a modified IFI procedure that incorporates device specific slip conditions is presented. The modified IFI procedure showed consistently better predictive capability than the conventional ASTM procedure on all the different devices considered in this study.

CHAPTER 1

PROBLEM STATEMENT

Skid resistance is the force developed when a tire that is fully or partially prevented from rolling slides along a pavement surface under lubricated conditions. Accidents due to skidding on pavement are a major concern of the aviation and highway industries. These accidents are generally attributed to skid resistance deficiencies on the pavement surface. Hence the tire pavement friction interaction mechanism is one of the most important issues of safe vehicle/aircraft operations on pavements.

Different models are available to simulate the tire pavement interaction and predict pavement friction. These models have different formats and outputs depending on the industry in which they were developed. The investigator was able to identify clearly two different industries in which different models were used. These are; the highway and aviation industries and the automobile industry. Different friction measuring devices have been developed by these industries to evaluate the frictional properties of a pavement surface. These devices operate under different principles; therefore, direct comparison between equipment is inappropriate.

The American Society for Testing and Materials (ASTM) provides specification for the standardization of different friction measuring devices and computation of different indices for comparison of friction values measured by different equipment on the same surface. Specifically, the International Friction Index (IFI) defined in ASTM E 1960 (ASTM E-1960-07, 2009) is used as the standard for comparison of friction values measured by different equipment. IFI has been developed in the Permanent International Association of Road Congresses (PIARC) International experiment (Wambold et. al.,

1995) for the purpose of harmonizing friction measurements from different equipment to a common calibrated index.

Furthermore, The National Aeronautics and Space Administration (NASA) has held Annual Runway Friction Workshops at the Wallops Flight Facility since 1993 on the eastern shore of Virginia. The main objective of this workshop is to calculate the IFI index from different devices that participate in it by evaluating the standardization parameters for each equipment. The workshop also serves to create an extensive friction database that would be used for subsequent research purposes.

1.1 Review of Literature on Friction

A comprehensive history of research on tire pavement interaction is available, because of the diverse efforts and background of many investigators interested in this particular topic. Many aircraft accidents have occurred around the world, particularly related to the aviation industry due to skidding. In some of these cases the aircraft had not been able to stop properly on the landing strip due to the improper understanding of the braking operation. There are many variables that are involved in this phenomenon. The understanding of each of these variables will help one to realize the magnitude of the problem that one faces and eventually design more reliable friction measuring techniques.

The coefficient of friction is defined as follows:

$$\mu = \frac{F_N}{F_S} \tag{1}$$

The coefficient of friction is an abstract quantity used to express the proportionality between the normal force (F_N) and the shear (frictional) force (F_S) of two parallel surfaces that are compressed together. Many devices operating under different mechanisms have been developed to measure the coefficient of friction of pavement surfaces. Unfortunately, different coefficient of friction values are obtained on the same surface when different devices are used; therefore direct comparison between coefficient

of friction obtained from different devices is inappropriate. The coefficient of friction is not a material property. In other words, one cannot state that a certain surface has a specific coefficient of friction. Instead, it is a system property with its magnitude depending on both two surfaces that are in contact. This is the reason why one must study the tire-pavement interaction as a system, instead of characterizing the surface only.

1.2 The Classic Laws of Friction

The classic laws of friction evolved from the early work of Amontons and Coulomb. These laws were based on empirical observations and can be summarized as follows:

(1) Friction is independent of the apparent or nominal contact area.
(2) Friction force is proportional to the normal load.
(3) Static coefficient of friction is greater that the kinetic coefficient of friction.
(4) Kinetic friction is independent of the sliding speed.

The friction at the rubber tire-pavement interface constitutes a complex phenomenon due to the viscoelastic nature of the rubber. Empirical work conducted by many investigators shows that the classical laws of friction are not valid on viscoelastic materials. Denny (1953) conducted laboratory experiments on rubber-like materials and showed that under contaminated conditions the coefficient of friction decreases with increasing contact pressure. Thirion (1946) confirmed the load dependence of rubber friction and proposed an empirical relationship between the coefficient of friction and pressure. Schallamach (1952) showed that the load dependence of rubber friction can be explained by assuming spherical surface asperities and elastic behavior of rubber in compression.

Although the mechanisms of tire-pavement friction interaction are not fully understood, the Molecular Attraction Theory, developed by Tomlinson and Hardy in the 1930s, seems to be the most accepted (Moore, 1975). The current investigation is limited to friction or skid resistance on wet pavement surfaces only.

1.3 Mechanics of Tire-Pavement Friction

Although the mechanisms of tire-pavement friction interaction are not fully understood, it is agreed in the literature that the frictional force is composed mainly of adhesion and hysteresis components (NCHRP, 2009). Tire rubber shear is another component that contributes to the frictional force, but its magnitude is negligible when compared to the adhesion and hysteresis force components. So one can express the frictional force as:

$$F = F_{adhesion} + F_{hysteresis} \tag{2}$$

If one divides both sides of the Equation (2) by the normal load, the following result is obtained:

$$f = f_a + f_h \tag{3}$$

Where f is the total coefficient of friction, and f_a and f_h are the components of the coefficient due to adhesion and hysteresis respectively. It can be seen that both f_a and f_h depend on the viscoelastic properties of the rubber:

$$f_a = K_1 s\left[\frac{E'}{p^r}\right]\tan\delta \qquad (r < 1) \tag{4}$$

and

$$f_h = K_2\left[\frac{p}{E'}\right]^n \tan\delta \qquad (n >= 1) \tag{5}$$

Where $tan\delta$ is the tangent modulus of the elastometer, defined as the ratio of energy dissipated to energy stored per cycle, p is the normal pressure, E' is the storage modulus or stress-strain ratio for the component of strain in phase with the applied stress, s is the effective shear strength of the sliding interface, r is an exponent with a value of about 0.2 and n is an index greater that the unity.

$$\tan\delta = \frac{E^{''}}{E^{'}} \tag{6}$$

and

$$E^{*} = E^{'} + jE^{''} \tag{7}$$

Where E^{*} is the complex modulus (equal to the stress-strain ratio in a viscoelastic body) and $E^{''}$ is the loss modulus which is equal to the stress-strain ratio for the component of strain 90^{o} out of phase with the applied stress.

The adhesion component of friction is due to the molecular bonding of exposed surface atoms of both surfaces (tire and pavement), followed by a stretch, break and relaxation cycle. Rubber has an elastomeric structure which is composed of flexible chains which are in constant state of thermal motion. A bond is produced between the separate chains in the surface of the tire and molecules of the pavement during tire-pavement interaction. Essentially, the rubber molecules jump a molecular distance to their new equilibrium position during the above cycle.

On the other hand, hysteresis forces are due to continuous draping of rubber over pavement aggregate asperities. The pressure distribution about the asperity depends on two distinct conditions:

(1) No sliding (no relative motion)
(2) In the presence of relative sliding

When there is no relative motion, the draping around the contact area and hence the pressure distribution is symmetrical about the asperity giving rise to no net horizontal frictional force. As the sliding begins, rubber accumulates in the leading edge of the asperity creating an asymmetrical pressure distribution producing a net friction force (unbalanced force) opposing the motion. At higher sliding speeds, the extent of the contact area decreases and approaches symmetrical conditions thus reducing hysteresis.

Figure 1 illustrates both mechanisms of adhesion and hysteresis; while Figure 2 shows the variation of adhesion and hysteresis with sliding speed.

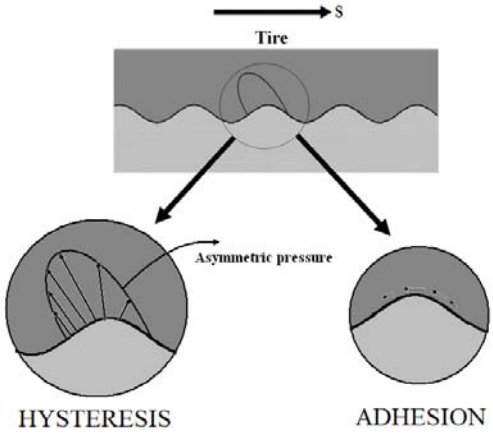

Figure 1 Mechanism of friction at the tire pavement interface (Adapted from Moore, 1975)

Based on the Figures 1, and 2, one can conclude that hysteresis is relatively independent of sliding speed (operational speed), but highly dependent on the pavement macrotexture. On the other hand, adhesion is dependent on both the operational sliding speed and the microtexture.

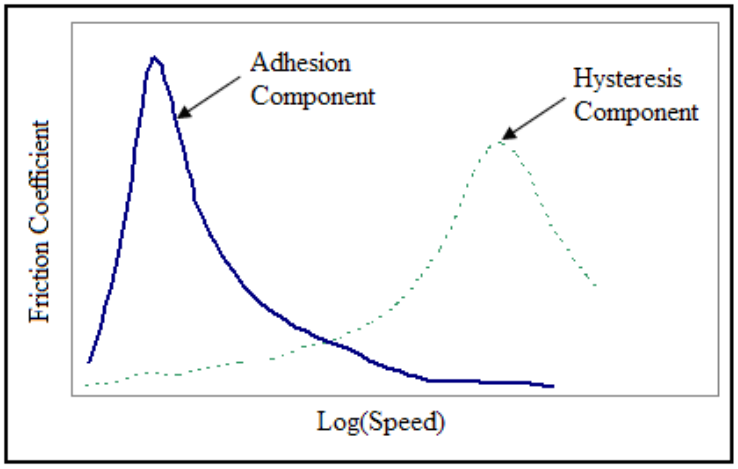

Figure 2 Friction components: Adhesion and Hysteresis (Adapted from Moore, 1975)

The knowledge acquired by studying the mechanics of tire-pavement interaction will enable one to better understand how the frictional measurement devices work, what their operational concepts are and hence what they eventually measure.

1.4 Models for Tire Pavement Interaction

The investigators recognize that the tire pavement interaction is viewed from different perspectives by different industries. Customized models developed by these industries provide specific information to those industries in areas of their general interest. Consequently there are two main industries that have proposed different model to predict the frictional properties of a pavement surface, namely: (1) the highway and aviation industries, and (2) the automobile industry.

1.4.1 Models of Highway and Aviation Industries

The highway and the aviation industries have created different empirical models in which they have tried to simulate the coefficient of friction using some measurable texture parameters of the pavement as explanatory variables (NCHRP, 2009). The most popular models are the Penn State University (PSU) model and the Rado model. These models serve as a basis for the PIARC model (Wambold et. al., 1995), which ultimately is used in the computation of IFI (Section 1.7).

1.4.2 Models of Automobile Industry

The automobile industries have also developed different models that are significant from the vehicle control point of view. Of these, two particular models stand out, namely, (1) The LuGre model and (2) Lumped model (Seneviratne et. al., 2009). These are dynamic models that focus on the properties of the tire itself rather than those of the pavement. Further details of the above models are found in the cited literature.

1.5 Friction Measuring Devices

As mentioned in Section 1, there is a necessity to evaluate accurately the frictional conditions of a pavement surface in order to prevent accidents and ensure safe highway and aviation operations. Reliable pavement surface friction information can be obtained from friction measuring vehicles or by laboratory methods.

1.5.1 Pavement Friction Measuring Vehicles

Different types of vehicles are capable of evaluating the frictional properties of a pavement surface. These devices can be subdivided into four different groups, depending on their operating mechanism. These mechanisms are: (1) the locked wheel, (2) side force, (3) fixed slip, and (4) variable slip. These vehicle subgroups operate under different principles simulating the relevant scenarios. This fact makes direct comparison between devices inappropriate.

The following are the different types of scenarios that these vehicles are designed to simulate:

(1) Locked wheel trailer → Emergency breaking situation without an Anti-Lock Braking Systems (ABS).
(2) Side force → stability in highway curves.
(3) Fixed slip and variable slip → simulated braking action with Anti-Lock Braking Systems (ABS).

One can observe that each device measures a different coefficient of friction on the same surface making difficult the decision making process about the exact or representative frictional conditions of a pavement surface. There are different friction measuring devices that are approved by the Federal Aviation Administration (FAA). Table 1 lists them and shows the different coefficient of friction thresholds specified by the FAA for different devices. The different threshold friction levels incorporated in Table 1 for different devices clearly shows that the pavement management community has acknowledged the incompatibility among different devices.

The data in Table 1 suggest that different devices may be correlated by using a linear model. This correlation is more or less achieved by the International Friction Index (IFI). Of the above, the two most commonly used vehicles used in the industry and the ones that would be the subject of this study are presented in the following sections.

Table 1 Friction level classification of runway pavement surfaces (Adapted from FAA, 1997)

Speed	40 mph			60 mph		
Friction Device / Level	Minimum	Maintenance Planning	New Design/ Construction	Minimum	Maintenance Planning	New Design/ Construction
Mu Meter	0.42	0.52	0.72	0.26	0.38	0.66
Dynatest Consulting, Inc. Runway Friction Tester	0.5	0.6	0.82	0.41	0.54	0.72
Airport Equipment Co. Skiddometer	0.5	0.6	0.82	0.34	0.47	0.74
Airport Surface Friction Tester	0.5	0.6	0.82	0.34	0.47	0.74
Airport Technology USA Safegate Friction Tester	0.5	0.6	0.82	0.34	0.47	0.74
Findlay, Irvine, Ltd. Griptester Friction Meter	0.43	0.53	0.74	0.24	0.36	0.64
Tatra Friction Tester	0.48	0.57	0.76	0.42	0.52	0.67
Norsemeter RUNAR (operated at fixed 16% slip)	0.45	0.52	0.69	0.32	0.42	0.63

1.5.1.1 Locked Wheel Trailer (LWT)

The Locked Wheel Trailer (LWT) is an equipment or device which is the most popular vehicle used by different Departments of Transportation (DOTs) to evaluate pavement condition. It operates under 100% slip conditions, which means that the wheel that is used to measure the coefficient of friction is completely prevented from rolling during testing. It is used to simulate the emergency braking condition without an ABS system. A more detailed operation standard can be found in the ASTM E 274 (ASTM E 274-06, 2009).

1.5.1.2 Runway Friction Tester (RFT)

The Runway Friction Tester (RFT) is a device that is typically used to evaluate the frictional properties of runways. It operates at approximately 15% of slip, in order to simulate the ABS action on the braking operation of aircrafts. The RFT is an approved continuous friction measuring device for which the threshold values for evaluating runway pavement condition can be seen in Table 1.

1.5.2 Laboratory Methods

Laboratory methods are available as alternatives for evaluating the frictional properties of a pavement surface. The cost of one of these devices is much lower compared to that of field friction measuring vehicles. There are two commonly devices used in the industry to evaluate surface frictional properties of a pavement in the laboratory. These are: The Dynamic Friction Tester (DFT) and the British Pendulum Tester (BPT).

1.5.2.1 Dynamic Friction Tester (DFT)

The Dynamic Friction Tester (DFT) can be employed to evaluate the surface frictional properties of a pavement. The measuring mechanism of the DFT is based on energy concepts with the loss of kinetic energy of a rotating disk resting on rubber sliders converted to an equivalent frictional force exerted by the pavement. DFT is capable of measuring friction over the sliding speed range of zero to 90 Km/h. A more detailed operation standard can be found in the ASTM E 1911 (ASTM E 1911-09, 2009). ASTM E 1960 advocates the use of DFT for the calibration of friction testing devices due to the high repeatability of DFT in IFI computations (Henry et. al., 2000). The DFT is used in conjunction with the Circular Track Meter (CT Meter) to calculate the IFI of a pavement surface. The CT Meter is a device used to evaluate texture properties of a surface, specifically the Mean Profile Depth (*MPD*) which is used to explain the friction-velocity dependency in the IFI model. A more detailed operation standard on the CT Meter can be found in the ASTM E 2157 (ASTM E 2157-01, 2009).

1.5.2.2 British Pendulum Tester (BPT)

The British Pendulum Tester (BPT) measures the frictional properties of pavement surfaces. The BPT measures friction at a low- sliding speed contact between a standard rubber slider and the pavement surface. The elevation to which the pendulum swings after contact provides an indicator of the frictional properties of the pavement surface

(NCHRP, 2009). The standard practice for measuring surface frictional properties using the British Pendulum Tester can be found in the ASTM E 303 (ASTM E 303-93, 2008).

1.6 Parameters Affecting Tire-Pavement Friction Interaction

In practice, engineers have tried to identify different characteristics of pavement texture that affect the tire-pavement interaction. Different parameters have been identified in the literature to have an effect on the tire pavement friction interaction. Generally these factors can be grouped into four different categories:

(1) Pavement surface characteristics.
(2) Vehicle operational parameters.
(3) Tire Characteristics.
(4) Environmental factors.

A detailed study illustrating the effect of these pavement surface characteristics on the friction measurement will be covered in the following sections.

1.6.1 Pavement Surface Characteristics

Pavement texture is perhaps the most important parameter related to the tire pavement friction interaction. A pavement surface should provide enough skid resistance to stop a vehicle in a panic braking situation. However friction should not be too excessive to produce mechanical wear in the tire structure. The pavement designer should find an optimum point where it would satisfy both requirements. Several studies performed at the PIARC (Wambold et. al., 1995) established three texture levels on pavements which describe different effects of frictional performance of a pavement surface. These levels are,

(1) Microtexture: it is a function of the aggregate asperities. Its magnitude ranges from 1 to 500 μm (0.5mm). Microtexture is related to μ_o, which has been correlated to the friction value obtained at zero sliding speed. It is also associated with the friction measurements of the Dynamic Friction Tester (DFT) obtained at a sliding speed of 20 km/h (DFT_{20}). The function of microtexture is to provide adhesional friction at the tire pavement interface under light contamination conditions, where there is still contact between the tire and the asperity tips.

(2) Macrotexture: it is a function of the arrangement and orientation of aggregates at the pavement surface. Its magnitude ranges from 0.5mm to 50mm. Macrotexture is related to the Speed Constant (S_p). Specifically S_p has been linearly correlated to *MPD,* and it can be calculated by using the CT Meter and the numerical correlation expressed in the ASTM E 1960 (Equation (12)). The macrotexture facilitates rapid drainage of water arrested in the pavement surface under the tire patch which could lead to hydroplaning conditions. The macrotexture of a pavement surface perform the same function performed by the treads in the tire.

(3) Megatexture: it results from pavement surface distress. Generally roughness with amplitude of 50 mm and larger is defined as megatexture (roughness). In the past, megatexture has been related to passenger comfort. One objective of the current study is to quantify the effect of megatexture on the normal load at the tire pavement interface. The magnitude of the megatexture varies depending on the nature of the profile. On a given pavement, although the microtexture and macrotexture remain more or less constant, possible changes in the normal load due to variable megatexture would be reflected in the frictional resistance, which at times could lead to longer braking distances. Megatexture (roughness) is evaluated by the International Roughness Index (*IRI*), following the specifications established in the ASTM E 1926 (ASTM E 1926-08, 2009).

Different pavement surfaces may present the same frictional properties at a certain sliding speed and yet have different frictional properties at other sliding speeds. Figure 3 illustrates two different surfaces that present the same frictional value at a sliding speed of 30km/h, but different friction-speed relationships due to different macrotexture properties. This illustrates the importance of defining all the texture parameters when reporting frictional values. Hence all of the above parameters must be determined in order to characterize the texture condition of a pavement surface.

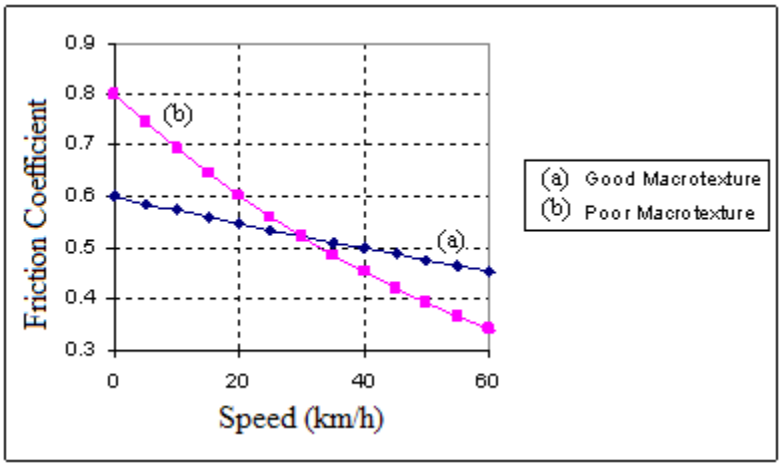

Figure 3 Texture effect on friction

As mentioned in Section 1.3 when one describes the details of the tire-pavement interaction mechanism, one has to consider the two frictional components, adhesion and hysteresis. These components are directly related to the different texture components of the pavement surface. Adhesion defined by microtexture is responsible for the frictional force at relatively low speeds (adhesion), while hysteresis defined by macrotexture is responsible for the frictional force at relatively high speeds.

1.6.1.1 Parameters Used for Texture Characterization

There are a number of different parameters used to quantify pavement texture. These are:

(1) Mean Profile Depth (*MPD*)

(2) International Roughness Index (*IRI*)

(3) Root Mean Square (*RMS*)

1.6.1.1.1 Mean Profile Depth (MPD)

The *MPD* is a parameter used to quantify pavement macrotexture. The standard practice for calculating the pavement *MPD* is established in the ASTM E 1845 (ASTM E 1845-01, 2009). A minimum of ten evenly space segments of 100 mm are needed for every 100 m of the test section for the computation of the *MPD*. Every segment is divided into two equal parts of 50 mm, and the peak value of the profile is determined for each of the 50 mm sub segments. The average of the two peaks is evaluated to obtain the Mean Segment Depth (*MSD*) of every segment. Finally, the average value of the *MSD* for all the segments of the measured profile is used to obtain the *MPD*. The *MPD* is linearly correlated to S_p (Equation (12)), which is one of the parameters used to report the IFI. The *MPD* quantifies the drainage capabilities of a pavement surface. For instance, a surface with higher *MPD* value will produce a more stable friction-velocity relationship (Figure 3(a)) than that with a surface with lower *MPD*, in which the friction will decrease rapidly with speed, under wet conditions (Figure 3(b)).

1.6.1.1.2 The International Roughness Index (IRI)

The International Roughness Index (*IRI*) was established by the World Bank with the intention of standardizing the longitudinal pavement profile evaluation (Sayers, 1995). *IRI* is based on a Quarter-Car Model, which is a "two degrees of freedom system" used to simulate the suspension system of a vehicle (Figure 4).

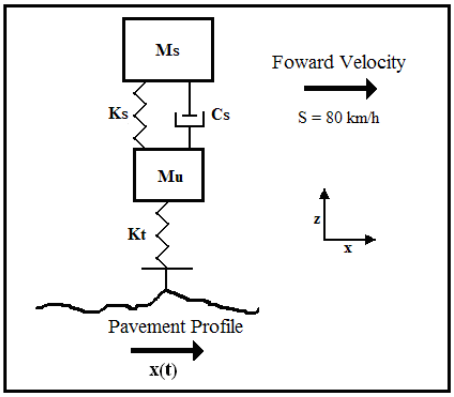

Figure 4 Quarter-Car Model

IRI is a portable quantity, which means that it can be computed independently of the device used to obtain the profile. *IRI* is defined as the cumulative displacement between the sprung and unsprung mass over the length of the profile. *IRI* is stable with time because it is based on the concept of a true longitudinal profile, rather than the physical properties of a particular vehicle. The standard practice for calculating the *IRI* is established in the ASTM E 1926 (ASTM E 11926-08, 2009).

$$IRI = \frac{1}{L}\int_0^{\frac{L}{S}} \left| \dot{z}_s - \dot{z}_u \right| dt \tag{8}$$

Where $\dot{z}_u$ and $\dot{z}_s$ are the velocities of the unsprung and sprung masses respectively. *L* is the length of the profile, and *S* is the velocity of the vehicle. *S* is fixed at 80 Km/h for *IRI* computations. The Quarter-Car Model can be used to evaluate the dynamic response of a particular vehicle to a given pavement profile using the appropriate model parameters for that vehicle (Figure 4). Then one would be able to evaluate the roughness effects of that pavement on the normal load at the tire pavement interface.

1.6.1.1.3 Root Mean Square (RMS)

The Root Mean Square (*RMS*), also known as the quadratic mean, is a statistical parameter used to characterize a pavement profile.

$$RMS = \frac{1}{N-1}\sqrt{\sum_{i=1}^{N} Y(i)^2} \tag{9}$$

Where Y(i) is the elevation of the profile at the i^{th} sample point, and *N* is the sample size.

1.6.2 Vehicle Operational Parameters

1.6.2.1 Slip Ratio

Friction researchers use the slip ratio term to indicate the difference between tire velocity and vehicle velocity, as indicated in Equation (10).

$$Slip = \frac{S - wR}{S} \tag{10}$$

Where S is the velocity of the vehicle, w is the angular velocity of the tire and R is the nominal radius of the tire. It is seen from Equation (10) that when the tire is rolling freely the slip must be 0 ($S = wR$). On the other hand when the tire is locked up the slip ratio is 1 ($wR = 0$). Locked wheels suffer severe localized wear under dry conditions since there is no rolling and subsequent uniform wear in the wheels when locked. Thus the material at the contact area between the wheel and the pavement surface is subjected to a frictional force that can lead to permanent deformation localized into one point only of the wheel. On the other hand, a rolling wheel distributes these effects in a uniform manner throughout the circumference; therefore the wear is considerably lower than that in the locked wheel condition.

Experimental work (NCHRP, 2009) shows that the maximum coefficient of friction for most surfaces is generally reached in a range between 0.1 and 0.2 slip ratio, depending on the type of surface, as shown in the Figure 5.

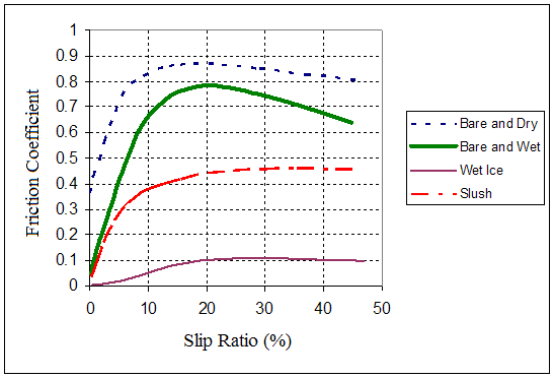

Figure 5 Coefficient of friction vs. Slip ratio on different surfaces (Adapted from NCHRP, 2009)

This is the principle on which Antilock Brake Systems (ABS) work. An ABS system recognizes that the maximum coefficient of friction is reached at a certain slip range, and hence controls the rotation of the tires for the slip ratio to be around that slip range. Thus ABS prevents the tires from locking, which provides vehicle stability, steerability and improves stopping capabilities. The ABS is an independent system in that only the wheels that are about to be locked will be pumped and slip-controlled, while the others will be subjected to the full braking pressure. Consequently this system would allow one to stop a vehicle within the shortest possible distance. A computer monitors the speed of each wheel, which is fed in to the ABS system (Mauer, 1995). When the system detects that one or more tires have locked up or are turning relatively slower compare to the remaining tires, the computer sends a signal to momentarily remove and re-apply the braking pressure to the affected tire to allow it to continue turning. This "pumping" of the brakes occurs at ten or more times a second, far faster then a human can pump the brakes manually.

1.6.2.2 Vehicle Speed

In general, the friction coefficient decreases with speed on wet conditions. This phenomenon is attributed to the facilitation of drainage under the tire. The higher the speed, the less time the water under the patch has to drain off. Pavement macrotexture (*MPD*) is usually used to explain the friction-velocity dependency. High macrotexture improves the drainage properties of the tire patch area, avoiding hydroplaning conditions. Figure 3 shows both the effects of pavement macrotexture and vehicle speed on the coefficient of friction.

1.6.3 Tire Characteristics

1.6.3.1 Tire Tread

The tire tread is a major factor when considering friction on contaminated pavement surfaces. Tire tread provides a drainage system to evacuate contaminants at the tire

pavement interface; thus having the same function as pavement macrotexture. The use of smooth tires is recommended when performing friction tests on a pavement surface, because then information specific to drainage capabilities and texture of the pavement can be obtained.

1.6.3.2 Tire Inflation Pressure

Tire inflation pressure is directly related to the tire stiffness. Hence frictional characteristics of a tire are related directly to its inflation pressure. Low tire pressures will be reflected in higher rolling resistance. Figure 9 shows the results from a load-deflection test performed by the investigator using the smooth tire of the Locked Wheel Tester. It is seen that the tire stiffness increases with increasing inflation pressure.

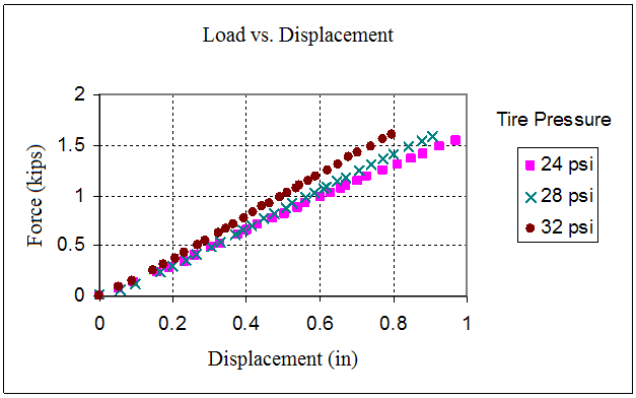

Figure 6 Effect of tire inflation pressure on tire stiffness

From Figure 6 one can infer the effects that tire inflation pressure would have on the vertical load at the tire pavement interface. As an example, a stiffer tire is more sensitive to a vertical displacement due to a profile than a softer tire.

1.6.4 Environmental Factors

A significant variation is observed in friction values measured on the same pavement surfaces at different times of the year. Several studies have suggested that this variation can be attributed to different environmental factors, such as rainfall, dry days preceding

the measurement, temperature, cumulative vehicles passes on test lane; and grease deposits, etc (Jayawickrama et. al., 1998).

1.6.4.1 Pavement Surface Temperature

Temperature has a significant effect on the frictional behavior of the tires, due to the viscoelastic nature of rubber. Friction in rubber like material generally decreases with increasing temperature. Temperature effect on friction is the main parameter responsible for seasonal variations of friction measurements. Therefore, it is necessary to apply a temperature correction to friction measurements in order to perform comparisons between those at different temperatures or different seasons of the year (Fuentes et. al., 2009).

1.7 International Friction Index (IFI)

As discussed in Section 1.5 different devices are available in the industry to measure the frictional properties of a pavement surface. As mentioned before, one of the issues surrounding these devices is that when the frictional characteristics of a pavement surface are evaluated using different friction measuring devices one sees significant deviations in their measurements. These friction measuring devices operate on different mechanisms and under different physical condition. Thus the observed differences would be obvious. As stated in Section 1.2 the coefficient of friction is not a material or a pavement surface property but is a property of the entire measuring system, which includes vehicle characteristics such as, slip ratio and tire pressure and waterfilm thickness. All these parameters change from device to device, so one should not be surprised of the difference on the measurements obtained from different devices on the same surface.

The PIARC International experiment (Wambold et. al., 1995) was conducted in Europe with the objective of developing a model that would be used to harmonize measurements obtained from different devices into a common calibrated index. Forty seven different friction measuring devices participated on the experiment and fifty four different sites, which covered a wide variety of pavement texture characteristics, were used to perform

the experiment. It was found that a simple linear regression could be used to correlate measurements from different devices. Consequently a friction index was proposed and later standardized by ASTM to be device independent, which implied that a certain pavement surface would have a specific index independent on the device used to obtain it. This index is the International Friction Index (IFI) as established in the ASTM E-1960. IFI defined in ASTM E 1960 is used currently as the standard for comparison of friction values measured by different equipment. The PIARC International experiment served as the base for harmonizing friction measurements from different equipment to a common calibrated index through IFI. IFI consists of two parameters: (1) Friction Number (*F60*) and (2) Speed Constant (*Sp*). It is typically reported as IFI (*F60, Sp*) and defined by Equations (11) and (12).

$$F60 = A + B * FRS * EXP\left[-\frac{(60 - S)}{S_p}\right] + C * MPD \tag{11}$$

$$S_p = a + b * MPD \tag{12}$$

Where *FRS* is the friction measurement obtained from a specific device at slip speed *S* (slip speed in km/h). *MPD* is the Mean Profile Depth is defined in Section 1.6.1.1.1. *F60* is the prediction of the calibrated Friction Number at 60 km/h and *Sp* is the prediction of the calibrated Speed Number, which was found in the PIARC experiment to be linearly correlated to the *MPD* (Wambold et. al., 1995); *A, B* and *C* are parameters specific to the friction measuring device while *a* and *b* are parameters considered to be specific to the texture measuring device used to measure the *MPD*. *A, B, C, a* and *b* are obtained by simple linear regression involving the relevant measured parameters in Equations (11) and (12), with the parameter *C* being used only when a ribbed tire is used for friction testing.

ASTM 1960 stipulates the use of DFT and CT Meter as standard equipment for the calibration of the IFI. Therefore the measurements obtained from these equipment (DFT_{20} and *MPD*) should be used as dependent variables when performing the simple linear

regression to obtain the characteristic parameters of the different equipment on calibration.

1.8 Scope of Investigation

A significant variation has been observed in coefficient of friction values measured on the same pavement surfaces at different times of the year. The objective of the first phase of this investigation is to evaluate the effect of the pavement temperature on the observed friction seasonal variations and propose a standardization procedure to correlate readings obtained at different times of the year using a given friction measuring device.

Different friction measuring devices available around the world are capable of evaluating the skid resistance properties of pavement surfaces. However, friction measurement values obtained from different devices on the same pavement surface are different, which makes the direct comparison between friction values obtained from different devices inappropriate. The current practice used to correlate friction measurements from different friction measuring devices is the International Friction Index (IFI). IFI is a mathematical model used to compare and harmonize frictional measurements taken from different equipment to a common calibrated index. The IFI assumes that there exists a linear correlation between measurements obtained from different frictional measuring equipment. IFI model uses DFT measurements obtained at 20 km/h as the standard friction measurement. However the DFT is a “spot” tester; which evaluates the frictional properties of a surface taking into account only a limited range of texture of the pavement (only micro and macro texture). On the other hand, conventional full scale friction testing equipment such as the Locked Wheel Tester, Runway Friction Tester, Grip tester etc. evaluate the frictional characteristics of a pavement over a specific length and hence their measurements are affected invariably by the dynamic effects arising from long-wave pavement roughness. The fact that DFT measurements, used for standardization, are not affected by long wavelength roughness, which affects all other full scale friction measuring vehicles, is a definitive issue in the current IFI standard. A second objective of

this investigation is to evaluate the effects that pavement roughness have on friction measurements.

Furthermore the IFI model assumes that the friction vs. speed dependency found in frictional measurements expressed by the Speed Constant (S_p) is accounted for by the pavement texture characteristics only. The parameter S_p dictates the speed variation of the wet friction measurements taken on a given pavement surface. Therefore another phase of the investigation would be directed at better understanding the principles underlying the concept of the International Friction Index (IFI) in general, and specifically the role played by the Speed Constant (S_p) in the IFI computations. The author believes that once the different factors that have an effect on friction measurements are identified, the IFI model can be revised to better correlate friction measurements obtained on the same pavement surface through time and among different friction measuring devices.

1.9 Organization of Dissertation

The following chapters represent a synthesis of research papers which address the respective issues described in Chapter 1. Chapter 2 presents a study of the different factors influencing the frictional measurements obtained using the DFT, while Chapter 3 describes the evaluation of the effect of roughness on skid resistance. Chapter 4 outlines an investigation evaluating the principles underlying the IFI, and a modified methodology proposed to evaluate the IFI parameters. Finally, Chapter 5 details the different conclusions obtained in this investigation.

CHAPTER 2

FACTORS INFLUENCING FRICTIONAL MEASUREMENT USING THE DYNAMIC FRICTION TESTER (DFT)

2.1 Introduction

Skid resistance on runways produced by the tire pavement friction interaction is an important element in aviation safety. Study of aircraft braking performance on runway surfaces has become so vital that organizations like NASA and FAA have developed research programs to evaluate the skid resistance available on runway pavement in order to ensure safe landing operations. Aircraft landing accidents continue to occur in many runways around the world. In some of these cases the aircraft had not been able to brake properly in the landing strip due to the improper understanding of the tire-pavement friction mechanism. There are many variables that are involved in this phenomenon. The understanding of each of these variables will help one to realize the magnitude of the problem that one faces and eventually design more reliable friction measuring techniques.

The International Friction Index (IFI) defined in ASTM E 1960 is used to harmonize friction measurements obtained from different equipment to a common calibrated index. The IFI would provide the means to evaluate the frictional characteristics of a pavement surface. ASTM E 1960 advocates the use of DFT for the calibration of a given friction testing equipment, as described in detail in Section 1.7.

The Dynamic Friction Tester (DFT) can be employed to evaluate the surface frictional properties of a pavement. A typical output from DFT is illustrated in Figure 7. In addition to its significance in IFI computations, many researchers have recognized the importance of the DFT in the area of skid resistance measurement (Wambold et. al., 1995). The above reasons led the author to conduct an investigation of the operation of the DFT, in

order to study the factors that could affect its measurements. The primary objective of this phase of the study was to identify the parameters that affect the friction measurements obtained from the DFT. Although this chapter is focused primarily on the temperature effects on the measured coefficient of friction values, other parameters that have significant impacts on DFT measurements were also identified in this study. These parameters are:

(1) Temperature of surface
(2) Temperature of water
(3) Site variability
(4) Water tank height
(5) Velocity
(6) Rubber slider

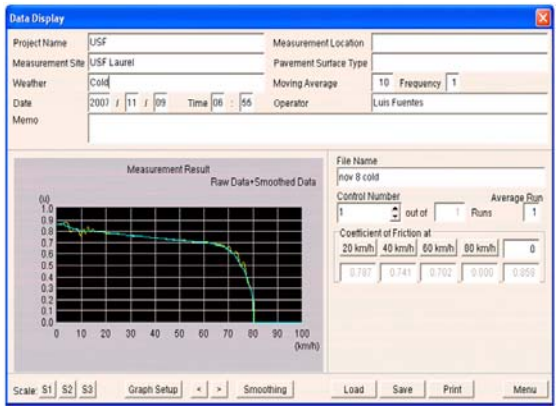

Figure 7 Typical output from the DFT

The author felt that seasonal variations in DFT measurements could mostly be explained by temperature effects, although the former has been proposed as an independent factor affecting friction measurements (Bazlamit et. al., 2005, and Jayawickrama et. al., 1998).

2.2 Experimental Setup

The author performed a field investigation within the University of South Florida campus to select a uniform test site for the experiment. Twelve (12) preliminary DFT measurements were performed at four (4) different sites. Finally the USF Laurel Drive site was selected because of its lowest spatial variation of friction, with a standard deviation of 0.01 at 20 km/h. This test site has an asphalt pavement that consists of a friction course of FDOT type S-3. DFT measurements were taken at the site at four (4) different levels of surface temperature and three (3) different levels of water temperature. Thus, twelve (12) different combinations of temperatures were used for testing. Four (4) DFT measurements were taken for each temperature combination to account for the spatial variation of friction. Surface temperatures were measured using an infrared sensor and every DFT measurement was performed on a dry spot. The different levels of temperature are seen in Table 2.

Table 2 Testing temperature combination

Surface		Water	
Temperature ^{o}F	Temperature Classification	Temperature ^{o}F	Temperature Classification
120 97 78 54	Hot (H) Hot Medium (HM) Medium (M) Cold (C)	135 75 34	Hot (H) Medium (M) Cold (C)

Effects of contaminants such as dust, sand, oil, grease and rubber particles were controlled by an intense clean up of the test site prior testing using a brush only with no chemicals, to avoid their effect on the friction measurement (Jayawickrama et. al., 1998). Any possible effects due to the height of the water level were eliminated by maintaining the water tank at an elevation of 0.6m above the DFT (ASTM E 1911-09, 2009). Moreover after each measurement the water tank was refilled back to the same level in order to maintain a constant water pressure throughout the experimentation.

Rubber sliders were replaced after twelve runs, as recommended in ASTM E 1911. It was observed in the present study that wear in the sliders was affected by the texture of the surface with rougher surfaces producing more wear.

The DFT is able to evaluate the coefficient of friction at different sliding speeds. However, DFT_{20} is used for IFI computations (Equation (11)) since DFT_{20} has provided the highest correlation to the IFI model in the PIARC International Experiment (Wambold et. al., 1995). By observation, the author was able to identify two different phenomena that could cause the change of the waterfilm thickness with speed. The first one is the rate of rotation of the disk, which at high angular speeds would induce a centrifugal force caused by the air movement under the disk, and the other one being the wiping effect produced by rubber sliders.

2.3 Results of Experiments

The results obtained from the 48 DFT measurements under different temperature combinations shown in Table 2 were subjected to a statistical study. Different software packages were used to perform the analysis, including Matlab, Excel and R. Figure 8 shows graphically the effect of the water temperature on the measured coefficient of friction at different speeds.

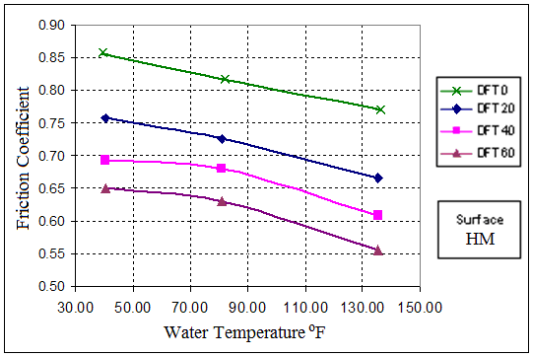

Figure 8 Average DFT measurements.
Friction Coefficient vs. Water Temperature in the range of 90 to 100 °F (Hot Medium)

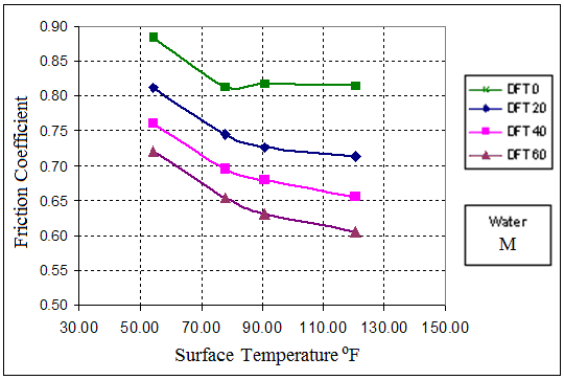

Figure 9 Average DFT measurements.

Friction Coefficient vs. Water Temperature in the range of 65 to 80 °F (Medium)

Four readings at each temperature combination were considered in the statistical analysis. It is observed in the Figures 8 and 9 that the coefficient of friction value decreases with increasing water temperature and surface temperature. Therefore it was necessary to perform a 3 parameter analysis to understand the combined effect of both surface and water temperature on coefficient of friction. This is illustrated in the 3D plot shown in Figure 4.

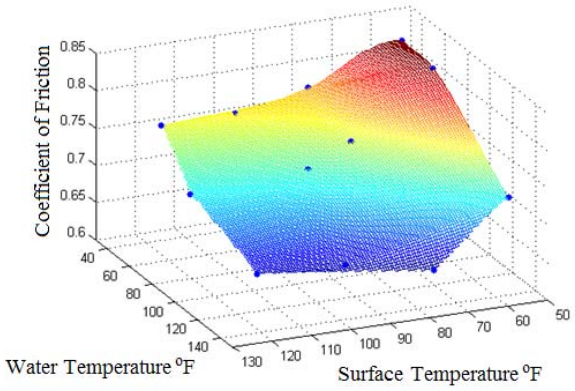

Figure 10 Combined effect of surface and water temperature on the coefficient of friction

In order to be able to explain the phenomenon of frictional variation due to temperature theoretically, one needs to understand the properties of the two types of materials that interact in producing pavement friction. The stiffnesses of both materials in contact, rubber and asphalt, are expected to decrease with increasing temperature (Bazlamit et.al., 2005).

Although the exact mechanisms of tire-pavement friction interaction are not fully understood yet, it is generally agreed in the literature that the frictional force is composed mainly of adhesion and hysteresis components (Moore, 1975). Shearing of tire rubber is another factor that contributes to the frictional force, although at a negligible magnitude when compared to the adhesion and hysteresis components. Moore, 1975, showed that the coefficient of friction decreases due to an increase of ΔT for any given sliding speed ***S*** in the operational speed ranges (Li et. al., 2004).

The decrease of coefficient of friction with the increase in water temperature could be attributed to the sensitivity of the hydrodynamic properties of water to temperature (Figure 11). The viscosity of water decreases as temperature increases thereby decreasing the boundary layer shear stress. This is because the shear stress in a Newtonian fluid is equal to the product of the viscosity and the time rate of strain (Bazlamit et.al., 2005).

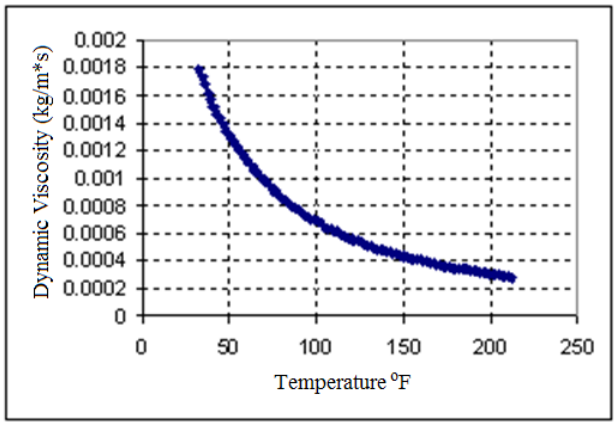

Figure 11 Change in dynamic viscosity of water with temperature

The least square regression method was used to analyze the relation between the two temperatures variables and the DFT_{20}. The friction measurements obtained on the different temperature combinations were used to obtain the regression presented in this paper. All possible regressions using the different potential explanatory variables are presented in Table 3. Different statistical parameters such as R^2, R^2_{pred} and C_p where used as criteria for the selection of the proposed model presented in Equation (13).

Table 3 All possible regressions

p	R^2	R^2_{pred}	C_p	p + 1	Variables
1	0.842	0.827	55.72	2	. . . . SW
1	0.740	0.714	97.06	2	. . . W2 .
1	0.729	0.702	101.53	2	. W . . .
1	0.250	0.175	295.45	2	S . . . .
1	0.220	0.142	307.33	2	. . S2 . .
2	0.945	0.933	16.05	3	S . . W2 .
2	0.923	0.906	25.04	3	S W . . .
2	0.923	0.906	25.06	3	. . S2 W2 .
2	0.900	0.878	34.38	3	. W S2 . .
2	0.868	0.839	47.39	3	. . . W2 SW
2	0.858	0.826	51.50	3	. W . . SW
2	0.843	0.809	57.35	3	S . . . SW
2	0.842	0.807	57.72	3	. . S2 . SW
2	0.741	0.683	98.80	3	. W . W2 .
2	0.302	0.147	276.24	3	S . S2 . .
3	0.981	0.974	3.61	4	S . S2 W2 .
3	0.965	0.952	10.18	4	S W S2 . .
3	0.953	0.935	15.20	4	S . . W2 SW
3	0.946	0.926	17.86	4	S W . W2 .
3	0.931	0.905	23.92	4	S W . . SW
3	0.925	0.897	26.39	4	. . S2 W2 SW
3	0.924	0.895	26.82	4	. W S2 W2 .
3	0.901	0.864	35.98	4	. W S2 . SW
3	0.896	0.857	37.94	4	S . S2 . SW
3	0.878	0.832	45.28	4	. W . W2 SW
4	0.984	0.975	4.40	5	S . S2 W2 SW
4	0.981	0.970	5.61	5	S W S2 W2 .
4	0.969	0.951	10.53	5	S W S2 . SW
4	0.953	0.926	16.95	5	S W . W2 SW
4	0.925	0.882	28.38	5	. W S2 W2 SW
5	0.985	0.973	6.00	6	S W S2 W2 SW

$$DFT_{20T} = 1.002 - 0.004404\,\mathrm{S} - 0.000005722\,\mathrm{W}^2 + 0.00001992 * \mathrm{S}^2 \qquad (13)$$

(R^2 = 98.1%, R^2 (pred) = 97.4%)

Where $DFT_{20T} = DFT_{20}$ measurement at temperature T, W = Water temperature in ^{o}F; and S = Surface temperature in ^{o}F. R^2_{pred} is determined by systematically removing each observation from the data set and estimating a regression equation, and finally determining how well the model predicts the removed observation. It is known that higher R^2_{pred} ensure models of greater predictive ability. The summary of the above statistics is shown in Table 4.

In order to develop the temperature correction the author used a standard surface temperature of 98 ^{o}F and a standard water temperature of 70 ^{o}F. After substituting the above standard values in Equation (13) to obtain standard DFT_{20} and subtracting the result from Equation (13) one obtains Equation (14). Equation (14) can be used to adjust *F60* (Equations (11)) to account for the temperature effect on DFT measurements.

$$\Delta DFT_{20T} = 0.2684 - 0.004404\,S - 0.000005722\,W^2 + 0.00001992 * S^2 \qquad (14)$$

Thus, ΔDFT_{20} can be considered as a correction factor that must be used on the Equation (11) to calculate the IFI parameter.

Table 4 Summary of statistics

Coefficients:	Estimate	Std. Error	t value	Pr(>|t|)	Significance level
(Intercept)	1.00E+00	3.62E-02	27.646	3.16E-09	0
S	-4.40E-03	8.87E-04	-4.966	0.0011	0.001
S2	1.99E-05	5.11E-06	3.897	0.00456	0.001
W2	-5.72E-06	3.37E-07	-16.994	1.46E-07	0
Residual standard error: 0.008496 on 8 degrees of freedom					
Multiple R-Squared: 0.9812, Predicted R-squared: 0.9741					
F-statistic: 139.1 on 3 and 8 DF, p-value: 3.057e-07					

Figures 12 and 13 illustrate the values corresponding to the fitted Equation (13) with respect to the actual measurements.

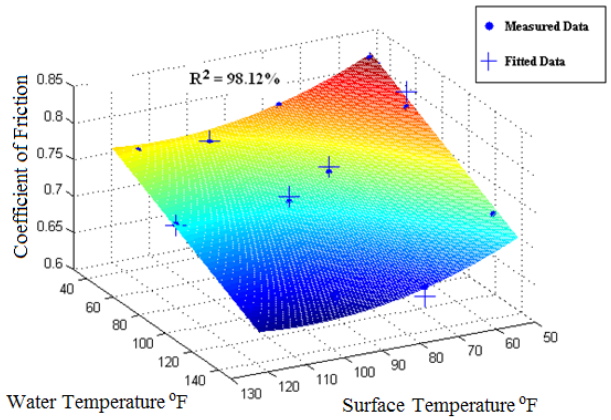

Figure 12 3D plot of model (Equation (13)) fitted surface and actual measurement of coefficient of friction

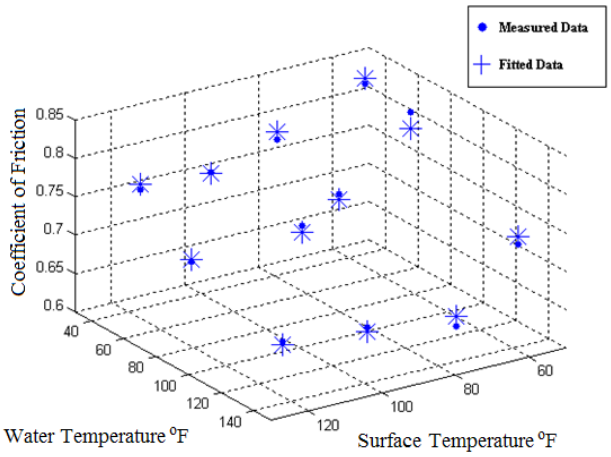

Figure 13 Plot of fitted data vs. measured DFT_{20} (Equation (13))

2.4 Variation of Friction Measurements due to Environmental Conditions

A significant variation has been observed in coefficient of friction values measured on the same pavement surfaces at different times of the year. In the literature, two different phenomena have been reported to have an effect on frictional measurements due to environmental conditions. They are (1) short term variation of friction, which has been attributed to different parameters such as rainfall, dry days preceding the measurement, cumulative vehicles passes on test lane; and grease deposits, etc (Jayawickrama et. al., 1998), and (2) seasonal variation (long term effects) which has been attributed to temperature and wear effects (Bazlamit et. al., 2005). Based on the findings reported in

Section 2.3, the author believes that a temperature correction factor should be used to account for the variation of friction measurements due to the seasonal variation. Figure 9 shows the seasonal variation of the skid number measured on an asphalt pavement site in Lucas County, Ohio (Bazlamit et. al., 2005). One can observe a periodic behavior of the skid number with respect to the time of the year.

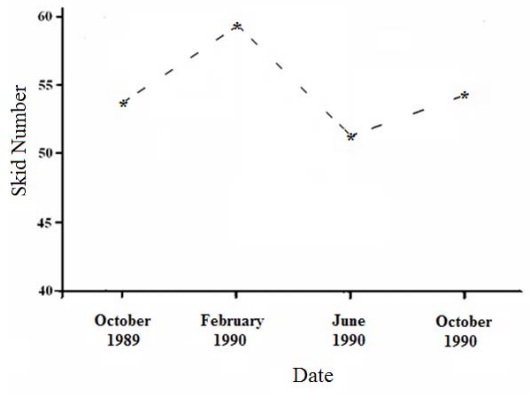

Figure 14 Typical seasonal variation of Skid Number for an asphalt pavement site located in Lucas County, Ohio (Adapted from Bazlamit et. al., 2005).

By determining the general air temperature trends of Lucas County, Ohio, from relevant sources (Weather Underground, (2007)), the author was able to plot the variation of the skid number with respect to the average air temperatures on the dates reported on Figure 14. It is seen from Figure 15 that the skid varies almost linearly with respect to only the temperature. This has been shown by the author in Figure 9 and can be predicted by Equation (13) formulated by the author.

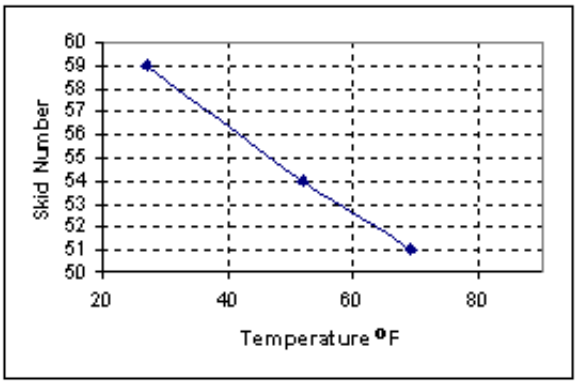

Figure 15 Skid Number vs. Temperature for an asphalt pavement site located in Lucas County, Ohio

CHAPTER 3

EVALUATION OF THE EFFECT OF PAVEMENT ROUGHNESS ON SKID-RESISTANCE

3.1 Significance and Standardization of Pavement Friction Measurements

Accidents due to pavement skid resistance deficiencies are a major concern of the aviation and highway industries. Skid resistance is developed when vehicle tires are fully or partially prevented from rolling under lubricated conditions and start to slide along a pavement surface. Hence modeling the mechanism of skid resistance generation due to the tire pavement friction interaction is a major issue in safe operation of vehicles and aircraft.

Lubricated mechanical systems operate in four different regimes of lubrication, namely: static friction, boundary lubrication, partial fluid lubrication and full fluid lubrication. Of these, the mechanics of static friction, boundary lubrication and full fluid lubrication are well understood as indicated in the literature (Armstrong, 1991). Skid resistance is particularly critical when water or other contaminants are present serving as lubricants at the tire pavement interface. Hence, the generation of pavement skid resistance must be investigated within the regime of partial fluid lubrication. However, the understanding of partial fluid lubrication is vague and only empirical studies have been conducted to study this phenomenon. The variation of skid resistance under partial fluid lubrication is complicated by its slip speed dependency. In the numerous empirical models that have been developed to address this variation, pavement texture parameters have been used as independent variables (Henry, 2000).

Since a multitude of devices are available for measurement of pavement skid resistance, there has been an imminent need for standardization of skid resistance measurements. The International Friction Index (IFI) is used to harmonize friction measurements obtained from different friction measuring devices to a common calibrated index (ASTM E-1960-07, 2009). The IFI concept is based on the assumption that the friction value of a given surface depends on the slip speed at which measurements are taken, the texture properties of the pavement surface (both micro and macrotexture) and characteristics of the device used to obtain the measurements. Hence, the ASTM E-1960-07 stipulates the use of Dynamic Friction Tester (DFT) and the CT Meter as the standard equipment for the calibration of the IFI. In the IFI method, DFT measurement obtained at 20 km/h (DFT_{20}) is considered the standard skid resistance value of a pavement and CT Meter is recommended as the standard instrument for evaluating S_p. DFT_{20} and S_p can be correlated to microtexture and macrotexture respectively (ASTM E-1960-07, 2009). The IFI concept also assumes the existence of a linear correlation between measurements obtained from different frictional measuring equipment. Hence any given friction measuring device can be calibrated against the DFT using two parameters; A and B inherent to the given device. The parameters A and B represent the intercept and slope, respectively, of the simple linear regression between the friction measurements of a specific device on different pavement surfaces and the corresponding measurements obtained using the DFT. These parameters could be used later for IFI computations using the given device or in the standardization of the readings of that device.

3.2 Limitations of the Current Friction Models

In the current pavement friction evaluation models, coefficient of friction is defined for a finite area of the pavement accounting only for micro and macrotexture. This is exemplified by the use of a spot tester such as DFT as a standard device in the IFI computation. On the other hand, in field evaluations, conventional full scale friction testing equipment are employed to evaluate the frictional characteristics of a pavement over a significant length. Hence, their measurements are affected invariably by the

dynamic effects arising from long-wave pavement roughness or megatexture. More specifically, in full scale friction measuring devices, a significant dynamic normal force is generated due to the mechanical vibration of its individual components in response to pavement roughness. The overall magnitude of megatexture (considered to be of amplitudes of 50 mm and larger) depends on the nature of the profile and it is typically evaluated by the International Roughness Index (*IRI*), following the specifications established in the ASTM E 1926-08 (ASTM E 1926-08, 2009). Dynamic changes in the normal load on a given pavement with variable megatexture and presumably more or less constant micro and macrotexture, would be manifested as reductions in skid resistance, leading to longer braking distance at times. In this regard, a number of studies have attributed skid related accidents to rough pavements (with high *IRI*) (Al-Masaeid, 1997, Tighe et. al., 2000, Davies et. al., 2004). Al-Masaeid observed that multiple-vehicle accidents increase as *IRI* increases and Davies et. al. also observed that skid related accidents involving multiple vehicles would increase with *IRI*. The current friction models which form the basis for IFI obviously do not incorporate the effect of pavement roughness on friction measurements.

In this study, an explanation or mechanism for the reduction in friction is shown to be due to megatexture and the resulting variations of normal load at the tire pavement interface and the well documented phenomenon of the reduction in rubber friction due to increased normal loads. Roth et. al. (1942) conducted an investigation on the friction produced by soft rubber compound commonly used in tire treads observing that the coefficient of friction decreases as the normal load and the pressure increase. However Roth et. al. have not proposed a viable mechanism for the observed reduction on the frictional force. Thirion (1946) also studied the influence of normal load in rubber friction being the first investigator to introduce adhesion as a friction generating mechanism on rubber like materials. Furthermore, Thirion observed that the coefficient of friction of rubber decreases hyperbolically with increasing normal pressure. Schallamach (1952) presented experimental evidence on the normal load dependency of rubber friction subsequently hypothesizing that the proportionality that exists between the frictional force and the true area of contact would be responsible for this phenomenon.

Therefore Schallamach proposed the following empirical equation to quantify the dependence of the coefficient of friction of rubber (μ) on the normal load (W).

$$\mu = cW^{-\frac{1}{3}} \tag{15}$$

The constant c has to be determined experimentally for a given velocity and interacting material types. Conventional frictional models do not also account for the normal load dependency of the coefficient of friction. Equation (15) reveals that for rubber the coefficient of friction decreases as the normal load increases.

3.3 Objectives of the Current Study

This phase of the investigation is focused on evaluating the impact of pavement megatexture on full-scale friction measuring devices in particular, through an understanding of the normal load variation caused by megatexture and the dependency of frictional coefficient on the normal load.

The specific objectives of this phase of the study documented in this chapter are;

(1) Experimental verification of the effect of pavement roughness on skid resistance.
(2) Experimental verification of the reduction in the coefficient of friction with increased normal load.
(3) Formulation of a simplified vibration model to interpret and quantify the changes in skid resistance due to pavement roughness.

3.4 Experimental Program

A detailed experimental program was planned and executed to achieve the first two objectives in the Section 3.3.

3.4.1 Equipment Used in the Study

The following state-of-the-art equipment were used to measure the parameters relevant to this study.

3.4.1.1 Circular Track Meter (CT Meter)

The CT Meter (ASTM E-2157 - 01(2005), 2009) is a device used to evaluate the macrotexture properties of a given surface. It specifically measures the Mean Profile Depth (*MPD*) which is used to express the friction-slip speed dependency in the IFI model (Equation 12).

3.4.1.2 Dynamic Friction Tester (DFT)

As described in Section 1.5.2.1 the Dynamic Friction Tester (DFT) (ASTM E 1911-09, 2009) can be employed to evaluate the surface frictional properties of a pavement. The measuring mechanism of the DFT is based on energy concepts with the loss of kinetic energy of a rotating disk resting on rubber sliders converted to an equivalent frictional force exerted by the pavement. DFT is capable of measuring friction over the sliding speed range from zero to 90 km/h.

3.4.1.3 Locked Wheel Tester (LWT)

As described in Section 1.5.1.1 the Locked Wheel Tester (LWT) (ASTM E 274-06, 2009) is the most popular device used by the U.S. Departments of Transportation (DOT) to evaluate skid-resistance of highway pavements. It operates at full (100%) slip conditions, whereby the wheel used to measure the coefficient of friction is completely prevented from rolling during testing. Thus, the LWT is used to simulate an emergency braking condition without an antilock braking system (ABS). The specific LWT used in this investigation was equipped with a profilometer capable of measuring *IRI* and *MPD* of the test wheel path. Smooth tires were used in this study since they allow one to better

evaluate the drainage capability of a pavement surface facilitating the comparison of pavement surfaces for skid resistance.

3.4.2 Selection of Test Sections

The first phase of experimentation was conducted to evaluate the effect of roughness on friction measurements. The specific goal of this phase was to show that significantly different friction measurements would be obtained using the LWT on two distinct sections possessing the same levels of microtexture and macrotexture, but different degrees of roughness.

In keeping with this objective, two pavement types (A and B) with different levels of roughness (*IRI*) were selected. Surface A was an asphalt pavement that consists of a friction course of Florida Department of Transportation (FDOT) type S-3, while surface B was an asphalt pavement consisting of a friction course of FDOT type FC-5. The next task was to select two sub-sections on each section (A and B) so that a significant difference in roughness (megatexture) was apparent between them. In each section A and B, a sub-section relatively rougher than the rest of the section was designated as the test site and another regular sub-section in close proximity to the test site was selected as the control site. Then after meticulous visual survey of both pavement sections, two sub-sections of each section were chosen as the test sites and the control sites. Both the DFT and the CT Meter were used to verify that the micro and macrotexture characteristics on both sub-sections were similar. Then five repeated friction measurements were obtained at three predetermined speeds on each sub-section using the LWT. After every friction measurement, an air blower (leaf blower) was used to remove the excess water from the wheel path of the LWT. The order in which the readings were taken was randomized to control all of the noise variables that were not of interest in this study, but that could have an effect on the measurements. The randomization also served to ensure that the measurements were unbiased with respect to the testing sequence. Friction measurements were reviewed with respect to the order in which they were performed to observe whether any specific trend would be observed as the friction measurements proceeded. No

definitive pattern such as a decreasing trend in the friction measurements at a specific speed was observed as measurements were repeated (Figure 16).

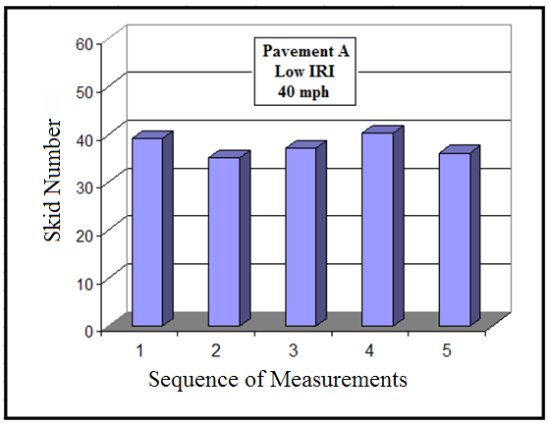

Figure 16 Evaluation of the effect of repeated measurements on the Skid Number

The second phase of the experiment was to evaluate the effect of the normal load on friction generated at the tire pavement interface. The specific goal of this phase was to illustrate that different friction measurements would be obtained by changing the load configuration of the LWT on the same surface. Four different levels of normal load were configured in the LWT to quantify its effect on friction measurements. Each time the desired variation in normal load was achieved by adding or removing appropriate weights from the LWT trailer. The modified weight configuration was designed so as to prevent any eccentricity at the tire pavement interface and maintain the static download force between the truck and the trailer within the range specified by ASTM E 274-06. The main aim of changing the static load on the skid-trailer was to expand the range of variation of the normal load induced by pavement roughness alone and provide a picture of the relationship between friction and roughness at a much higher resolution. In this phase of the experiment, since friction had to be measured in each test under the designated normal load, testing was limited to "relatively" smooth surfaces in order to prevent dynamic changes in the normal load caused by pavement roughness from becoming a confounding factor.

To achieve the above conditions, two additional pavements surfaces (C and D) were selected. Surface C is an asphalt pavement that consists of a friction course of FDOT type FC-5, while surface D is an asphalt pavement that consists of a friction course of FDOT type FC-12.5. These friction courses are the most abundant in Florida's highway network. FC-5 is an open graded surface type generally used on highways with speed limits higher than 50 mph, and FC-12.5 is a dense graded surface type used on highways with speed limits lower than 50 mph. Five friction measurements were performed using the LWT at each of the two predetermined speeds for selected design load combinations on each surface. After every friction measurement, a leaf blower was used to remove the excess water from the wheel path of the LWT. The order in which these readings were obtained was randomized to control all the extraneous (noise) variables that could affect the friction measurements. After every friction measurement, the LWT was recalibrated for the updated load configuration.

3.5 Results of Texture Analysis

Figure 17 present different descriptive statistics of *MPD* (from CT Meter) and DFT_{20} (from the DFT) used for the texture comparison between the control and the test sections of both pavement surfaces A and B. From Figure 17 it is observed that there is no significant difference in macrotexture (indicated by *MPD*) and microtexture (indicated by DFT_{20}) between the test and control sub-sections on both pavements A and B.

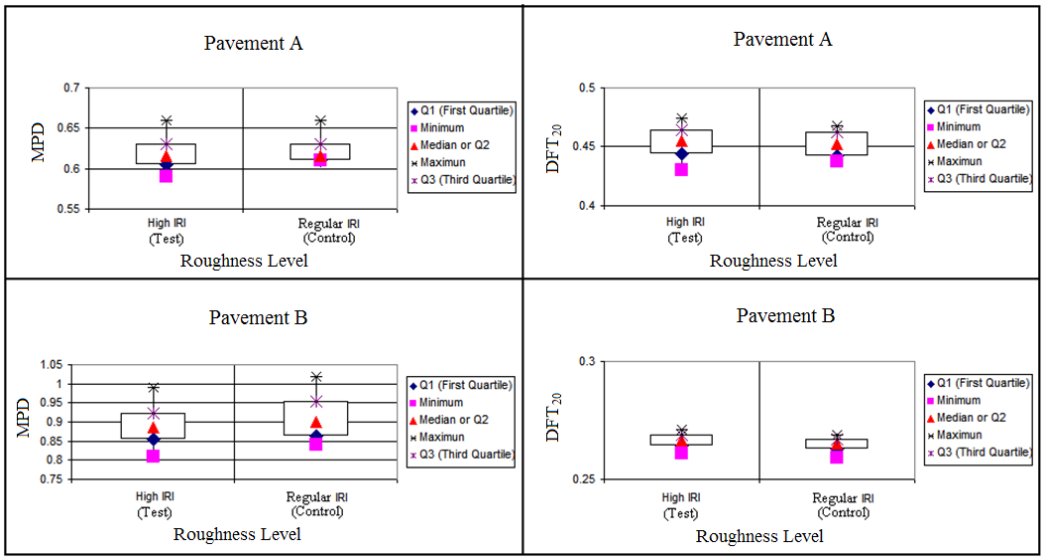

Figure 17 Box-Plots of texture comparison between test and control sections of pavements A and B

In order to verify that the random variations in *MPD* and DFT_{20} within each (A and B) section are not statistically significant, an effects model of the following form was used:

$$y_{ij} = \mu + \tau_i + \varepsilon_{ij} \begin{cases} i = 1,2 \\ j = 1,2,3,4 \end{cases} \tag{16}$$

where y_{ij} is the j^{th} observation of the i^{th} treatment, μ is a parameter common to all treatments called the overall mean. In this case μ would be the overall DFT_{20} or *MPD* mean of the pavement surface; τ_i is a parameter unique to the i^{th} treatment called the i^{th} treatment effect, which in this case would be roughness. The null hypothesis would be that $\tau_i = 0$, implying that the effect of roughness on the test and control sub-sections is zero for the measurements obtained using the DFT and the CT Meter. Tables 5-8 present the analysis of variances (ANOVA) of texture (*MPD* and DFT_{20}) for both pavements A and B with roughness as the treatment factor.

Table 5 Analysis of variance of microtexture (DFT_{20}) on pavement A

Source of Variation	Degrees of Freedom	Sum of Squares	Mean Square	F_0	P-Value
Roughness	1	0.000008	0.000008	0.0213	0.8887
Residuals	6	0.0022515	0.00037525		

Table 6 Analysis of variance of microtexture (DFT_{20}) on pavement B

Source of Variation	Degrees of Freedom	Sum of Squares	Mean Square	F_0	P-Value
Roughness	1	0.0000061	0.000006125	0.3411	0.5805
Residuals	6	0.000107	0.000017958		

Table 7 Analysis of variance of macrotexture (*MPD*) on pavement A

Source of Variation	Degrees of Freedom	Sum of Squares	Mean Square	F_0	P-Value
Roughness	1	0.00005	0.00005	0.0698	0.8005
Residuals	6	0.0043	0.0007167		

Table 8 Analysis of variance of macrotexture (*MPD*) on pavement B

Source of Variation	Degrees of Freedom	Sum of Squares	Mean Square	F_0	P-Value
Roughness	1	0.000112	0.000112	0.0184	0.8965
Residuals	6	0.036675	0.006113		

From Tables 5-8, it can be observed that in all four cases the P-value is significantly high at a significance level (α) of 0.1, which leads to acceptance of the null hypothesis (Equation (16)) that the difference in roughness is not significant ($\tau_i = 0$) for the DFT_{20} and *MPD* measurements within the test and control sub-sections of pavements A and B. This leads to the conclusion that the test and control sites only differ in roughness (megatexture) and not in micro and macrotexture properties.

3.6 Results of Friction Testing

3.6.1 Effect of Roughness on Friction

Figures 18 and 19 show the *IRI* (International Roughness Index), *RN* (Ride Number), which is another indicator of roughness, *MPD* and the DFT_{20} evaluations of the test and control sub-sections of pavements A and B respectively. It must be noted that the parameters *IRI* and *RN* are computed in accordance with the ASTM E 1926-08 and ASTM E 1489-08 (ASTM E 1489-08, 2009) respectively, using the laser profiler of the LWT.

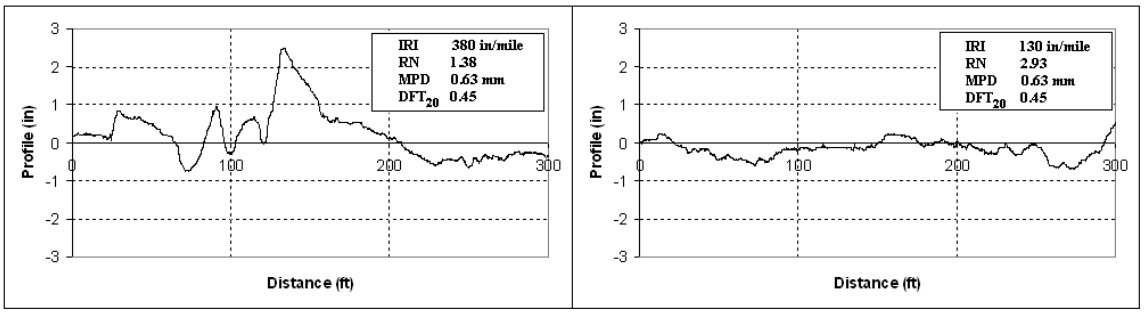

(a) Rough (test) (b) Regular (control)

Figure 18 Measured roughness characteristics of sub-sections of pavement A

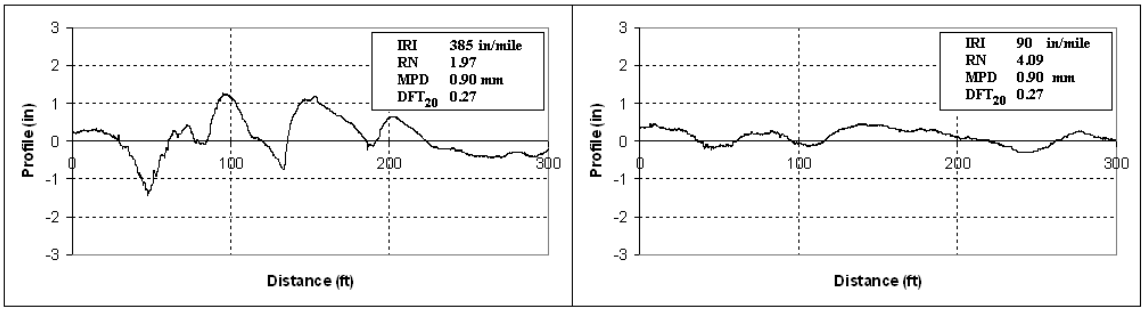

(a) Rough (test) (b) Regular (control)

Figure 19 Measured roughness characteristics of sub-sections of pavements B

Figure 20 depicts the friction measurements on pavement A and B at sub-sections of regular (control) and high (test) roughness. It can be observed that on both pavements, at a given speed, the skid number decreases as the roughness increases.

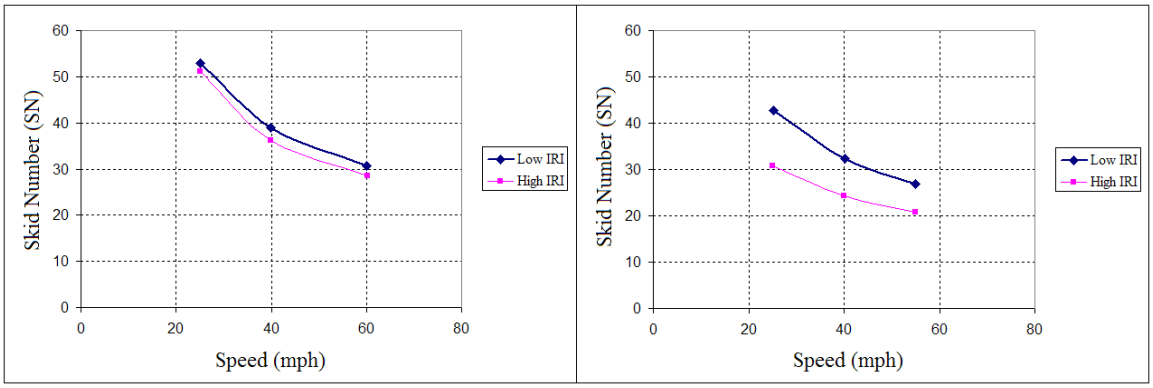

Figure 20 Effect of roughness on the Skid Numbers of (a) pavement A and (b) pavement B

It is also seen from Figure 20 that the roughness ranges encountered in pavements A and B contribute to Skid Number reductions of 6% and 20% respectively. In addition an ANOVA study was also performed to investigate the significance of the reduction in *SN* due to roughness and the interaction between speed and roughness. The results of ANOVA are given in Tables 9-10.

It can be concluded from Tables 9-10 that the roughness variation has a statistically significant effect on frictional measurements, at a 90% level of confidence (P-values << α (= 0.1)). It also appears that the plots in Figure 20 have parallel trends with respect to speed, indicating that there is no significant interaction between roughness and speed. However, one would expect the interaction between speed and roughness to affect the friction measurements, since the speed of the moving LWT determines how the roughness of the pavement surface is "felt" by the LWT in terms of the rate of change in elevation with time (Gillespie et. al., 1993).

In this respect, it can be observed from Table 9 that the interaction variable (speed*roughness) has no significant effect on *SN* in pavement A, where as Table 10 shows that the P-value for the interaction variable is much lower than α (0.1), indicating its significance on *SN* measurements. One possible explanation for this anomaly could be that a specific predominant roughness wavelength encountered on pavement B excites one of the natural frequencies of the suspension system of the LWT at a specific speed, a condition that does not occur on pavement A.

Table 9 Analysis of variance of friction measurements (*SN*) including the interaction variable Speed*Roughness on pavement A

Source of Variation	Degrees of Freedom	Sum of Squares	Mean Square	F_0	P-Value
Speed	1	2449.43	2449.43	186.2531	8.34E-13
Roughness	1	40.3	40.3	3.064	0.09282
Speed*Roughness	1	0.02	0.02	0.0012	0.97237
Residuals	24	315.63	13.15		

Table 10 Analysis of variance of friction measurements (*SN*) including the interaction variable Speed*Roughness on pavement B

Source of Variation	Degrees of Freedom	Sum of Squares	Mean Square	F_0	P-Value
Speed	1	856.41	856.41	408.967	2.20E-16
Roughness	1	546.13	546.13	260.797	4.524E-15
Speed*Roughness	1	43.88	43.88	20.955	0.0001025
Residuals	26	54.45	2.09		

In order to provide support for the above hypothesis the profiles of pavements A and B were plotted in Figure 21 in the frequency domain. First a Fast Fourier Transform (FFT) was performed on the profiles to obtain the wave number (w_n) spectrum and then the frequency spectrum, *f*, corresponding to any evaluation speed (*S*) was determined using Equation (17).

$$f = w_n * S \tag{17}$$

where *f* is frequency (cycles/sec), and w_n is the pavement wavenumber (cycle/length).

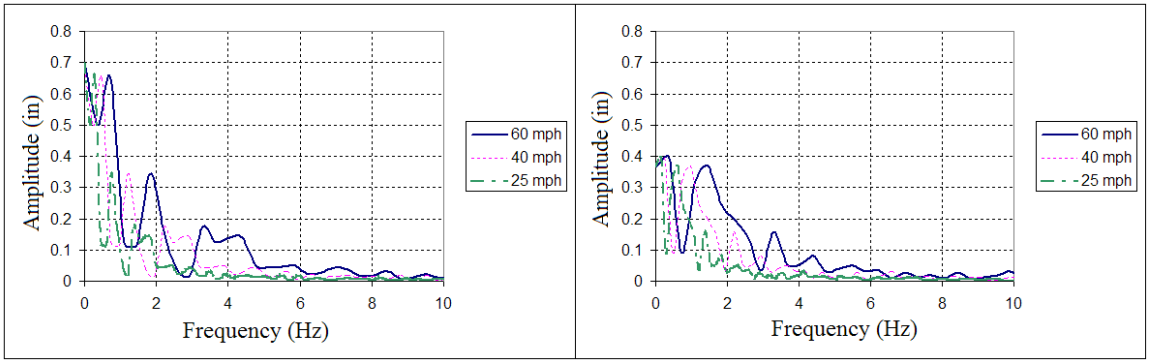

Figure 21 Frequency decomposition of the pavement profiles

It can be seen from Figure 21 that the principal frequency components of the profiles of pavement A and B (for the three speeds used) lie in the ranges of 0.2 - 0.8 Hz, and 0.5 - 2 Hz, respectively. Since one of the natural frequencies of the LWT is found to be 1.8 Hz (Section 3.7), the dynamic response of the LWT is magnified on pavement B. This illustrates that the relationship between friction and roughness can be confounded by speed effects when testing pavements where one predominant roughness wavelength can interact with the operational speed to produce a resonant condition of the LWT.

3.6.2 Effect of the Normal Load on Friction

In the second phase of the experimental program, testing was conducted to investigate the effects of the normal load on friction measurements. Figure 22 presents the frictional measurements taken on pavements C and D (Section 3.4.2) by varying the normal load at two distinct speeds. The typical static normal load of the LWT is 1085 lb, as stipulated in the ASTM standards. From Figure 22 one can observe that *SN* follows an inverse S shape, where *SN* remains constant for low normal loads until a certain limiting normal load is reached at which *SN* starts to decrease as the load increases, and finally reaches a residual *SN*. It must be noted that at a fixed normal load the reduction in *SN* at higher speeds (Figure 22) is an established fact as seen in Equation (27) (Henry et. al., 1978, ASTM E-1960-07, 2009).

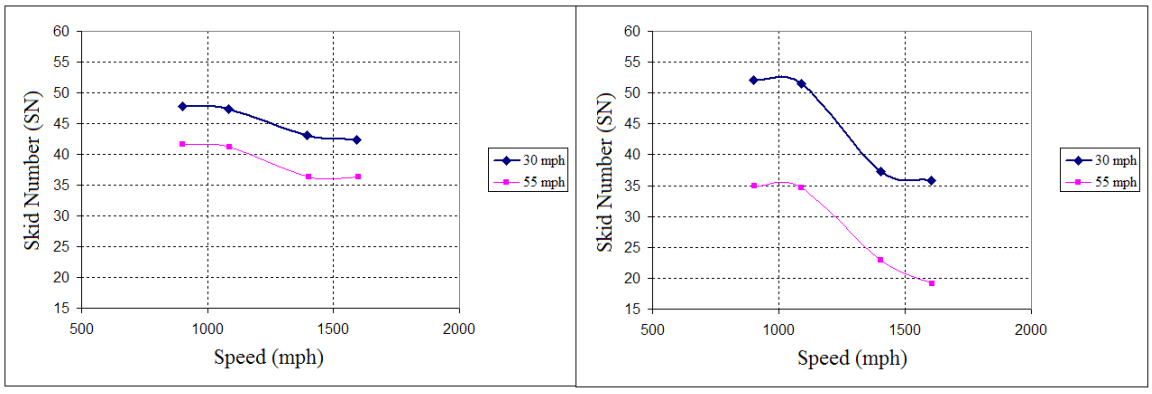

Figure 22 Effect of normal load on Skid Numbers on: (a) pavement C and (b) pavement D

ANOVA was also performed to verify the significance of the dependence of normal load on *SN*. From the results of this analysis shown in Tables 11-12 one can see that the P-

value representing the factor, load, is approximately zero, leading to the conclusion that the normal load is statistically significant in friction measurements.

Table 11 Analysis of variance of friction measurements (*SN*) on pavement C based on Speed and Normal Load

Source of Variation	Degrees of Freedom	Sum of Squares	Mean Square	F_0	P-Value
Speed	1	376.86	376.86	237.714	2.20E-16
Load	3	238.72	79.57	50.193	9.17E-13
Residuals	35	55.49	1.59		

Table 12 Analysis of variance of friction measurements (*SN*) on pavement D based on Speed and Normal Load

Source of Variation	Degrees of Freedom	Sum of Squares	Mean Square	F_0	P-Value
Speed	1	2670.45	2670.45	921.39	2.20E-16
Load	3	2077.02	692.34	238.88	2.20E-16
Residuals	35	101.44	2.9		

However, the ANOVA results shown in Tables 11-12 do not provide adequate information to distinguish the normal load levels at which the significant differences in the measured average *SN* values occur. In order to verify that the mean *SN* values measured under two selected normal loads are significantly different from one another, one could carry out multiple independent sample t-tests, each time performing a pair-wise comparison of the corresponding *SN* means. However when one performs *n* simultaneous independent sample t-test comparisons, one would expect the Type I error (α) to accumulate *n* times, thus inflating it to the point that the studies would no longer produce meaningful results. In order to address this issue, a technique known as Tukey's HSD (Honestly Significant Difference) test (Montgomery, 2008) was executed to control the family-wise error rates. In this investigation, the HSD test was used specifically to determine as to which of the *SN* means measured at selected load level pairs were significantly different from each other. Tukey's test is a hypothesis test where a pairwise comparison of means is performed in which the overall significance level is exactly α (Type error I). Tukey's test turns out to be conservative when compared to results obtained by performing multiple independent sample t-tests, making the conclusions

drawn from this analysis more meaningful. The results of the Tukey's HSD test are demonstrated in Tables 13-14 and Figure 23.

Table 13 and 14 show that the P- values for combinations #2, 3, 4 and 5 are equal to zero, enabling one to reject the null hypothesis that the *SN* is the same at those load combinations. This observation is further supported by the confidence intervals obtained using the Tukey's HSD test which are plotted in Figure 23(a) and Figure 23(b). Furthermore, the above results also show that that there is no significant difference between the mean *SN* measured at load combination #1 in both Tables 13 and 14; and in combination #6 in Table 13. Although the very low P value corresponding to the combination #6 in Table 14 suggests that there is a difference in *SN* for that combination, one can observe in Figure 23(b) that the corresponding confidence interval for the difference in means almost contains the value of zero. This slight anomaly is pronounced only at the speed of 50 mph as seen in Figure 23(b). Results of the data analysis provided in Tables 13-14 and Figure 23 further support the inverse S shape proposed for the *SN* vs. load variation seen in Figures 22(a) and 22(b) . Hence, the following mathematical representation, which captures S-shape dependencies, is used to model *SN* with respect to normal load.

Table 13 Pairwise comparison among Skid Numbers means at different load configuration using Tukey's HSD Test for pavement C

Combination #	Load Pair Combination (lb)	Difference of *SN* means between Load levels	Lower *SN* Limit of Confidence Interval	Upper *SN* Limit of Confidence Interval	P-Value
1	1085-900	-0.2374102	-1.79763	1.32281	0.9763147
2	1400-900	-4.76	-6.278607	-3.241393	0
3	1600-900	-5.2015174	-6.685209	-3.717826	0
4	1400-1085	-4.5225898	-6.08281	-2.96237	0
5	1600-1085	-4.9641072	-6.490364	-3.43785	0
6	1600-1400	-0.4415174	-1.925209	1.042174	0.8527597

Table 14 Pairwise comparison among Skid Numbers means at different load configuration using Tukey's HSD Test for pavement D

Combination #	Load Pair Combination (lb)	Difference of *SN* means between Load levels	Lower *SN* Limit of Confidence Interval	Upper *SN* Limit of Confidence Interval	P-Value
1	1085-900	-0.8330	-2.8863	1.2203	0.6954
2	1400-900	-13.4076	-15.4137	-11.4015	0
3	1600-900	-16.2307	-18.3402	-14.1211	0
4	1400-1085	-12.5746	-14.5807	-10.5685	0
5	1600-1085	-15.3977	-17.5072	-13.2881	0
6	1600-1400	-2.8231	-4.8867	-0.7594	0.0040

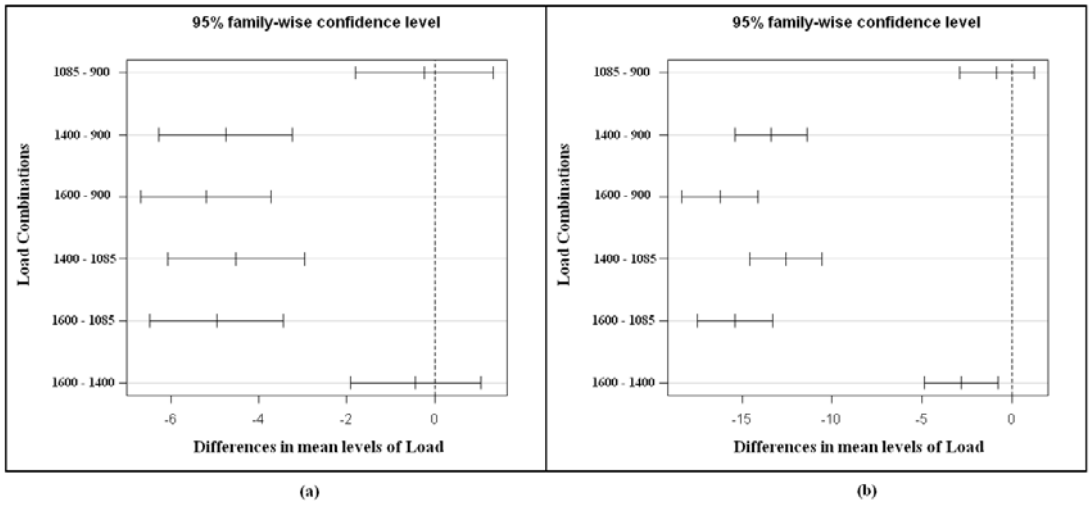

Figure 23 Confidence intervals for all differences in means of all pair of load combination on: (a) pavement C and (b) pavement D

$$SN = SN_o + \frac{SN_r - SN_o}{1 + \exp\left[-\frac{W - w_i}{b}\right]} \tag{18}$$

where $\boldsymbol{SN}_o$ is the ***SN*** at relatively low loads, $\boldsymbol{SN}_r$ is the residual ***SN*** at relatively high loads, ***W*** is the normal load, ***b*** is the width of the inverse S shape curve along the w axis, and $\boldsymbol{w_i}$ is the inflection point of the curve, as shown in Figure 24. For a particular LWT, the parameters ***b*** and $\boldsymbol{w_i}$ can be determined using nonlinear regression or curve fitting techniques. It can be envisioned that Equation (18) would have a wider field applicability to include any vehicle compared to an equivalent laboratory format developed by

Schallamach (1952) in Equation (15). Figure 25 shows the results of fitting Equation (18) for pavements C and D.

An interesting observation from Figure 25 is that the values of the parameters w_i and b do not seem to depend on either the operational speed or the pavements, suggesting that they could be inherent parameters of the measuring device (LWT). Equation (18) will be used in Section 3.7 to simulate the friction measurements under different dynamic conditions. The parameters of Equations (18) that are listed in Table 15 represent the two pavements C and D.

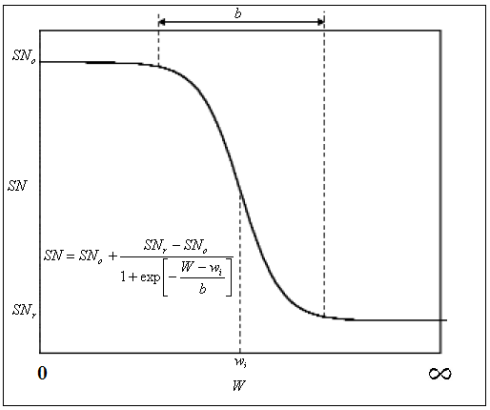

Figure 24 Nonlinear model representing the effect of Normal Load on Skid Numbers

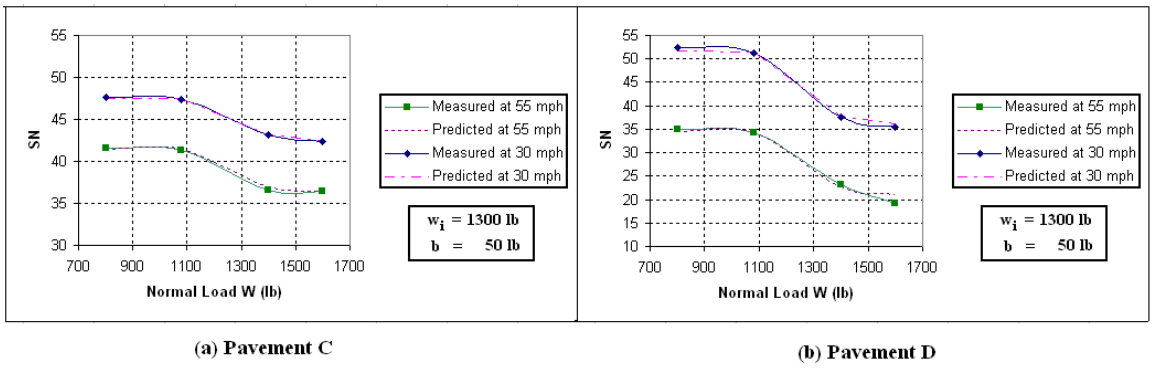

Figure 25 Measured vs. Predicted Load-*SN* relationship at different speeds

Table 15 Parameters characterizing the friction-load dependency of pavements C and D

Surface	Speed (mph)	*b* (lb)	*wi* (lb)	SN_o	SN_r
C	30	50	1300	47.5	41.5
C	55	50	1300	42.5	36.4
D	30	50	1300	51.7	34.5
D	55	50	1300	35	21

3.6.3 Explanation of the Abnormal *SN* vs. Load Behavior

Skid resistance is commonly explained theoretically by the molecular attraction theory (Moore, 1975) that states that the friction generated at the tire pavement interface is composed of two main components; adhesion and hysteresis (Equation (3) on Section 1.3).

From Section 1.3 it can be seen that both f_a and f_h depend on the viscoelastic properties of rubber. Also one can see from Equation (4) that the adhesion component decreases as the normal pressure increases. On the other hand, Figure 2 illustrates how the two components contribute to the overall coefficient of friction as the speed changes. Li et. al., 2003, showed that the adhesion component dominates the frictional coefficient at general operational speeds (20 – 60 mph).

Hence, one could use the above facts to formulate the following explanation for the *SN* vs. Load behavior presented in Figures 24 and 25. Although Equations (4) and (5) show opposing trends of "*f*" as the normal load changes, based on Figure (2) one could expect the adhesion component to dominate the overall *f* within normal operational speeds (Li et. al., 2003). Therefore *f* would decrease with the normal pressure (*p*).

3.7 Modeling the Dynamic Effects of Pavement Roughness

3.7.1 Model Development and Validation

To simulate the dynamic response of the LWT trailer, and specifically assess the variation of the normal load at the tire pavement interface due to road roughness, a rigid-body vibration dynamic model with two-degrees of freedom was formulated for one half of the LWT (Figure 26). For this purpose, six model parameters: two masses M_w and M_t, the two spring stiffnesses K_w and K_t, and the two damping coefficients C_w, and C_t are defined. As seen in Figure 26, M_w (unsprung mass) is the combined mass of one half of the vehicle axle, and the single trailer tire, while M_t (sprung mass) is half the total mass of the trailer without M_w. K_t is the stiffness coefficient of the suspension of the trailer as provided by the manufacturer and verified later from laboratory testing, and K_w is the stiffness coefficient of the tire established from tire testing in the laboratory. C_t is the damping coefficient of the trailer (the shock absorber), and C_w is the damping coefficient of the tire. It must be noted that the above model does not include the additional normal force resulting from the back torque produced on the testing wheel due to the frictional force. The two damping coefficients were determined using experimental modal analysis followed by back-calculation from measured response of the LWT when subjected to a defined profile input. The experimental measurements will be described in the validation procedure. Table 16 defines the values of the above parameters.

The proposed model (Figure 26) constrains the motion in the vertical direction and the vertical displacements are defined using the variables $q_t(t)$ and $q_w(t)$, measured from a pre-determined baseline. The displacement input to the system is provided by the road profile. Equation (19) can be used to transform the spatially defined profile, $y = f(x)$, to a time dependent vertical displacement input $y(t)$.

$$t = \frac{x}{S} \tag{19}$$

where x is the longitudinal distance along a given pavement profile, and S is the operational speed of the LWT. By providing the facility of converting the variations in the pavement to a forced displacement on a time scale, Equation (19) enables one to investigate the interaction between speed and roughness (Gillespie, 1993).

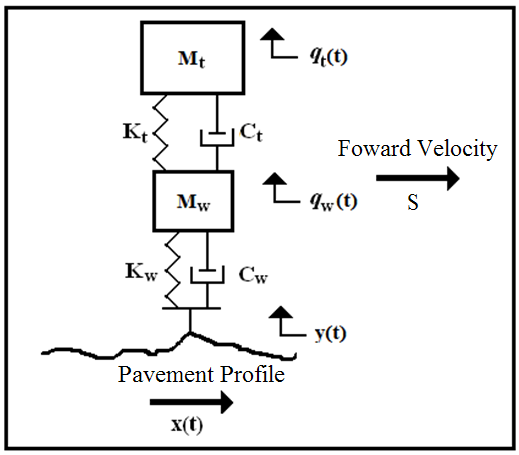

Figure 26 LWT half trailer vibration model

Table 16 Dynamic model parameters

Parameter	Description	Magnitude	Units
M_t	Sprung mass	440	Kg
M_w	Unsprung mass	60	Kg
C_t	Suspension damping	3.5	kNs/m
C_w	Tire damping	0.5	kNs/m
K_t	Suspension stiffness	70	kN/m
K_w	Tire stiffness	265	kN/m

The equations of motion can be written in state space variable form (Cauchy form) as

$$\dot{\underline{z}} = A\underline{z} + \underline{b}y + \underline{c}\dot{y} \tag{20}$$

where $\dot{y}$ is the first derivative of the profile with respect to time and $\underline{z}$ is the array of state variables (Equation (21)) that defines the motion of the system. A, $\underline{b}$ and $\underline{c}$ arrays are defined as follows using the model parameters:

$$\underline{z} = \begin{bmatrix} q_t & \dot{q}_t & q_w & \dot{q}_w \end{bmatrix}^T \tag{21}$$

$$A = \begin{bmatrix} 0 & 1 & 0 & 0 \\ -\frac{K_t}{M_t} & -\frac{C_t}{M_t} & \frac{K_t}{M_t} & \frac{C_t}{M_t} \\ 0 & 0 & 0 & 1 \\ \frac{K_t}{M_w} & \frac{C_t}{M_w} & -\frac{(K_t + K_w)}{M_w} & -\frac{(C_t + C_w)}{M_w} \end{bmatrix} \tag{22}$$

$$\underline{b} = \begin{bmatrix} 0 & 0 & 0 & \frac{K_w}{M_w} \end{bmatrix}^T \tag{23}$$

$$\underline{c} = \begin{bmatrix} 0 & 0 & 0 & \frac{C_w}{M_w} \end{bmatrix}^T \tag{24}$$

Runge-Kutta method is used to solve Equation (20) for any given input profile expressed in the time domain as *y(t)*.

In order to validate the above model and evaluate its damping parameters, the LWT was instrumented with two accelerometers attached at two specific locations of the LWT (as shown in Figure 27) to measure the corresponding accelerations (motion) of the trailer frame (M_t) and the axle (M_w). Then, a simple test was designed in which LWT was moved rapidly over a pavement bump (Figure 28) at a speed of 4.2 mph inducing a sudden excitation on it. During this test, the acceleration records of the trailer frame and the axle that approximate the motion of the two lumped masses of the model (Figure 26) were recorded. Profile measurements of the separate pavement bump needed for the prediction model in Equation (20) was measured using a rod and level.

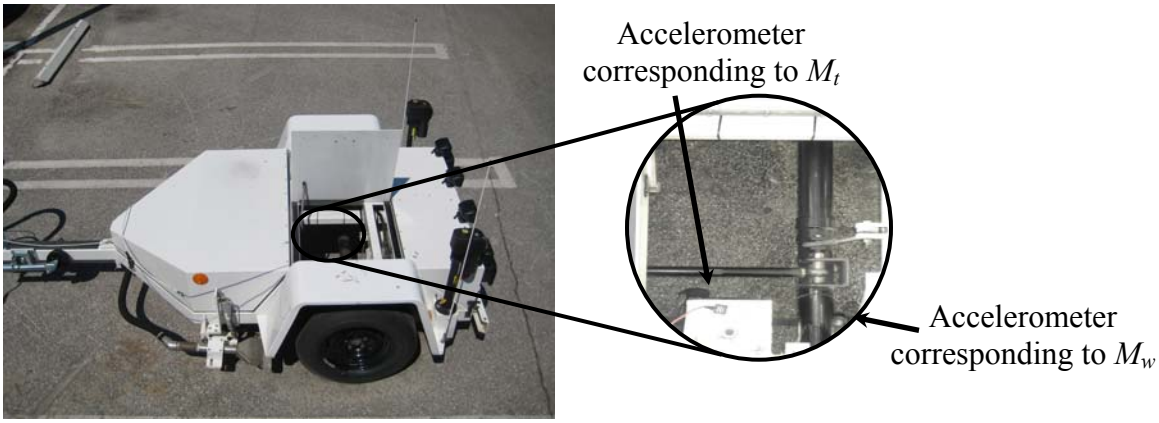

Figure 27 Instrumentation on the LWT

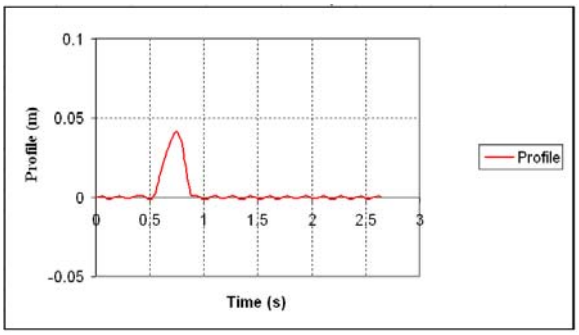

Figure 28 Input profile for the validation of the system (pavement bump)

Figure 29 presents the frequency spectrum of the acceleration corresponding to M_t. The spectrum reveals the two natural frequencies of the system, which represent the principal modes of motion (degrees of freedom) of the LWT. These can be calculated by solving the eigenvalue problem of Equation (20). The computed natural frequencies of the system are 1.8 Hz and 11.9 Hz, which shows excellent agreement between the predicted and measured natural frequencies. Figure 30 displays a comparison between the actually measured and the model predicted vertical velocities of the two masses or the corresponding components of the system when the LWT traveled over the bump described on Figure 28 at 4.2 mph. The vertical velocity was obtained by integrating the measured acceleration with time. One can observe in Figure 29 that the theoretical model captures both the high and the low frequency modes of the response.

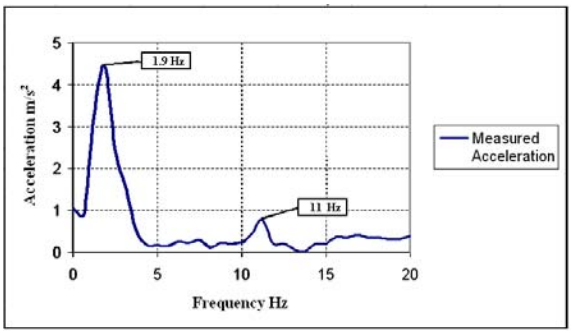

Figure 29 Frequency spectrum of the accelerometer readings corresponding to M_t

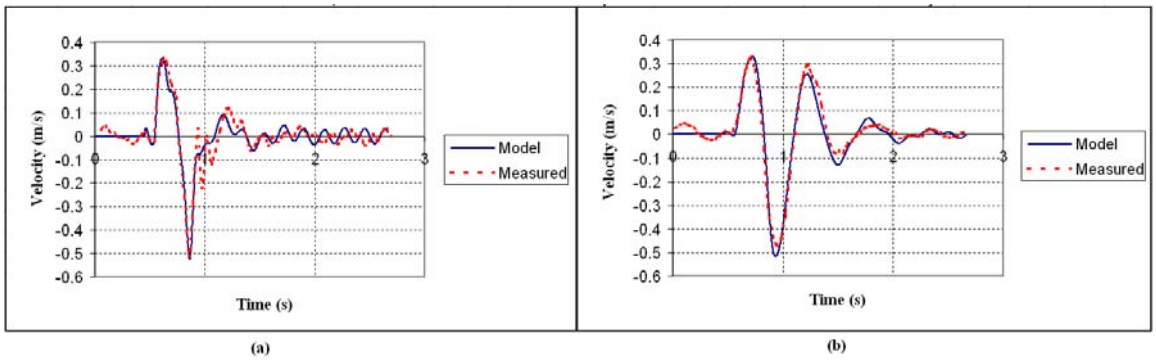

Figure 30 Measured and predicted velocities of: (a) M_w and (b) M_t

3.7.2 Simulation of Friction Measurements

Using the solution of the above validated model (Equations (20)-(24)) and Equation (25), one can determine the dynamic normal load induced at the tire pavement interface due to roughness as

$$W = W_{static} - K_w(q_w - y) - C_w(\dot{q}_w - \dot{y}) \tag{25}$$

where W and W_{static} are the dynamic load during operation and the load caused by only the masses at static equilibrium at the tire pavement interface.

With the statistically established SN vs. W relationship for LWT (Equation (18)) and the model for predicting the dynamic variations of the normal load W along a given profile (Equation (25)) one can simulate the effect of profile roughness on pavement skid resistance. In this process, for a given input pavement profile, one can predict W at any

time using Equation (25) and use Equation (18) to obtain the instantaneously effective *SN*. The average *SN* can then be calculated for a sufficiently long profile length. Figure 31 shows average *SN* values obtained from the above procedure for the simulated pavements profiles using the friction characteristics of pavements C and D at two specific speeds, plotted with respect to the corresponding *IRI*. The *IRI* values for the simulated profiles were calculated in accordance with the algorithm provided by the ASTM standards.

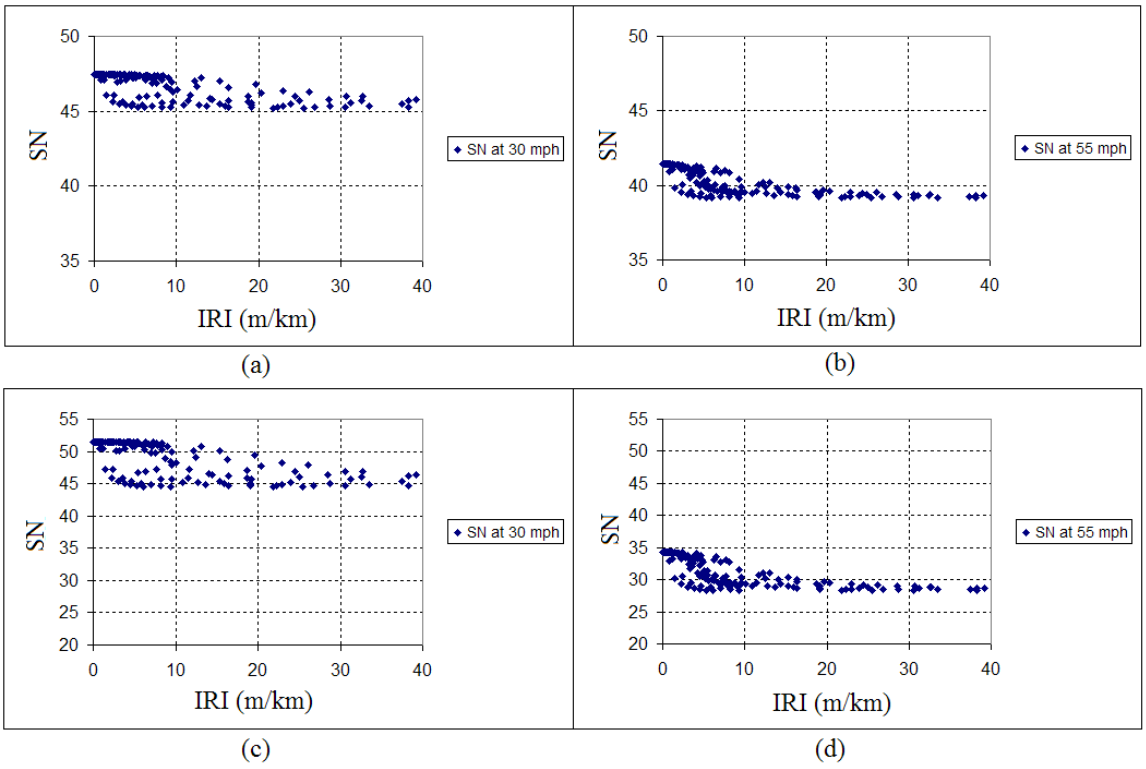

Figure 31 *SN* vs. *IRI* on the simulated profile of (a) pavement C at 30 mph, (b) pavement C at 55 mph, (c) pavement D at 30 mph, and (d) pavement D at 55mph

Figure 31 shows a highly scatter plot between *SN* and *IRI*. It can be seen that at relatively low values of *IRI* (0 to 10 m/km), which are usually encountered in real pavement profiles, there is no apparent correlation between *SN* and *IRI*. However, at high *IRI* values, as expected, *SN* shows a decreasing trend with increasing *IRI*. The ill-definition of the *SN* vs. *IRI* relationship, seen particularly at usually encountered *IRI* values, can be attributed to the dependency of the *IRI* parameter on the natural frequencies of the Quarter-car model used in the *IRI* computation. *IRI* is a standard parameter that is used to

evaluate the roughness condition of a pavement profile calculated from a dynamic model that simulates the motion of a Quarter-car (ASTM E 1926-08, 2009). In order to verify this explanation, profiles were simulated over a large range of wavenumbers and amplitudes. Figure 32 shows the *IRI* obtained from the simulated profiles plotted against the corresponding amplitude and the frequency. The frequency in Figure 32 was obtained using the operational speed of 80 km/h, as stipulated in the ASTM E1926 for *IRI* computations.

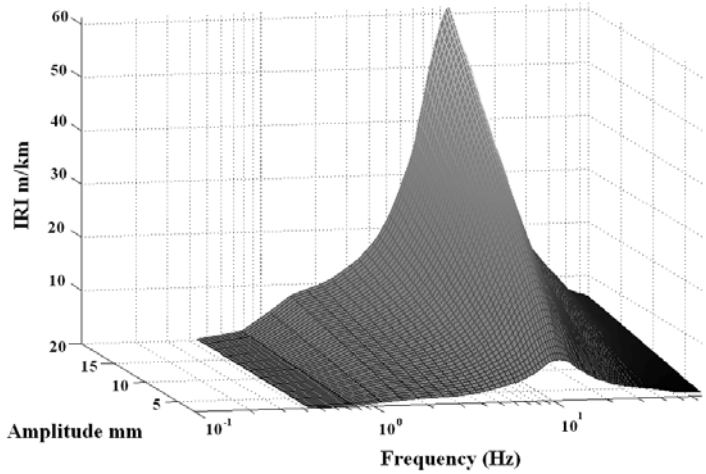

Figure 32 3D representation of *IRI* with respect to frequency and amplitude

In Figure 32 one can observe that at two specific frequencies the *IRI* gets magnified. These frequencies correspond to the natural frequencies of the Quarter-car model used to compute the *IRI*. Therefore, it is seen that *IRI* is quite sensitive to the dynamic characteristics of the Quarter-car model and exhibits a non-monotonic relationship with respect to roughness, with many conditions of roughness producing the same *IRI*. Therefore one can conclude that although *IRI* is used as a standard to evaluate the roughness of pavements it is not an appropriate parameter for expressing the *SN* vs. roughness relationship. The non-monotonic nature of the *IRI* vs. roughness relationship (Figure 32) clearly explains why multiple values of *SN* correspond to a given *IRI* in Figure 31. Furthermore, even if one expresses the variation in the *SN* values measured by LWT with respect to more appropriate roughness parameters of the pavement profile, e.g. wavelength and amplitude, one could expect a non-monotonic relationship because the natural frequencies of the LWT itself can produce a resonance effect. To illustrate this,

the vibration model (Equation (18) and (19)-(25)) was used to predict the *SN* values that would be measured by the LWT on simulated pavement profiles with *SN* vs. *W* characteristics similar to that of pavement D, as seen in Table 16. The simulated profiles were obtained by using simple sine waves of constant amplitude of 20 mm and a wide range of wavelengths. Figure 33 shows the predicted variation of *SN* throughout the frequency spectrum corresponding to the range of input wavelength and the sharp recess in *SN* corresponding to the predominant LWT frequency of 1.8 Hz.

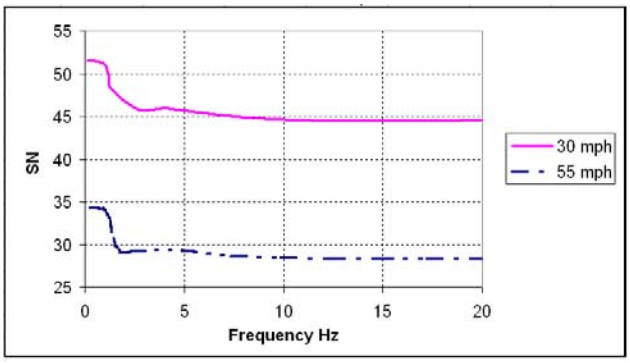

Figure 33 *SN* vs. Frequency of simulated pavement D with amplitude of 20 mm

This study shows that the Dynamic Load Coefficient (*DLC*) is appropriate for representing the effect of roughness on *SN*. *DLC* is used typically to assess the dynamic variation of the normal load at the tire pavement interface of a given vehicle for a specific combination of pavement roughness and vehicle speed (Gillespie, 1993). It is defined as

$$DLC = \frac{\sigma_W}{W_{Static}} \tag{26}$$

where σ_W is the standard deviation of the normal load (W) variation, obtained from Equation (25) in response to a given pavement profile.

Since the variation of *SN* with roughness is triggered by the dynamic variation of the normal load, *SN* vs. *DLC* provides a single-value relationship for a given pavement and speed. Consequently Figure 34 shows *SN* vs. *DLC* plots to be of monotonic inverse S shapes as seen before in Figures 24 and 25. Figure 34 was constructed as follows: The

DLC for a given pavement with a known profile (y) can be determined from Equations (20)-(26). Also, using Equation (18) and the corresponding parameters found in Table 15, one can estimate *SN* values measured by the LWT on that pavement. Hence, this study suggests the use of the well-defined curves in Figure 34 to define the effect of roughness and speed on the measured *SN*.

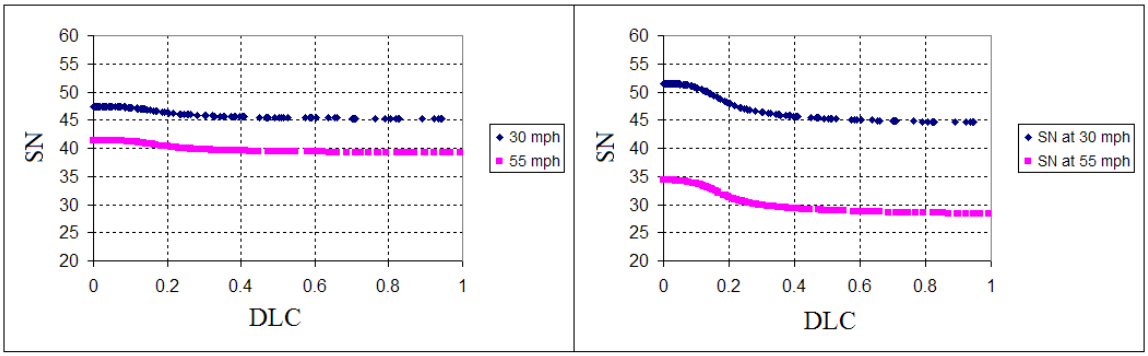

Figure 34 *SN* vs. *DLC* on (a) pavement C and (b) pavement D

CHAPTER 4

EVALUATION OF THE SPEED CONSTANT (S_p) AND ITS EFFECT ON THE CALIBRATION OF FRICTION MEASURING DEVICES

4.1 Standardization of Friction Measurements

Accidents due to skidding on pavements are a major concern of the aviation and highway industries. These accidents are generally attributed to skid resistance deficiencies on those pavement surfaces. Skid resistance force is developed when a vehicle tire that is fully or partially prevented from rolling slides along a pavement surface under lubricated conditions. Skid resistance has been associated with pavement texture, starting with Henry et al., 1978, who used different pavement texture characteristics for the prediction of skid resistance variation with slip speed. In the above work, pavement microtexture, which depends on the surface of aggregate asperities with its magnitude ranging from 1 to 500 μm (0.5 mm), is associated with the skid resistance at low vehicle slip speeds. Furthermore, pavement macrotexture, which depends on the arrangement and orientation of aggregate particles on the pavement surface with its magnitude ranging from 0.5 mm to 50 mm, is used to evaluate the skid resistance-speed relationship by correlating it to the rate at which surface wetting water can escape from the tire footprint during skid resistance measurements.

Penn State Model (NCHRP, 2000) employs the Henry et. al., 1978, concept and introduces a variable called the percent normalized gradient (*PNG*) to express the skid resistance-speed dependency as;

$$SN(S) = SN_0 * e^{-\left(\frac{PNG}{100}S\right)} \quad (27)$$

where *SN* is the Skid Number measured at slip speed *S*, and SN_0 is the Skid Number at zero slip speed. SN_0 has been shown to be correlated to pavement microtexture. *PNG* is the percent normalized gradient which describes the rate of decrease of skid resistance with the slip speed. Henry et. al., 1978, have shown that *PNG* is more or less constant on a given surface, and that it is correlated to the pavement macrotexture. SN_o and *PNG* can be evaluated by performing a simple linear regression of frictional measurements on a given surface at different slip speeds. It must be noted that Locked Wheel Testers (LWT) had been used primarily to gather the frictional data that lead to these original formulations.

Since then, several equipment capable of evaluating frictional characteristics of pavement surfaces have been developed around the world. It has been observed frequently that different devices would produce different friction measurements when used on the same pavement surface. Hence, a problem arises when frictional measurements obtained from different devices are compared by personnel from different agencies in runway operational and management decision making. During the Permanent International Association of Road Congress (PIARC) international experiment held in Europe in 1992 a series of experiments were conducted with one of its objectives being the development of a model that would address the differences in frictional measurements among various friction measuring devices.

The International Friction Index (IFI) (Section 1.7) was developed consequent to the PIARC international experiment, and it is used as the standard to evaluate frictional characteristics of pavement surfaces. IFI is used to harmonize measurements obtained from different frictional measuring devices to a common calibrated friction index. The IFI concept is based on the assumption that the friction value of a given surface depends on the slip speed at which the measurements are taken, texture properties of the pavement surface (both micro and macrotexture) and characteristics of the device used to obtain the measurements.

The PIARC model (Wambold et. al., 1995) introduces the Speed Constant (S_p) to replace the *PNG*/100 parameter of Equation (27) as follows:

$$FRS = FR_0 * e^{-\left(\frac{S}{S_p}\right)} \tag{28}$$

where FR_0 is the friction at zero slip speed. By rearranging Equation (28) one can obtain Equation (29), to express *FR60* in terms of *FRS* and *S*,

$$FR(60) = FRS * e^{\left(\frac{S-60}{S_p}\right)} \tag{29}$$

where *FRS* is the friction measurement obtained from a specific device at slip speed *S* and *FR(60)* is the predicted value of friction corresponding to a slip speed of 60 km/h. S_p has been considered as a constant with units of speed that characterizes the drainage properties of a given surface which is correlated to the pavement macrotexture.

On the other hand, the IFI of a given pavement consists of two parameters: (1) Friction Number (*F60*) and (2) Speed Constant (S_p). It is typically reported as IFI (*F60,* S_p) and defined by Equations (11) and (12).

4.1.1 Investigation of the Validity of the IFI Concept

Different researchers have reviewed the standardization or harmonization procedure defined by the International Friction Index (IFI) concept. Flintsch et. al., 2009, conducted an investigation using the data collected from the devices used by the consortium members in the 2008 Virginia Smart Road Rodeo on different pavement surfaces. The results obtained from this investigation did not produce harmonious results among the devices used when the original PIARC calibration parameters were used. Flintsch et. al., 2009, were able to improve the agreement between *F60* values obtained from their devices by performing a renewed correlation and modifying the *A*, *B* and *C* coefficients originally proposed in the PIARC experiment. In addition, Flintsch et. al., 2009, proposed that the discrepancies

seen in the IFI values calculated from different devices used in their investigation could be solved by reevaluating the original coefficients (*A, B,* and *C*) that were determined in the PIARC international experiment and used in IFI computations. Furthermore Flintsch et. al., 2009, also proposed the implementation of equations specific to each friction measuring devices to calculate the S_p , but claimed to have obtained relatively weak correlations (coefficients of determination) associating S_p to pavement macrotexture for all the devices used. However Flintsch et. al., 2009, obtained improved correlations between S_p and *MPD* using power models, with the highest coefficient of determination (R^2) being 0.56.

National Cooperative Highway Research Program (NCHRP), 2009, summarizes the guidelines for management of pavement friction on existing pavement surfaces and the development of the IFI model. Although Section 4 of NCHRP, 2009, reaffirms the ASTM E 1960 stipulation that the S_p depends on pavement texture parameters and the texture measuring device *only*, in its Appendix E it is clearly stated that on the same surface, different *friction measuring devices* would produce a different set of parameters, *F60* and S_p. This reinforces the hypothesis that different friction measuring devices would produce different friction-speed dependencies on the same pavement surface as defined by their characteristic S_p parameters.

Transport Canada Publication No TP 14289E, 2003, presents a comprehensive method for modelling the braking performance of aircraft tires on wet pavements. This model acknowledges the importance of the coefficient of friction as a system property by incorporating additional parameters such as the vertical load, tire parameters and the waterfilm thickness to predict the friction-speed relationship.

4.1.2 Assumptions Governing the IFI Concept

Based on ASTM E 1960 the Speed Constant (S_p) in Equation (12) depends on the macrotexture characteristics of the pavement surface and the method used to determine the macrotexture. In other words, the current International Friction Index (IFI) concept

implies that the friction-speed relationship that is established based on friction measurements on a given pavement surface at different slip speeds is a characteristic of that pavement only. It must be noted that S_p defines the gradient of the semi log (friction) vs. speed relationship. Hence, for a given pavement surface any friction measuring device should produce a friction-speed gradient defined by Equation (12). If Equation (12) truly represents the *FRS* vs. *S* gradient for any device on a given pavement surface, then, as illustrated in Figure 35, *FR60* predicted from Equations (12) and (29) would be invariant of the slip speed used for its calculation.

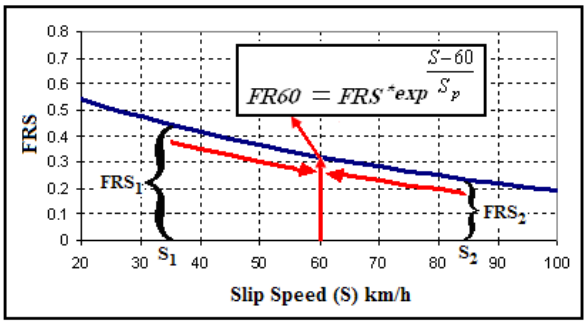

Figure 35 Relation among *FRS*, *S*, *FR60* and S_p

The coefficient of friction (μ) is a system modeling property used to express the proportionality between the normal force (F_N) and the shear (frictional) force (F_S) on two parallel surfaces that are in contact. μ is known to be dependent on both surfaces that are in contact as well as several other external factors (Booser, 1989). The predominant factors that affect the interaction include the normal load, contact pressure, slip speed, and the thickness of the waterfilm when friction is evaluated under wet conditions. These factors are generally different from one friction measuring device to another and therefore, one can expect the assumption of the friction-speed gradient that solely depends on the pavement surface texture to have a limitation when the measuring device changes.

4.2 Objectives of the Current Investigation

The objective of this phase of the investigation is to evaluate the principles underlying the IFI concept, especially the definition of the S_p parameter. The author also needed to understand the role played by S_p in producing different *FR60* values when *FR60* is evaluated from friction measurements obtained at different slip speeds on the same pavement surface, contrary to the IFI implication that it would be independent of the slip speed used for its calculation. Finally the author expects to illustrate how the existing S_p evaluation procedure can be modified to produce more consistent IFI calibration parameters (*A* and *B*). The data used for the investigation would be obtained from the data acquired during the Wallops Runway Friction workshops conducted in May 2007 and May 2008.

4.3 Data Collection

Over more than a decade runway pavement frictional data have been collected on an annual basis at the friction workshops held at the Wallops Flight Facility in Virginia, with the purpose of improving the understanding of the concept of skid resistance. An additional aim of the above workshop has been to produce an extensive friction database for harmonization of the friction measurements from the different devices used worldwide. At this workshop, frictional and texture measurements have been obtained over 14 different surfaces available at Wallops using a variety of friction and texture measuring devices. These surfaces have been constructed covering a large range of microtexture and macrotexture for the purpose of investigating the intricate behavior tire pavement frictional interaction.

Wallops Runway Friction Workshop conducted in May 2007 included 12 full scale friction measuring devices, namely, 2 E274, SFT, 3 GT, SARSYS, 2 BV11, RFT, Mu METER, and NAC DFT. The plan was for every vehicle to take a total of 10 measurements at two different operational speeds (65 and 95 km/h) on the above

surfaces. Some of the devices were unable to accomplish this task and hence appropriate adjustments have been made in the analysis.

In addition, the Wallops Runway Friction Workshop conducted in May 2008 included 15 full scale friction measuring devices, namely, 3 E274, SFT, 2 GT, SARSYS, 2 BV11, 3 RFT, Mu METER, TWO, and NAC DFT, which were used to evaluate the same surfaces at 4 different vehicle speeds (50, 65, 80 and 95 km/h). At both the above workshops the Circular Track Meter (CT Meter) was used to evaluate the texture characteristics of the tested pavement surfaces and provide the means to compute the S_p of every surface using Equation (12).

4.4 Analysis of Data

4.4.1 Effect of the Slip Speed on *FR60*

A preliminary study was performed using the 2007 NASA Wallops data to investigate the effect of the slip speed on *FR60*. At this stage four devices were selected to perform the analysis; Illinois E274, TC SFT85, FAA RFT and the DND GT. The S_p was calculated on different surfaces (Table 17) according to ASTM standards using the CT Meter and Equation (12), with the recommended *a* and *b* parameters of 14.2 and 89.7 respectively. Then the friction measurements taken at the two different measuring speeds (65 and 95 mph) were converted to *FR60* using Equation (29) based on the assumption that the friction-speed variation would be defined accurately by the S_p parameter. Appropriate slip speeds were used for the *FR60* calculations for the devices that operate at slip ratios different from 100%.

It was mentioned in Section 4.1.2 that based on the fundamental concepts that were used in formulating the IFI that one would expect the same value of *FR60* to be calculated from different slip speeds, when using the S_p parameter obtained from the CT Meter and the *a* and *b* values recommended by the ASTM E 1960 procedure. In this regard Figure 36 presents some descriptive statistics of interest on the average *FR60* values calculated

for the four devices on pavement surface E at the two measuring speeds (65 and 95 km/h) employed in the Wallops workshop in 2007.

Table 17 Texture characteristics of tested pavement surfaces on 2007

SITE	*MPD*	S_p (km/h)
A	0.433	53.01
B	1.764	172.42
C	2.232	214.44
D	0.512	60.16
E	0.415	51.46
F	1.333	133.77
G	1.929	187.20
ECHO 1	0.690	76.06
ECHO 2	0.706	77.50
EK 1	0.176	30.02
EK 2	0.446	54.18
EK 3	0.653	72.74
EK 4	0.340	44.67
R 4	0.956	99.95

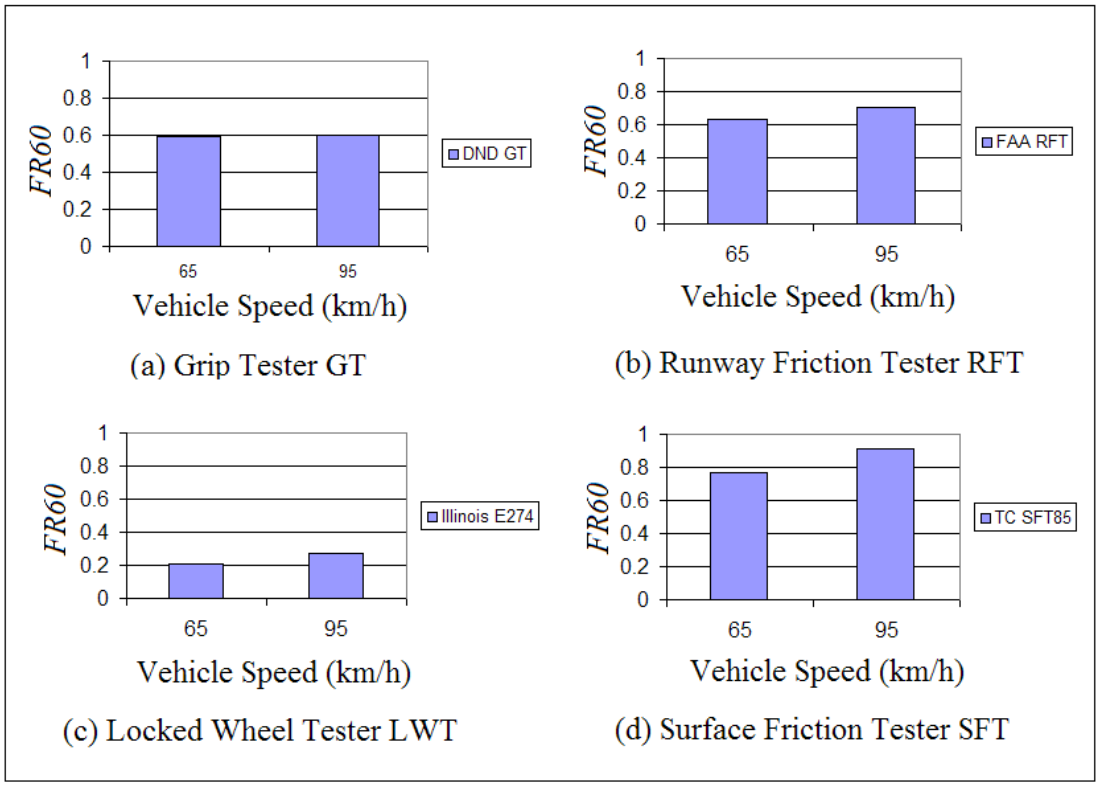

Figure 36 *FR60* values obtained from different devices on the same pavement surface E

One can observe from Figure 36 that the values of *FR60* do not show a constant trend. In order to prove statistically that the *FR60* magnitudes obtained from different slip speeds are not equal, a hypothesis test was performed. A pooled t-test was used to compare the mean of the *FR60* values obtained from different slip speeds and a t-distribution was used for statistical inference. The standard deviations of the populations were unknown and hence they were assumed to be different. The test statistic of the t-distribution, T_d, for d degrees of freedom can be expressed as

$$T_d = \frac{FR60_{S1} - FR60_{S2}}{\sqrt{\frac{\sigma_{S1}^2}{n1} + \frac{\sigma_{S2}^2}{n2}}} \tag{30}$$

where $FR60_{S1}$ and $FR60_{S2}$ are the average values of the *FR60s* obtained from testing at slip speeds *S1* and *S2* respectively. $\sigma_{S1}^2, \sigma_{S2}^2$, and *n1*, *n2* are the corresponding sample standard deviations and the sample sizes respectively. d can be expressed by;

$$d = \frac{\left[\left(\frac{\sigma_{S1}^2}{n1}\right) + \left(\frac{\sigma_{S2}^2}{n2}\right)\right]^2}{\frac{\left(\frac{\sigma_{S1}^2}{n1}\right)^2}{n1-1} + \frac{\left(\frac{\sigma_{S2}^2}{n2}\right)^2}{n2-1}} \tag{31}$$

Tables 18-21 present the statistical summary of this study of *FR60* values from the 2007 NASA Wallops database. A p-value lower than 0.05 would indicate that the null hypothesis ($FR60_{S1} = FR60_{S2}$) should be rejected at 95% confidence level. Since one can observe that the vast majority of such p-values are less than 0.05 in Tables 18-21, it can be concluded that the null hypothesis defined as the *FR60* values computed from different slip speeds are similar can be rejected at a 95% confidence level.

Table 18 Comparison of *FR60* means obtained from different slip speeds using the FAA RFT07

Section	$FR60_{S1}$	$FR60_{S2}$	*n1*	*n2*	σ_{S1}	σ_{S2}	*d*	*Td*	p-value
A	0.529	0.665	10	10	0.019	0.058	11	6.995	0.00001
B	0.842	0.913	10	10	0.029	0.026	18	5.683	0.00001
C	0.808	0.834	10	10	0.037	0.026	17	1.799	0.04489
D	0.504	0.570	10	10	0.026	0.033	18	4.970	0.00005
E	0.634	0.700	10	10	0.041	0.082	14	2.304	0.01854
F	0.827	0.790	10	10	0.019	0.042	13	2.556	0.01196
G	0.945	0.900	10	10	0.023	0.034	16	3.446	0.00166
Echo 1	0.626	0.659	10	10	0.046	0.051	18	1.517	0.07335
EK 1	0.256	0.285	10	10	0.072	0.086	18	0.823	0.21067
EK 2	0.677	0.852	10	10	0.039	0.062	16	7.520	0.00000
R 4	0.471	0.494	10	10	0.044	0.026	15	1.404	0.09038
Echo 2	0.646	0.692	10	10	0.035	0.054	16	2.247	0.01956
EK 3	0.555	0.557	10	10	0.050	0.070	17	0.100	0.46088
EK 4	0.510	0.537	10	10	0.054	0.048	18	1.188	0.12513

Table 19 Comparison of *FR60* means obtained from different slip speeds using the DND GT07

Section	$FR60_{S1}$	$FR60_{S2}$	*n1*	*n2*	σ_{S1}	σ_{S2}	*d*	*Td*	p-value
A	0.600	0.733	10	10	0.035	0.194	10	2.149	0.02859
B	0.704	0.769	10	10	0.018	0.086	10	2.326	0.02115
C	0.685	0.736	10	10	0.019	0.051	12	2.913	0.00651
D	0.615	0.724	10	10	0.029	0.191	10	1.772	0.05343
E	0.594	0.598	10	10	0.026	0.325	10	0.034	0.48670
F	0.706	0.690	10	10	0.025	0.175	10	0.296	0.38652
G	NA	NA	NA	NA	NA	NA	NA	NA	NA
Echo 1	0.603	0.566	10	10	0.032	0.048	16	2.043	0.02893
EK 1	0.271	0.364	10	10	0.030	0.035	18	6.355	0.00000
EK 2	0.667	0.723	10	10	0.035	0.061	15	2.536	0.01142
R 4	NA	NA	NA	NA	NA	NA	NA	NA	NA
Echo 2	NA	NA	NA	NA	NA	NA	NA	NA	NA
EK 3	NA	NA	NA	NA	NA	NA	NA	NA	NA
EK 4	NA	NA	NA	NA	NA	NA	NA	NA	NA

Table 20 Comparison of *FR60* means obtained from different slip speeds using the Illinois E274-07

Section	$FR60_{S1}$	$FR60_{S2}$	*n1*	*n2*	σ_{S1}	σ_{S2}	*d*	*Td*	p-value
A	0.210	0.303	8	7	0.030	0.055	10	3.965	0.00133
B	0.521	0.519	10	10	0.022	0.014	16	0.198	0.42274
C	0.542	0.506	10	10	0.026	0.007	11	4.261	0.00067
D	0.251	0.363	10	10	0.033	0.028	18	8.166	0.00000
E	0.204	0.273	10	8	0.020	0.059	9	3.115	0.00621
F	0.469	0.454	10	8	0.076	0.030	13	0.597	0.28026
G	0.584	0.518	10	9	0.032	0.023	17	5.178	0.00004
Echo 1	0.325	0.337	10	7	0.011	0.043	7	0.701	0.25310
EK 1	0.075	0.082	10	5	0.008	0.018	5	0.886	0.20815
EK 2	0.247	0.252	10	10	0.018	0.016	18	0.616	0.27270
R 4	0.236	0.277	10	10	0.024	0.011	13	4.964	0.00013
Echo 2	NA	NA	NA	NA	NA	NA	NA	NA	NA
EK 3	0.233	0.337	10	10	0.046	0.027	15	6.122	0.00001
EK 4	0.150	0.103	10	10	0.042	0.009	10	3.489	0.00292

Table 21 Comparison of *FR60* means obtained from different slip speeds using the TC SFT85-07

Section	$FR60_{S1}$	$FR60_{S2}$	*n1*	*n2*	σ_{S1}	σ_{S2}	*d*	*Td*	p-value
A	0.702	0.912	10	10	0.015	0.034	13	17.824	0.00000
B	0.892	0.981	10	10	0.014	0.016	18	13.183	0.00000
C	0.862	0.912	10	10	0.028	0.021	17	4.455	0.00017
D	0.655	0.824	10	10	0.022	0.034	16	13.269	0.00000
E	0.771	0.916	10	10	0.042	0.073	15	5.404	0.00004
F	0.899	0.960	10	10	0.014	0.039	12	4.679	0.00027
G	0.981	1.031	10	10	0.007	0.024	11	6.425	0.00002
Echo 1	0.752	0.826	10	10	0.034	0.030	18	5.133	0.00003
EK 1	0.428	0.525	10	10	0.055	0.044	18	4.360	0.00019
EK 2	0.849	1.081	10	10	0.041	0.060	16	10.102	0.00000
R 4	0.650	0.660	10	10	0.019	0.027	17	0.981	0.17012
Echo 2	0.741	0.803	10	10	0.033	0.053	16	3.118	0.00331
EK 3	0.733	0.780	10	10	0.033	0.039	18	2.932	0.00446
EK 4	0.638	0.777	10	10	0.038	0.050	17	7.037	0.00000

The results presented in Tables 18-21 and the discussion in Section 4.1.2 lead to the conclusion that the S_p values computed for each surface based on Equation (12) and the ASTM E 1960 recommended parameters *a* and *b* do not represent the true friction-slip speed dependency of that surface with respect to all the friction measuring devices.

4.4.2 Speed Constant (S_p) and the Significance of the *a* and *b* Parameters

The conclusions drawn in Section 4.4.1 certainly illustrates the need for revision of Equation (29) especially with respect to the S_p proposed by ASTM E1960 which stipulates the S_p to be computed using Equation (12). To illustrate this need further, a correlation analysis was performed between the *MPD* values obtained on the tested pavement surfaces using the CT Meter at the 2008 NASA Wallops workshop, and the S_p parameters that were obtained by fitting the model expressed in Equation (32) (linearized form of Equation (28)) to the experimental friction data obtained by different friction measuring devices at different slip speed, on each tested pavement surface. The results from this analysis can be seen in Figure 37 and Table 22.

$$\ln(FRS) = \ln(FR_0) - \left(\frac{1}{S_p}\right) * S \tag{32}$$

From Figure 37 one can observe the weak correlation that exists between the *MPD* and the experimental S_p values obtained from all the friction measuring devices. Although one can observe an increasing trend of S_p with *MPD* in Figure 37, the coefficient of determination (R^2) which is an indicator of the proportion of the variability in the data set that is accounted for by the statistical model, is only 0.257. This indicates that most of the variability present in the data is not explained by the predictor included in the linear model which in this case is the *MPD*.

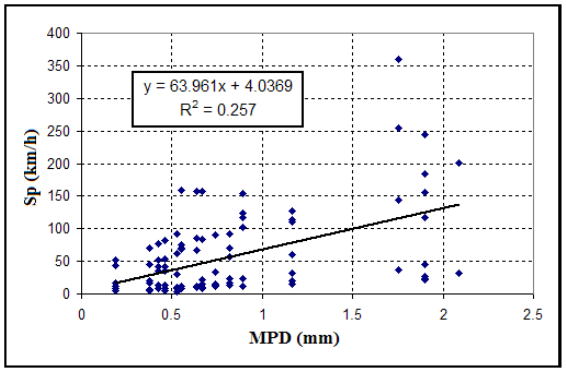

Figure 37 MPD vs. S_p obtained experimentally for all friction measuring devices using the 2008 NASA Wallops data

An additional summary of the statistical analysis performed on the *a* and *b* parameters of the linear model in Figure 37 is presented in Table 22. One can see that the 95% confidence intervals of the parameter *b* do not contain the value recommended in the ASTM standard. It is also noted that the *b* parameter is the one that represents the rate of change of the S_p parameter with the pavement macrotexture. The above results further reinforce the need realized in Section 4.4.1 to revise the current values (*a* =14.2 and *b* = 89.7) used in the ASTM for the computation of the S_p parameters in Equation (12).

Table 22 Statistical analysis of the *a* and *b* parameters of the model presented in Figure 37

Coefficient	Magnitude	Confidence Interval Lower 95% Value	Confidence Interval Upper 95% Value	ASTM Values
a	4.036	-16.797	24.871	14.2
b	63.961	41.927	85.995	89.7

4.4.3 Device Dependency of the *a* and *b* Parameters

From the scatter plot and the low R^2 seen in Figure 37 one could conclude that there is a weak correlation between *MPD* and S_p, when the data from all friction measuring devices is used for regression analysis indiscriminately. Consequently, 2008 NASA Wallops runway friction workshop data was used to further investigate the device dependency of *a* and *b* parameters. Table 23 presents the texture conditions of the different pavement surfaces that were included in the above workshop. The *MPD* values in Table 23 are measured using the CT Meter, and the S_p values were computed using Equation (12), using the ASTM recommended *a* and *b* values. When Tables 23 and 17 are compared one can observe that there have been no major changes in the texture conditions on the Wallops pavements surfaces between years 2007 and 2008.

Figure 38 presents the friction measurements of three representative friction measuring devices (FAA RFT, VTTI GT and USF 274) obtained during the 2008 Wallops workshop plotted against the corresponding slip speeds. It is noted that although the testing speeds were similar, the slip speeds varies from one device to another since each device operates at its characteristic slip ratio. The line labeled as the standard device in Figure 38

represents the friction-speed trend that a device should follow in accordance with Equations (28)-(29) and (12) using S_p values presented in Table 23. However from Figure 38 one can also observe that, on any given pavement surface, different friction measuring devices plot friction-speed relationships that deviate significantly from the standard plot defined by the ASTM. On the other hand, one can observe that the only vehicle that seems to follow the standard device is the USF LWT which operates at a slip ratio of 100%, while the other devices (FAA RFT and VTTI GT) that operate at slip ratios in the range of 10-20% present a seemingly steeper slope, with friction decreasing faster with slip speed. The reason for the observed deviation from the standard trend could be that the actual friction-speed behavior of a given friction measuring device is different than the general trend suggested by Equation (12), with the use of the ASTM recommended parameters a = 14.2, and b = 89.7. It is important to realize that these parameters (a and b) have been evaluated statistically, based on the results of all the devices used in the PIARC experiment (Wambold et. al., 1995). The data dependency of the S_p vs. *MPD* relationship was illustrated in Figure 37 in a minor scale, where different values (a and b) were obtained. Hence the standard values of a and b would not be very much applicable to any particular device.

Table 23 Texture characteristics of tested pavement surfaces on 2008

Surface	*MPD*	S_p (k/hr)
A	0.55	63.535
B	1.753333	171.474
C	2.09	201.673
D	0.64	71.608
E1	0.426667	52.472
E2	0.46	55.462
F	1.163333	118.551
G	1.896667	184.331
Echo1	0.82	87.754
EK1	0.19	31.243
EK2	0.526667	61.442
R4	0.893333	94.332
Echo2	0.74	80.578
EK3	0.67	74.299
EK4	0.373333	47.688

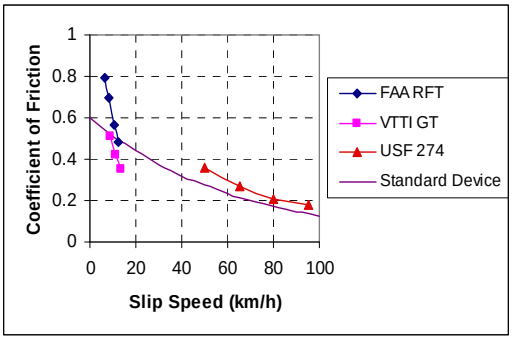

(a) Surface A

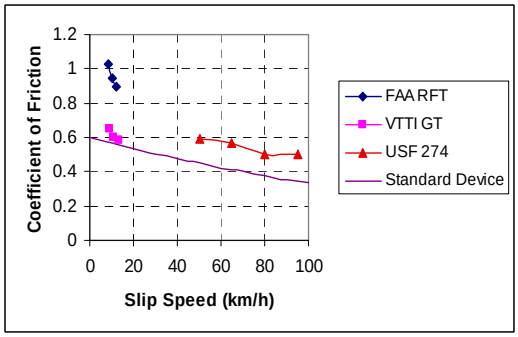

(b) Surface B

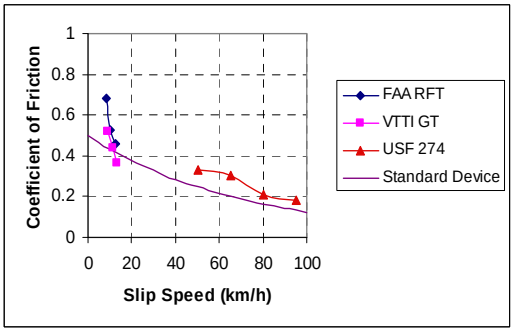

(c) Surface D

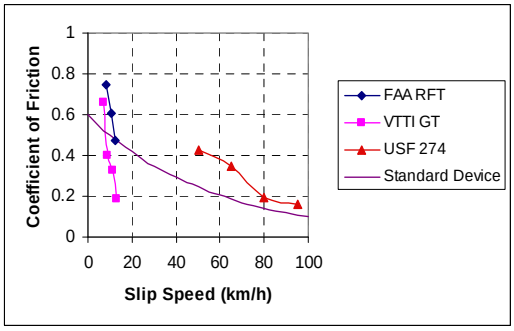

(d) Surface E2

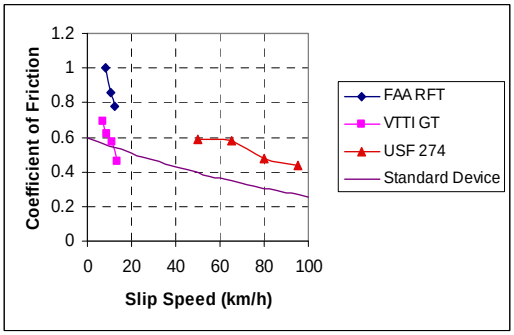

(e) Surface F

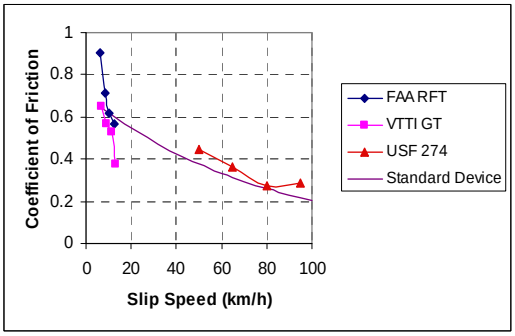

(d) Surface Echo2

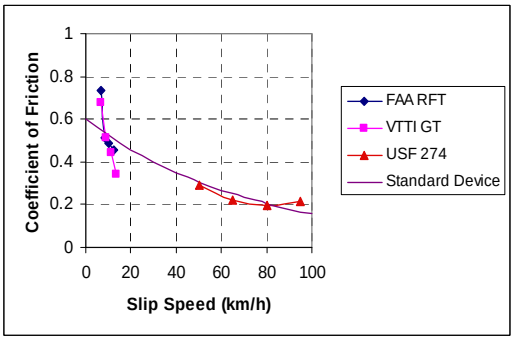

(f) Surface EK3

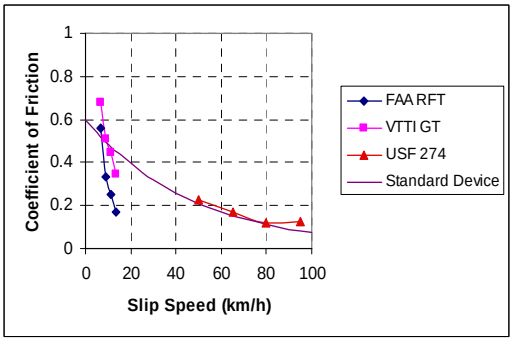

(g) Surface EK4

Figure 38 Measured coefficient of friction vs. slip speed relationships of friction measuring devices on test pavement surfaces

The trends seen in Figure 38 and the illustration in Figure 39 could be used to explain the anomaly found in Tables 18-21; where it was proven statistically that the *FR60* values for a given device would not be the same when computed from different slip speeds. As an example, if one were to extract FAA RFT data from Figure 38(d) and calculate the *FR60* from two different slip speeds using the S_p calculated from Equation (12) with the standard parameters associated with pavement macrotexture, one would obtain two completely different numbers (0.47 and 0.32) instead of the actual value of 0.18 as illustrated in Figure 39.

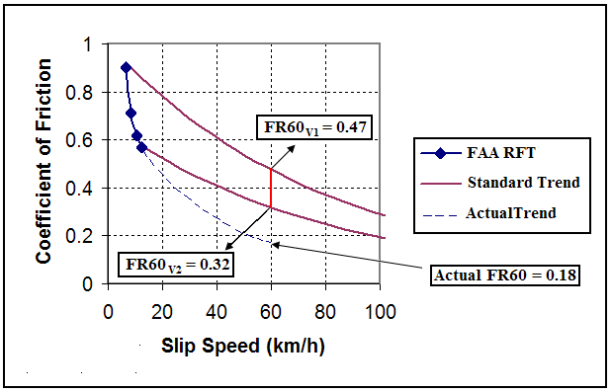

Figure 39 *FR60s* calculated from different slip speeds on surface Echo2 for the 2008 FAA RFT

Based on these findings, if one were to correlate the data presented in Figure 37 using carefully selected clusters of data specific to each device, *a* and *b* parameters that would be more representative of that device could be obtained. Then these revised parameters could be used in Equation (12) to capture the actual friction-speed dependency for that particular device. Figure 40 presents such individual correlations between S_p vs. *MPD* for different devices used in the 2008 NASA Wallops Runway Friction workshop. One can see from Table 24 that the coefficients of determination found when associating S_p to *MPD* for each specific device are significantly higher than that seen in Figure 37, where all the devices were included in the regression analysis.

Table 24 presents the summary of the statistical analysis obtained from the tests results plotted in Figure 40. 95% confident intervals for the magnitude of the parameters *a* and *b* is provided to illustrate their variation from one device to another. Table 24 also includes a summary of the statistical analysis for the devices associated with Figure 40 which were

also used for testing in 2007, to illustrate how the relevant parameters vary over time. In summary, by using the *a* and *b* parameters specific for each device in Equation (12) one would be able to better predict the friction measurement at 60 km/h based on a single friction measurement at any other slip speed. This would certainly address the issue illustrated in Tables 18-21 where different *FR60* values were obtained when they were calculated from different slip speeds.

Table 24 Statistical analysis on the *a* and *b* parameters for different friction measuring devices

Device	Coefficient *a*			Coefficient *b*			R^2
	Magnitude	CI Lower 95%	CI Upper 95%	Magnitude	CI Lower 95%	CI Upper 95%	
VTTI GT	1.265	-3.325	5.855	16.116	11.168	21.063	80.76%
DND GT08	5.642	-19.976	31.261	59.812	29.492	90.133	65.89%
DND GT07	5.848	3.409	8.288	20.342	15.843	24.841	80.05%
Dynatest RFT	7.506	1.138	13.874	9.555	3.171	15.940	49.66%
FAA RFT08	5.919	4.022	7.816	8.470	6.251	10.688	89.23%
FAA RFT07	3.680	-0.406	7.766	11.752	7.771	15.734	79.33%
USF RFT	-2.241	-5.409	0.927	25.109	21.271	28.947	95.51%
USF E274	28.386	-5.101	61.873	90.640	58.632	122.648	74.22%
VDot E274-08	29.981	-19.442	79.404	110.592	53.304	167.880	71.24%
VDot E274-07	37.071	-48.793	122.936	126.055	2.270	249.839	40.80%
PTI E274	31.200	2.130	60.269	75.577	46.394	104.760	79.23%

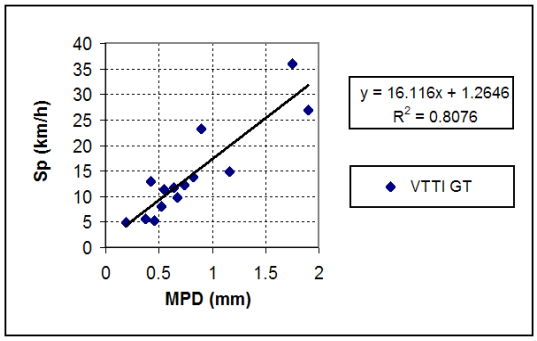

(a) VTTI Grip Tester

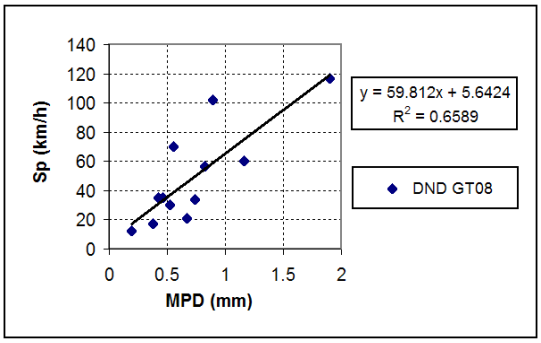

(b) DND Grip Tester

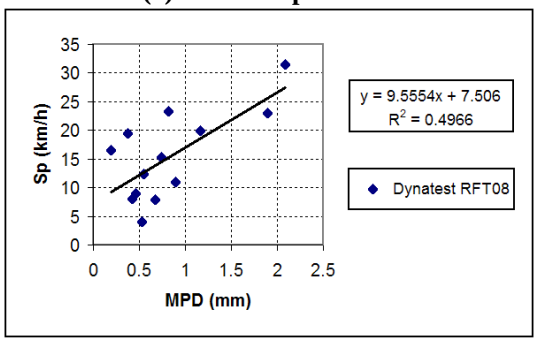

(c) Dynatest Runway Friction Tester

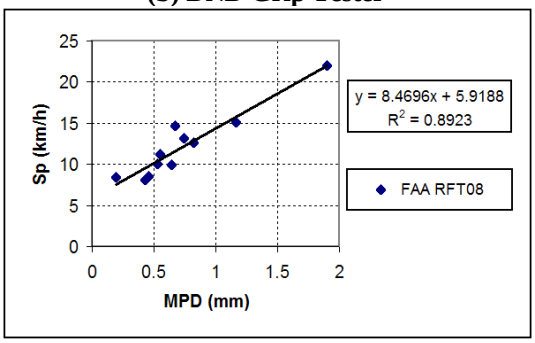

(d) FAA Runway Friction Tester

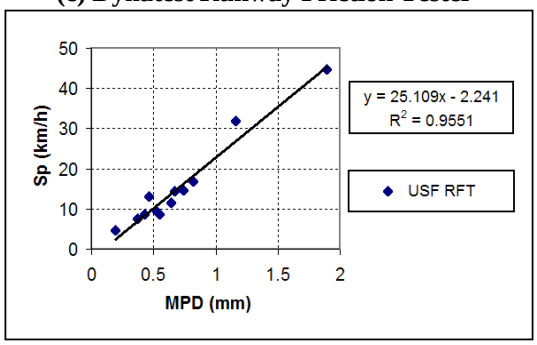

(e) USF Runway Friction Tester

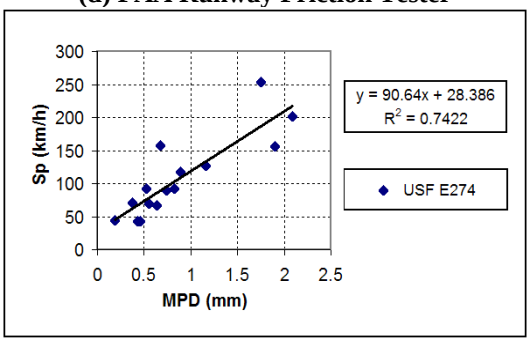

(f) USF Locked Wheel Tester

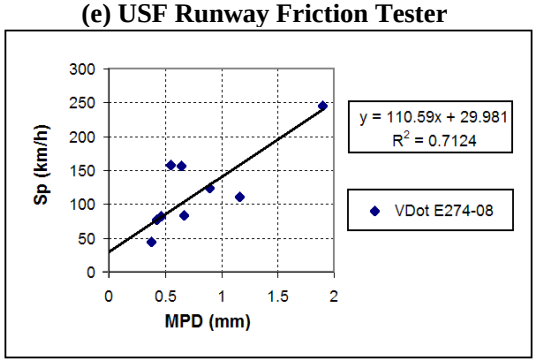

(g) VDot Locked Wheel Tester

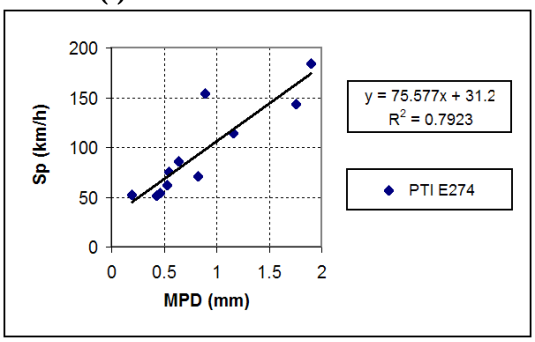

(h) PTI Locked Wheel Tester

Figure 40 S_p vs. *MPD* for the different specific devices used in the 2008 NASA workshop

4.4.4 Slip Speed Sensitivity of the *A* and *B* Parameters

The final phase of the investigation was to assess the impact of device specific S_p vs. *MPD* relationship on the device calibration parameters *A* and *B*. First, in order to evaluate the sensitivity of the parameters *A* and *B* to the slip speed, these parameters were calculated from two different sets of measurements taken at specific slip speeds *S1* and *S2* for the friction measuring devices presented in Table 24. *A* and *B* parameters listed in Table 25 were determined by first computing the *FR60* for ten different surfaces from friction measurements made at the specified slip speeds using Equation (12) with the ASTM suggested *a* and *b* (14.2 and 89.7) values relevant to the CT Meter and then linearly correlating them to the corresponding *F60* values obtained using the Dynamic Friction Tester (DFT) (Equation (11)). Since no ribbed tires were used for this analysis *C* was consider to be 0. By comparing the values obtained by using $FR60_{S1}$ and $FR60_{S2}$ in Table 25, one can observe clearly the effect of the measuring slip speed on the parameters *A* and *B*. It is evident that the slip speed is a crucial variable in determining the calibration parameters *A* and *B* based on the current ASTM standard. The deviation within each parameter (*A* and *B*) due to the difference in the slip speed can be expressed by Equation (33), were the average *A* and *B* values were used to compute the percent deviation.

$$\%Deviation = \frac{\left|A_{FR60S1} - A_{FR60S2}\right|}{\frac{A_{FR60S1} + A_{FR60S2}}{2}} \tag{33}$$

where A_{FR60S1} and A_{FR60S2} are the parameters *A* computed from the two different sets of measurements taken at specific slip speeds *S1* and *S2* respectively. The corresponding form of Equation (33) was used to compute the deviation in the parameter *B*.

The effect of the operational slip speed seems to lead to deviations of as much as 164% for parameter *A* (for the PTI E274) and 30 % for *B* (for the VDot E274-07). Considering all the devices used, the average deviations for parameters *A* and *B* computed according to ASTM standards were 37% and 13% respectively.

On the other hand, the modified *A* and *B* parameters shown in Table 26 were calculated using the conventional format, but using the revised *a* and *b* parameters specific to every friction measuring device shown in Table 24. It is evident from Table 26 that the modified *A* and *B* are less dependent on the slip speed. The deviations associated with the modified values are significantly less with the highest being a 56% for the parameter *A* (for the PTI E274) and 15% for the parameter B (for the VDot E274-07). The revised *a* and *b* parameters reduced the average deviation of *A* and *B* to 11% and 6% respectively, for all the devices used.

Table 25 *A* and *B* parameters calculated in accordance with ASTM standards

Device	$FR60_{S1}$		$FR60_{S2}$		%Deviation	
	A	*B*	*A*	*B*	*A*	*B*
VTTI GT	0.145	0.727	0.229	0.692	45%	5%
DND GT08	0.135	0.771	0.165	0.726	20%	6%
DND GT07	0.153	0.726	0.187	0.849	20%	16%
Dynatest RFT	0.155	0.658	0.200	0.708	25%	7%
FAA RFT08	0.180	0.458	0.217	0.505	18%	10%
FAA RFT07	0.178	0.589	0.199	0.677	11%	14%
USF RFT	0.166	0.675	0.203	0.699	20%	4%
USF E274	0.123	0.680	0.088	0.728	33%	7%
VDot E274-08	0.132	0.572	0.155	0.466	16%	20%
VDot E274-07	0.067	0.699	0.099	0.517	39%	30%
PTI E274	0.099	0.562	0.010	0.708	164%	23%

Table 26 *A* and *B* parameters calculated using revised *a* and *b* parameters

Device	$FR60_{S1}$		$FR60_{S2}$		%Deviation	
	A	*B*	*A*	*B*	*A*	*B*
VTTI GT	0.322	1.878	0.323	1.961	0%	4%
DND GT08	0.207	0.784	0.216	0.758	5%	3%
DND GT07	0.315	1.539	0.315	1.760	0%	13%
Dynatest RFT	0.298	2.878	0.300	2.900	1%	1%
FAA RFT08	0.329	2.485	0.329	2.483	0%	0%
FAA RFT07	0.309	2.253	0.309	2.387	0%	6%
USF RFT	0.325	1.031	0.323	1.096	1%	6%
USF E274	0.122	0.677	0.130	0.674	7%	1%
VDot E274-08	0.119	0.604	0.136	0.565	13%	7%
VDot E274-07	0.075	0.699	0.112	0.600	41%	15%
PTI E274	0.102	0.556	0.057	0.626	56%	12%

4.4.5 Effect of the Use of a Modified S_p Parameter in IFI Standard Correlation

The data presented in Tables 25 and 26 illustrates the improvements that the use of a modified S_p parameter would provide to the stability of the parameters *A* and *B* with respect to the measuring slip speed. However this information does not indicate whether the improved approach predicts better *F60* than the current approach. On the other hand, it is clear that the use of a modified S_p parameter would capture the actual friction vs. speed gradient of a given device and therefore predict better *FR60* independent on the *FRS* used on the computations, as illustrated on Figure 39. This fact alone is a significant improvement in the current procedure since it provides a better tool to evaluate the actual *FR60* of a given pavement to be used in the decision making process of a pavement management system. Furthermore, in order evaluate Equation (11) and illustrate which method (ASTM or modified S_p method) produces a better correlation between the two variables *F60* and *FR60,* Figures 41-42 and Tables 27-28 are presented.

One can observe from Figure 41 that even though the parameters *A* and *B* are speed invariant when using the modified S_p procedure, the ASTM method produces a better coefficient of determination (R^2). One can also observe that the R^2 obtained using the ASTM method is significantly sensitive to the measuring speed, producing lower values at higher measuring speeds ($R^2_{S1} > R^2_{S2}$ with S1 < S2). The %Errors in Tables 27-35 were calculated from the average fitted error obtained for the different pavement surfaces used at the calibration stage, where the corresponding *A* and *B* parameters were obtained. The corresponding calibration for Dynatest RFT is seen in Figure 41.

The above observation is further supported by the results in Table 27 where the same trend occurs in different independent devices used in the analysis. When Tables 27 and Table 28 are compared, one can see that only the devices that operate at 100% slip condition (USF E274, VDot E274-08 and PTI E274) show a significant improvement when the modified S_p method is used (as illustrated in Figure 42).

The phenomenon observed with the devices that operate at a slip range of 10-20% occurs because these devices present a relatively steep friction speed gradient, as illustrated in Figure 38. Given the slip condition of the devices that operate at this slip range, the operational slip speed would be significantly low compared to a device that operates at 100% slip condition. When friction values obtained from any of the devices at any given slip speed (*FRS*) is used to predict the *FR60* using Equation (29), with the appropriatly modified *a* and *b* parameters, one realizes that these values would asymptotically approach zero given the steep friction slip gradient that these devices present (Figure 38). It is realized that *FR60* is the friction value predicted for 60 km/h, which is significantly higher than the normal operating slip speeds of these devices. This condition is further illustrated in Figures 41(c) and 41(d) where it can be seen that the *FR60* values concentrate in the region close to zero.

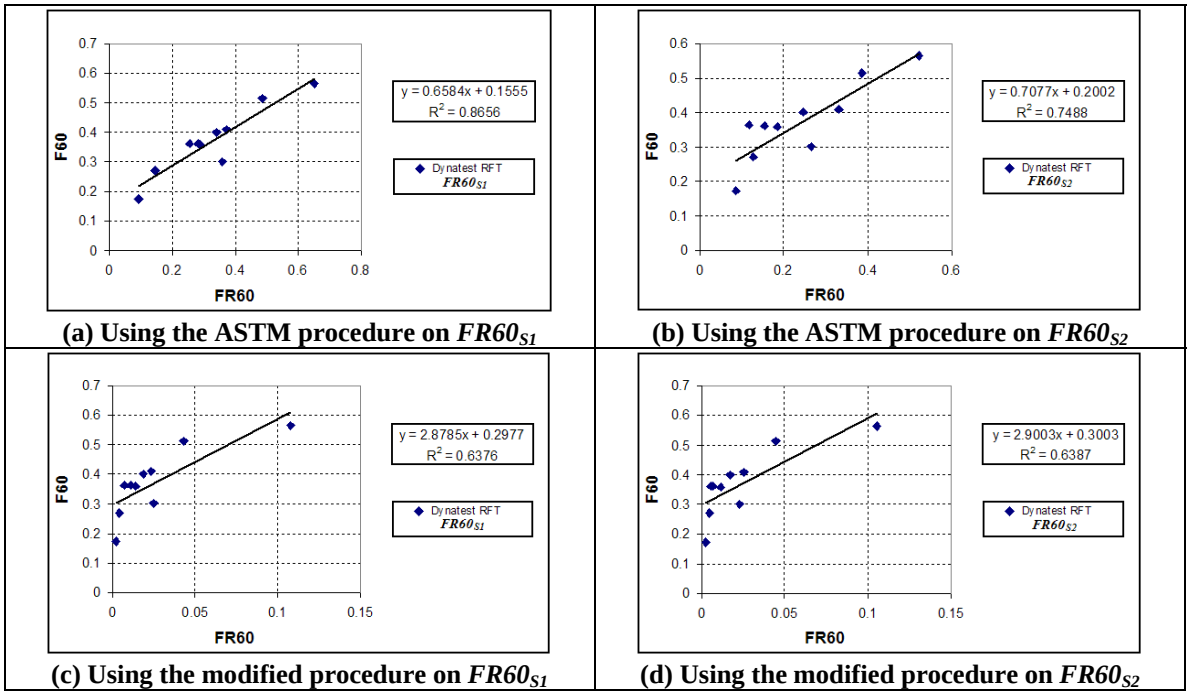

(a) Using the ASTM procedure on $FR60_{S1}$ **(b) Using the ASTM procedure on $FR60_{S2}$**

(c) Using the modified procedure on $FR60_{S1}$ **(d) Using the modified procedure on $FR60_{S2}$**

Figure 41 Dynatest RFT correlations for Equation 11

Table 27 Evaluation of the correlation between *FR60* obtained at different slip speeds and *F60* values using the ASTM method

Device	%Deviation		$FR60_{S1}$	$FR60_{S2}$	%Error	
	A	*B*	R^2	R^2	$FR60_{S1}$	$FR60_{S2}$
VTTI GT	44.9%	5.0%	0.835	0.690	8.7%	13.5%
DND GT08	19.7%	6.1%	0.833	0.794	8.1%	9.9%
Dynatest RFT	25.2%	7.2%	0.866	0.749	10.2%	15.3%
FAA RFT08	18.2%	9.8%	0.918	0.888	8.0%	9.7%
USF RFT	20.2%	3.6%	0.928	0.932	6.6%	6.8%
USF E274	32.7%	6.8%	0.893	0.895	8.7%	9.1%
VDot E274-08	15.8%	20.4%	0.856	0.598	7.5%	13.6%
PTI E274	164.4%	23.0%	0.856	0.835	10.1%	11.5%

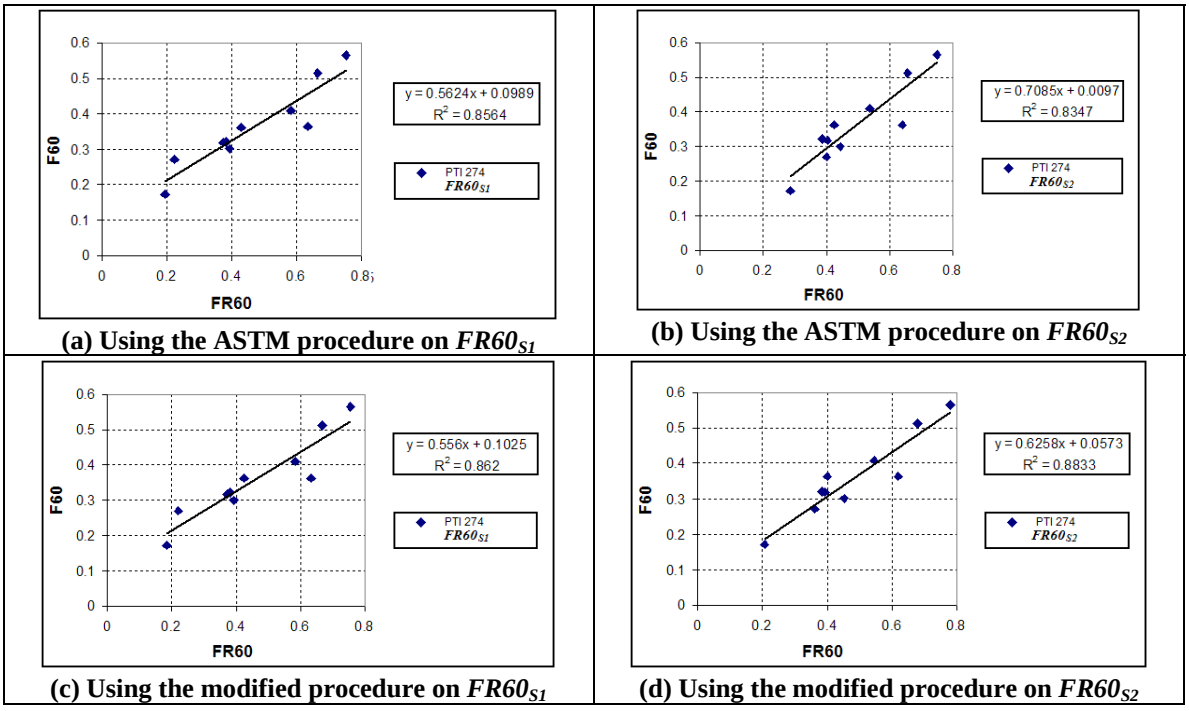

(a) Using the ASTM procedure on $FR60_{S1}$

(b) Using the ASTM procedure on $FR60_{S2}$

(c) Using the modified procedure on $FR60_{S1}$

(d) Using the modified procedure on $FR60_{S2}$

Figure 42 PTI 274 correlations for Equation 11

Table 28 Evaluation of the correlation between *FR60* obtained at different slip speeds and *F60* values using the modified S_p method

Device	%Deviation		$FR60_{S1}$	$FR60_{S2}$	%Error	
	A	*B*	R^2	R^2	$FR60_{S1}$	$FR60_{S2}$
VTTI GT	0.1%	4.3%	0.568	0.551	20.6%	21.0%
DND GT08	4.5%	3.3%	0.810	0.778	11.0%	12.0%
Dynatest RFT	0.9%	0.8%	0.638	0.639	18.9%	18.9%
FAA RFT08	0.1%	0.1%	0.616	0.614	15.8%	15.8%
USF RFT	0.6%	6.2%	0.611	0.634	18.5%	18.2%
USF E274	6.8%	0.5%	0.894	0.893	8.9%	8.6%
VDot E274-08	13.0%	6.6%	0.884	0.763	6.6%	11.0%
PTI E274	56.4%	11.8%	0.862	0.883	9.9%	8.8%

In the light of the above information, one could suggest that the relationship observed between *FR60* and *F60* is not linear when values obtained from devices operating at slip range of 10-20% are used. At this point it must be realized that the *F60* values used for the standardization of any given friction measuring device are obtained using the DFT, which is also a device that operates at 100% slip conditions.

Alternatively, one could use a power transformation on the *FR60* values to obtain a linear relation between the *F60* and the corresponding transformed *FR60* data. Tables 29-35 present results of the analysis of implementing different power transformation to the *FR60* values. It can be seen from Tables 29-35 that the use of power transformation on the *FR60* values improves significantly the correlations of the devices that operate at slip ranges of 10-20%. The devices that operate at 100% slip conditions did not show any improvement when power transformations were used compared to the results presented in Table 28. One can conclude that this was because there was already a linear relationship between *FR60* values of the devices that operate at 100% slip conditions and the DFT *F60*, and hence no transformation of the data would be necessary for further improvement on these particular devices.

Table 29 Evaluation of the correlation between transformed *FR60* using the "logarithm transformation" and *F60* values using the modified S_p method at different slip speeds

Device	%Deviation		$FR60_{S1}$	$FR60_{S2}$	%Error	
	A	*B*	R^2	R^2	$FR60_{S1}$	$FR60_{S2}$
VTTI GT	0.3%	1.0%	0.728	0.718	12.2%	12.1%
DND GT08	0.4%	3.8%	0.735	0.732	12.1%	11.5%
Dynatest RFT	0.1%	2.0%	0.824	0.781	9.2%	11.9%
FAA RFT08	0.1%	0.2%	0.946	0.943	5.0%	5.1%
USF RFT	0.7%	4.7%	0.678	0.689	13.9%	13.8%
USF E274	0.6%	1.7%	0.877	0.886	8.7%	7.9%
VDot E274-08	7.6%	22.9%	0.812	0.638	9.3%	14.1%
PTI E274	4.8%	21.7%	0.815	0.848	10.0%	10.0%

Table 30 Evaluation of the correlation between transformed *FR60* using the "square root" transformation and *F60* values using the modified S_p method at different slip speeds

Device	%Deviation		$FR60_{S1}$	$FR60_{S2}$	%Error	
	A	*B*	R^2	R^2	$FR60_{S1}$	$FR60_{S2}$
VTTI GT	1.4%	0.6%	0.728	0.695	16.0%	16.7%
DND GT08	15.6%	3.6%	0.821	0.800	8.1%	8.0%
Dynatest RFT	5.1%	3.2%	0.768	0.738	14.3%	15.8%
FAA RFT08	0.3%	0.3%	0.808	0.805	12.1%	12.1%
USF RFT	0.7%	2.4%	0.816	0.831	12.4%	11.9%
USF E274	13.1%	1.5%	0.905	0.907	6.9%	7.0%
VDot E274-08	69.8%	13.9%	0.852	0.706	7.8%	12.5%
PTI E274	60.2%	16.7%	0.846	0.875	9.5%	8.5%

Table 31 Evaluation of the correlation between transformed *FR60* using the "cube root" transformation and *F60* values using the modified S_p method at different slip speeds

Device	%Deviation		$FR60_{S1}$	$FR60_{S2}$	%Error	
	A	*B*	R^2	R^2	$FR60_{S1}$	$FR60_{S2}$
VTTI GT	3.2%	2.5%	0.789	0.749	12.0%	13.0%
DND GT08	236.3%	3.6%	0.804	0.789	9.3%	8.5%
Dynatest RFT	13.4%	3.7%	0.802	0.762	12.1%	14.2%
FAA RFT08	0.6%	0.3%	0.881	0.877	9.6%	9.7%
USF RFT	0.9%	1.6%	0.899	0.911	8.7%	8.3%
USF E274	5.6%	1.6%	0.900	0.904	7.1%	6.6%
VDot E274-08	36.9%	16.7%	0.839	0.684	8.3%	13.1%
PTI E274	37.7%	18.4%	0.837	0.868	9.6%	8.9%

Table 32 Evaluation of the correlation between transformed *FR60* using the "fourth root" transformation and *F60* values using the modified S_p method at different slip speeds

Device	%Deviation		$FR60_{S1}$	$FR60_{S2}$	%Error	
	A	*B*	R^2	R^2	$FR60_{S1}$	$FR60_{S2}$
VTTI GT	5.1%	3.1%	0.810	0.770	10.0%	11.2%
DND GT08	20.6%	3.6%	0.791	0.779	9.9%	9.2%
Dynatest RFT	71.0%	3.7%	0.814	0.771	11.1%	13.6%
FAA RFT08	1.3%	0.3%	0.913	0.908	8.3%	8.4%
USF RFT	1.3%	1.4%	0.927	0.938	7.1%	6.6%
USF E274	4.1%	1.6%	0.896	0.901	7.5%	6.7%
VDot E274-08	31.1%	18.2%	0.833	0.673	8.5%	13.4%
PTI E274	31.9%	19.2%	0.832	0.864	9.7%	9.1%

Table 33 Evaluation of the correlation between transformed *FR60* using the "fifth root" transformation and *F60* values using the modified S_p method at different slip speeds

Device	%Deviation		$FR60_{S1}$	$FR60_{S2}$	%Error	
	A	*B*	R^2	R^2	$FR60_{S1}$	$FR60_{S2}$
VTTI GT	7.1%	3.3%	0.815	0.776	9.1%	10.3%
DND GT08	12.5%	3.6%	0.782	0.772	10.4%	9.7%
Dynatest RFT	35.2%	3.5%	0.819	0.775	10.5%	13.2%
FAA RFT08	4.1%	0.3%	0.928	0.923	7.4%	7.6%
USF RFT	1.7%	1.4%	0.929	0.939	5.9%	5.6%
USF E274	3.4%	1.7%	0.893	0.899	7.8%	6.9%
VDot E274-08	28.7%	19.1%	0.829	0.666	8.7%	13.5%
PTI E274	29.2%	19.7%	0.829	0.861	9.8%	9.3%

Table 34 Evaluation of the correlation between transformed *FR60* using the "sixth root" transformation and *F60* values using the modified S_p method at different slip speeds

Device	%Deviation		$FR60_{S1}$	$FR60_{S2}$	%Error	
	A	*B*	R^2	R^2	$FR60_{S1}$	$FR60_{S2}$
VTTI GT	9.7%	3.2%	0.813	0.777	8.5%	9.8%
DND GT08	9.7%	3.6%	0.775	0.766	10.7%	10.0%
Dynatest RFT	16.1%	3.4%	0.822	0.777	10.2%	12.9%
FAA RFT08	5.1%	0.3%	0.936	0.931	6.8%	7.1%
USF RFT	2.4%	1.4%	0.919	0.929	7.0%	6.8%
USF E274	3.0%	1.7%	0.891	0.897	7.9%	7.1%
VDot E274-08	27.4%	19.7%	0.826	0.662	7.9%	13.6%
PTI E274	27.6%	20.0%	0.827	0.859	9.8%	9.4%

Table 35 Evaluation of the correlation between transformed *FR60* using the "seventh root" transformation and *F60* values using the modified S_p method at different slip speeds

Device	%Deviation		$FR60_{S1}$	$FR60_{S2}$	%Error	
	A	*B*	R^2	R^2	$FR60_{S1}$	$FR60_{S2}$
VTTI GT	13.6%	3.1%	0.809	0.775	8.6%	9.5%
DND GT08	8.2%	3.7%	0.770	0.762	10.9%	10.2%
Dynatest RFT	11.1%	3.3%	0.823	0.778	9.9%	12.7%
FAA RFT08	1.6%	0.2%	0.941	0.936	6.4%	6.7%
USF RFT	3.2%	1.5%	0.905	0.914	8.0%	7.8%
USF E274	2.8%	1.7%	0.889	0.896	8.0%	7.2%
VDot E274-08	6.8%	7.0%	0.824	0.658	8.0%	13.7%
PTI E274	45.8%	33.1%	0.825	0.858	9.8%	9.4%

Figure 43 provides a tool to analyze the effect of the power transformation, λ, on the average coefficient of determination (R^2) of the correlation between *F60* and transformed *FR60* values for friction measuring devices that operate in the 10-20% slip range. It can be seen from Figure 43 that the fifth root power transformation (λ = 1/5) maximizes the R^2 value. Therefore, the information provided in Figure 43 would help one to select the optimum power transformation that would enhance the fitting capabilities of the proposed transformed model. It must be noted that a λ value of zero corresponds to the logarithmic transformation. However the results of Figure 43 would not provide one with the predictive capabilities of each power model.

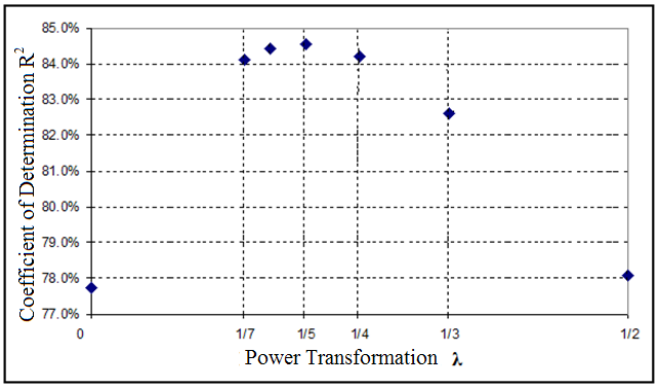

Figure 43 Power Transformation vs. R^2 on the friction measuring devices that operate in the 10-20% slip condition range

4.4.6 Prediction Capabilities of the Proposed Models

In order to evaluate which of the proposed power transformation yields the highest predictive capability, *F60* values were calculated for different friction measuring equipment on three independent pavement surfaces. The following computations were performed:

(1) Calculate *FR60* values using Equation (29) using the corresponding modified S_p parameter for the different devices on the respective surfaces.

(2) Calculate *F60* values using Equation (11) with the appropriate *A* and *B* parameters that are characteristic to both the friction measuring device and transformation used on the corresponding transformed *FR60* values.

F60 values were also computed using the traditional ASTM procedure. The result of this analysis is presented in Tables 36-43, which also contain the standard *F60* value obtained using the DFT. Of these, Tables 41-43 only compare the general ASTM method with the linear modified S_p method, since it has been shown before that a transformation of the data was not necessary for the Locked Wheel Testers that operate at 100% slip.

Table 36 Summary of predicted *F60* values for the different method used for the VTTI GT

Surface	*F60* Values								
	DFT	ASTM	λ = 0	λ = 1/2	λ = 1/3	λ = 1/4	λ = 1/5	λ = 1/6	λ = 1/7
A	0.318	0.270	0.371	0.322	0.328	0.336	0.341	0.346	0.349
D	0.322	0.283	0.389	0.340	0.350	0.359	0.365	0.369	0.372
E1	0.340	0.235	0.327	0.295	0.288	0.290	0.293	0.296	0.299

Table 37 Summary of predicted *F60* values for the different method used for the DND GT08

Surface	*F60* Values								
	DFT	ASTM	λ = 0	λ = 1/2	λ = 1/3	λ = 1/4	λ = 1/5	λ = 1/6	λ = 1/7
A	0.318	0.371	0.384	0.365	0.372	0.375	0.377	0.378	0.379
D	0.322	0.368	0.387	0.370	0.376	0.379	0.381	0.382	0.383
E1	0.340	0.299	0.326	0.297	0.304	0.309	0.312	0.314	0.316

Table 38 Summary of predicted *F60* values for the different method used for the Dynatest RFT

Surface	*F60* Values								
	DFT	ASTM	λ = 0	λ = 1/2	λ = 1/3	λ = 1/4	λ = 1/5	λ = 1/6	λ = 1/7
A	0.318	0.280	0.337	0.324	0.326	0.328	0.330	0.331	0.332
D	NA	NA	NA	NA	NA	NA	NA	NA	NA
E1	0.340	0.264	0.294	0.298	0.294	0.293	0.293	0.293	0.293

Table 39 Summary of predicted *F60* values for the different method used for the FAA RFT08

Surface	*F60* Values								
	DFT	ASTM	λ = 0	λ = 1/2	λ = 1/3	λ = 1/4	λ = 1/5	λ = 1/6	λ = 1/7
A	0.318	0.285	0.351	0.335	0.336	0.338	0.340	0.341	0.342
D	0.322	0.289	0.368	0.346	0.350	0.353	0.355	0.357	0.359
E1	0.340	0.290	0.320	0.319	0.314	0.313	0.313	0.313	0.314

Table 40 Summary of predicted *F60* values for the different method used for the USF RFT

Surface	*F60* Values								
	DFT	ASTM	λ = 0	λ = 1/2	λ = 1/3	λ = 1/4	λ = 1/5	λ = 1/6	λ = 1/7
A	0.318	0.268	0.386	0.321	0.327	0.336	0.344	0.351	0.356
D	0.322	0.283	0.398	0.341	0.353	0.364	0.372	0.377	0.381
E1	0.340	0.246	0.361	0.295	0.287	0.289	0.296	0.303	0.309

Table 41 Summary of predicted *F60* values for the different method used for the USF E274

Surface	*F60* Values		
	DFT	ASTM	Modified
A	0.318	0.292	0.304
D	0.322	0.306	0.312
E1	0.340	0.314	0.307

Table 42 Summary of predicted *F60* values for the different method used for the VDot E274-08

Surface	*F60* Values		
	DFT	ASTM	Modified
A	0.318	0.368	0.355
D	0.322	0.353	0.343
E1	0.340	0.430	0.406

Table 43 Summary of predicted *F60* values for the different method used for the PTI E274

Surface	*F60* Values		
	DFT	ASTM	Modified
A	0.318	0.296	0.303
D	0.322	0.285	0.298
E1	0.340	0.290	0.288

In order to evaluate the predictive capabilities of the proposed methods predicted *F60* values were compared to the corresponding standard *F60* obtained using the DFT following the stipulations of the ASTM standards. The results of this analysis are presented in Tables 44-51.

Table 44 Summary of predicted *F60* % Errors for the different method used for the VTTI GT

Surface	%Error							
	ASTM	λ = 0	λ = 1/2	λ = 1/3	λ = 1/4	λ = 1/5	λ = 1/6	λ = 1/7
A	15.0%	16.8%	1.3%	3.3%	5.5%	7.4%	8.8%	9.9%
D	12.0%	20.6%	5.4%	8.7%	11.4%	13.2%	14.5%	15.5%
E1	30.9%	3.8%	13.2%	15.2%	14.9%	13.9%	12.9%	12.0%

Table 45 Summary of predicted *F60* % Errors for the different method used for the DND GT08

Surface	%Error							
	ASTM	λ = 0	λ = 1/2	λ = 1/3	λ = 1/4	λ = 1/5	λ = 1/6	λ = 1/7
A	16.5%	20.7%	14.8%	16.9%	17.9%	18.5%	18.9%	19.2%
D	14.3%	20.2%	14.8%	16.7%	17.7%	18.2%	18.6%	18.9%
E1	12.1%	4.2%	12.8%	10.5%	9.1%	8.2%	7.6%	7.1%

Table 46 Summary of predicted *F60* % Errors for the different method used for the Dynatest RFT

Surface	%Error							
	ASTM	λ = 0	λ = 1/2	λ = 1/3	λ = 1/4	λ = 1/5	λ = 1/6	λ = 1/7
A	11.9%	6.1%	1.8%	2.6%	3.2%	3.6%	4.0%	4.2%
D	NA	NA	NA	NA	NA	NA	NA	NA
E1	22.5%	13.6%	12.3%	13.5%	13.8%	14.0%	14.0%	14.0%

Table 47 Summary of predicted *F60* % Errors for the different method used for the FAA RFT08

Surface	%Error							
	ASTM	λ = 0	λ = 1/2	λ = 1/3	λ = 1/4	λ = 1/5	λ = 1/6	λ = 1/7
A	10.4%	10.4%	5.3%	5.6%	6.2%	6.8%	7.2%	7.6%
D	10.3%	14.3%	7.2%	8.4%	9.5%	10.3%	10.9%	11.3%
E1	14.9%	6.0%	6.3%	7.7%	8.0%	8.0%	7.9%	7.7%

Table 48 Summary of predicted *F60* % Errors for the different method used for the USF RFT

Surface	%Error							
	ASTM	λ = 0	λ = 1/2	λ = 1/3	λ = 1/4	λ = 1/5	λ = 1/6	λ = 1/7
A	15.6%	21.4%	0.8%	2.8%	5.6%	8.2%	10.3%	12.0%
D	12.1%	23.4%	5.8%	9.7%	12.9%	15.3%	17.0%	18.2%
E1	27.8%	6.0%	13.4%	15.8%	14.9%	13.0%	11.0%	9.1%

Table 49 Summary of predicted *F60* % Errors for the different method used for the USF E274

Surface	%Error	
	ASTM	Modified
A	8.1%	4.3%
D	5.0%	3.3%
E1	7.6%	9.7%

Table 50 Summary of predicted *F60* % Errors for the different method used for the VDot E274-08

Surface	%Error	
	ASTM	Modified
A	15.9%	11.6%
D	9.4%	6.4%
E1	26.3%	19.4%

Table 51 Summary of predicted *F60* % Errors for the different method used for the PTI E274

Surface	%Error	
	ASTM	Modified
A	6.8%	4.8%
D	11.7%	7.5%
E1	14.8%	15.3%

A summary of the results in Tables 44-48 is presented in Table 52, in terms of the average %Errors for different devices that operate in the slip range of 10-20%. In addition, Table 53 summarizes the average %Errors of the devices that operate under full braking locked wheel (slip = 100%) conditions.

Table 52 Summary of the average predicted % Errors of the devices that operate in the range of 10-20% slip condition

Device	Average %Error							
	ASTM	$\lambda = 0$	$\lambda = 1/2$	$\lambda = 1/3$	$\lambda = 1/4$	$\lambda = 1/5$	$\lambda = 1/6$	$\lambda = 1/7$
VTTI GT	19.3%	13.7%	6.6%	9.1%	10.6%	11.5%	12.1%	12.4%
DND GT08	14.3%	15.0%	14.1%	14.7%	14.9%	15.0%	15.0%	15.1%
Dynatest RFT	17.2%	9.9%	7.1%	8.0%	8.5%	8.8%	9.0%	9.1%
FAA RFT08	11.9%	10.2%	6.3%	7.2%	7.9%	8.3%	8.6%	8.9%
USF RFT	18.5%	17.0%	6.7%	9.4%	11.1%	12.2%	12.8%	13.1%
Overall Average	16.2%	13.2%	8.1%	9.7%	10.6%	11.2%	11.5%	11.7%

Table 53 Summary of the average predicted % Errors of the devices that operate at 100% slip condition

Device	Average %Error	
	ASTM	Modified
USF E274	6.9%	5.8%
VDot E274-08	17.2%	12.5%
PTI E274	11.1%	9.2%
Overall Average	11.7%	9.1%

Table 52 shows that the power transformation with $\lambda = ½$ produces a consistently lower average %Error for all the friction measuring devices that operate in the slip range of 10-20%. It is also seen in Table 52 that the overall average of the averages %Errors using the conventional ASTM method yield a value of 16.2% when all the devices are considered, while the corresponding value for the square root transformation is 8.1%. This shows that the proposed transformation reduces the prediction error significantly. On the other hand, Table 53 shows that the modified linear S_p method produces consistently better results for the Locked Wheel testers (slip = 100%) compared to the conventional ASTM method.

4.4.7 Modified International Friction Index

Based on the findings of this investigation, a modified methodology is proposed to compute the International Friction Index (IFI). The modified methodology is summarized by the following steps:

(1) Select a set of at least ten pavement surfaces that contain a wide variety of both macrotexture and microtexture. The macrotexture and the microtexture are to be evaluated using the *MPD* parameter and the DFT_{20}. *MPD* values must be in the range of 0.25-1.5mm, while DFT_{20} values are to be in the range of 0.30-0.90.

(2) Measure the coefficient of friction at different speeds on the selected pavement surfaces.

(3) Fit the friction data to Equation (32) for every pavement surface to obtain the different experimentally obtained S_p values. Determine the calibration constant (*a* and *b*) from a linear regression between the experimentally obtained S_p values and the *MPD*.

(4) Using the friction device to be calibrated, determine the friction values (*FRS*) of the test pavements and calculate the *FR60* using Equation (29), with the appropriate S_p parameter determined in step (3).

(5) Use Equations (34) and (35) to obtain the standard friction parameters of the test pavement surfaces:

$$S_p = 14.2 + 89.7MPD \tag{34}$$

$$F60 = 0.081 + 0.732 * DFT_{20} * EXP\left[-\frac{40}{S_p}\right] \tag{35}$$

If the friction device to be calibrated operates in the slip range of 10-20%, then follow step (6a);

(6a) Determine the calibration constant (A and B) from a linear regression using Equation (36), where λ is equal to ½.

$$F60 = A + B * \left(FR60\right)^{\lambda} \tag{36}$$

On the other hand, if the friction device to be calibrated operates at 100% slip conditions, then follow step (6b);

(6b) Determine the calibration constant (A and B) from a linear regression using Equation (11).

CHAPTER 5

CONCLUSIONS

The ASTM standards dictate DFT to be used for calculating IFI (ASTM E-1960-07, 2009). Therefore an experimental investigation was performed to study the factors that influence the DFT measurements. The results from the investigation indicated that a number of parameters must be controlled in order to obtain consistent results on the same pavement surface on different trials.

The results also indicate a strong dependence among DFT_{20} and the temperatures of water and the pavement surface. Generally, as the temperature increases DFT_{20} values decrease. It is also concluded that the temperature effect on friction is the main parameter responsible for seasonal variations of friction measurements. Therefore, it is necessary to apply a temperature correction to DFT readings in order to perform comparisons between measurements taken at different temperatures or different seasons of the year. The authors suggest that a standard temperature be established in order to perform the above correction more systematically. The average temperature of the summer season seems to be the most fitting standard temperature. This is because coefficient of friction values are generally lower during high summer temperatures and in the absence of a temperature correction the risk of over-prediction of coefficient of friction exists.

It is suggested in ASTM E1911 that the water tank must be maintained 0.6 m above the DFT to eliminate possible effects due to the elevation of the water tank height. However, when performing multiple tests at the same location, the water level inside the tank subsides thus changing the water pressure of the system. Therefore, in order to maintain constant water pressure, the water in the tank must be continuously replenished during continued testing.

In the second phase of this research program an experimental and analytical investigation was performed to study the effect of pavement roughness on friction measurements. Significant experimental evidence was presented in this investigation to illustrate that increased pavement roughness decreases the measured *SN* (skid number or 100*coefficient of friction). Although the investigation was limited to LWT measurements, this finding could be extended to other vehicles as well as to explain the results of previous investigations attributing skid related accidents to pavement roughness.

Furthermore, the current International Friction Index (IFI) standard for characterizing the frictional properties of a pavement surface does not consider pavement roughness as a required parameter for estimation of IFI. This is because it advocates the use of the Dynamic Friction Tester (DFT), which is a "spot" tester, as the calibration device. In this research it was concluded that even when the DFT measures the same friction value on different pavement sections with similar texture conditions, full scale friction measuring device such as the LWT would produce different friction readings if the roughness condition changes from one section to another. In order to account for this phenomenon, an additional parameter accounting for roughness effects could be included in the regression analysis used in IFI computations. A parameter appropriate for this purpose can be found by extending this research further.

Since the primary factor that contributes to the variation of *SN* with roughness is the dynamics of the normal load, a rigid-body two-degree-of-freedom system was used successfully to model the variation of normal load at the tire pavement interface of the LWT. The stiffness and damping properties of the model were estimated by direct laboratory measurements and back-calculation from field experimental data. The natural frequencies and velocities predicted by the theoretical model showed excellent agreement with the corresponding experimental measurements performed subsequently.

It was also shown experimentally that a quantifiable nonlinear relationship exists between rubber friction and the normal load. This relationship was combined with the above

vibration model to explain the dependency of friction (*SN*) on roughness. In addition, a procedure was also formulated to predict the pavement friction response (measurable *SN*) of LWT on any known profile. It can be visualized that the same general trend of *SN* vs. roughness would also be exhibited by other vehicles as well.

Different parameters that have the potential to define the effects of roughness on friction measurements were studied. It was found that the International Roughness Index (*IRI*) is sensitive to the properties of its inherent Quarter-car model, and hence it is not an accurate predictor of the *SN* vs. roughness relationship. However, the Dynamic Load Coefficient (*DLC*), commonly used to evaluate the effect of heavy vehicles on pavements structures, was found to be an adequate estimator of the roughness effects on measured friction. This preliminary investigation showed that isolated testing of rough pavement sections with excessively high *DLC* values produce relatively lower *SN* values than smoother pavement sections with the same texture characteristics. It is the authors' belief that *SN* values should only be used as a reference for maintenance purposes. A *SN* value measured at 100% slip does not necessarily represent the actual friction conditions encountered by any given vehicle that could very well operate under a different braking mechanism. Therefore the conclusions of this research cannot be used to associate measured *SN* values with the potential for skid-related accidents of automobiles.

The findings of this investigation would provide better characterization of pavement friction in current models by incorporating pavement roughness. They would also lead to formulation of more meaningful and safer Pavement Management System (PMS) decision-making criteria with respect to the rehabilitation of rough pavements, which will not only address the serviceability, but also the safety issues.

In the final phase of this research a comprehensive study was performed using the data collected from 2007 and 2008 Wallops Friction Workshops to understand the concept of Speed Constant and investigate its effect on the IFI-based calibration of friction measuring devices. The following were the main findings of this study; (1) different *FR60* values were calculated from different slip speeds on the same pavement surface

using the S_p vs. *MPD* relationship recommended in the ASTM. (2) *a* and *b* parameters specific to both the friction measuring device and the pavement would capture the true friction speed dependency, enabling one to predict more accurate *FR60* values for a given surface. The modified S_p parameter captures the real friction speed gradient of a given device, hence predicting better *FR60* independent on the *FRS* used on the computations. This fact alone is a significant improvement in the current procedure since it provides a better tool to evaluate the actual *FR60* of a given pavement to be used in the pavement management decision-making process. By not using the *a* and *b* parameters specific for the friction measuring device one could mischaracterize the frictional characteristics of a pavement surface and hence disseminate misleading information for the pavement management decision-making process. (3) *A* and *B* device calibration parameters which were calculated in accordance with ASTM standards were sensitive to the slip speed used in their calculation. Different *A* and *B* parameters were obtained when friction measurements at different slip speeds were used for its calculation. Furthermore by using device dependent S_p parameters the slip speed dependency of the parameters *A* and *B* can be reduced significantly.

This investigation also indicated that there is a linear correlation between *F60* obtained from devices that operate at 100% slip conditions and the standard friction measuring device DTF, which also operates under the same slip conditions. On the other hand the relationship between *F60* values obtained from the standard device, DFT, and the *F60* values obtained using friction measuring devices that operate in the slip range of 10-20% was found to be nonlinear. However, it was found that the use of a power transformation on the *F60* values obtained using friction measuring devices that operate in the slip range of 10-20% would produce a linear relationship between the standard *F60* values obtained using the DFT and the corresponding transformed *F60* values. The revised *A* and *B* parameters corresponding to the different devices used in this investigation were then calculated using the proposed modifications. The above values presented were less sensitive to the speed at which the tests were performed, and also possessed a much higher coefficient of determination than the corresponding parameters obtained using the conventional ASTM method.

Based on the results of the investigation the authors felt that the current procedure used by ASTM for calculation of the International Friction Index (IFI) could be modified slightly, particularly with respect to (1) the procedure used for the calculation of the Speed Constant and (2) the methodology used for correlating the *FR60* values to the standard DFT *F60* measurements. Although it has been well documented that a direct relationship between the frictional speed dependency and macrotexture exists, the results of this study indicate that the *a* and *b* parameters used in the ASTM procedure should be specific to the device used for testing. This is necessary to compensate for the effects of the specific frictional measuring device, since it has been observed that different frictional measuring devices generate their own characteristic frictional speed trends on the same pavement surface. Therefore, the authors suggest these parameters be calculated by correlating the experimental S_p parameters obtained from data clusters corresponding to specific friction measuring devices to the *MPD* of different pavement surfaces covering a wide variety of macrotexture. Finally, a modified IFI procedure that incorporates device specific slip conditions into its computations is proposed. The modified IFI procedure consistently produced more accurate predictions than the conventional ASTM procedure on all the different devices considered in this study.

REFERENCES

Al-Masaeid, H. R. (1997) "Impact of Pavement Condition on Rural Road Accidents". Canadian Journal of Civil Engineering, Vol. 24, No. 4, 1997, pp. 523–532.

Armstrong-Hèlouvry, B (1991) "Control of Machines with Friction", The Springer International Series in Engineering and Computer Science, Vol. 128.

ASTM: "Standard Test Method for Skid Resistance of Paved Surfaces Using a Full-Scale Tire", Standard No E274-06, ASTM 2009.

ASTM: "Standard Test Method for Measuring Surface Frictional Properties Using the British Pendulum Tester", Standard No E303-93, ASTM 2008

ASTM: "Standard Practice for Computing Ride Number of Roads from Longitudinal Profile Measurements Made by an Inertial Profile Measuring Device", Standard No E1489 - 08, ASTM 2009

ASTM: "Standard Practice for Calculating Pavement Macrotexture Mean Profile Depth", Standard No E1845-01(2005)e1, ASTM 2009

ASTM: "Standard Test Method for Measuring Paved Surface Frictional Properties Using the Dynamic Friction Tester", Standard No E1911-09, ASTM 2009

ASTM: "Standard Practice for Computing International Roughness Index of Roads from Longitudinal Profile Measurements", Standard No E1926-08, ASTM 2009.

ASTM: "Standard Practice for Calculating International Friction Index of a Pavement Surface", Standard No E1960-07, ASTM 2009

ASTM: "Standard Practice for Measuring Pavement Macrotexture Using the Circular Track Meter", Standard No E2157-01 (Reapproved 2005), ASTM 2009

Bazlamit, S. Reza, F. (2005), "Changes in Asphalt Pavement Friction Components and Adjustment of Skid Number for Temperature". Journal of Transportation Engineering, Volume 131, Issue 6, pp. 470-476.

Booser, E. R. (1989).CRC Handbook of Lubrication: Theory and Practice of Tribology Volume II. CRC Press, Boca Raton, Fl, pp 39-47.

Cenek P.D. and Davies R.B. (2004) "Crash Risk Relationships for Improved Safety Management of Roads", Proc Towards Sustainable Land Transport, Wellington, New Zealand.

Denny, D. F., (1953) "The Influence of Load and Surface Roughness on the Friction of Rubber-Like Materials", Proc. Phys. Soc., Series B, 66, 721-727.

ESDU International plc, (2003). Development of a Comprehensive Method for Modelling Performance of Aircraft Tires Rolling or Braking on Dry and Precipitation-Contaminated Runways TP 14289E. Transportation Development Centre: Transport Canada.

Federal Aviation Administration (1997). "Measurement, Construction, and Maintenance of Skid-Resistant Airport Pavement Surfaces", U.S. Department of Transportation, AC No**:** 150/5320-12C.

Flintsch, G. W; de Leon Izeppi, E. D; McGhee, K. K and Roa, J. A. Evaluation of the International Friction Index Coefficients for Various Devices. Transportation Research Board Annual Meeting 2009 Paper #09-3240, Washington, D.C.

Fuentes, L. Gunaratne, M. (2009) "Factors Influencing Frictional Measurement Using the Dynamic Friction Tester (DFT)", Presented at 88th Meeting of the Transportation Research Board .Paper #09-0100. Washington, D.C.

Gillespie, T D; Karamihas, S M; Sayers, M W; Nasim, M A; Hansen, W ; Ehsan, N ; Cebon, D. (1993) "Effects of Heavy-Vehicle Characteristics on Pavement Response and Performance", NCHRP Report 353, Transportation Research Board, Washington DC.

Henry, J.J., Hironari Abe, Shulchi Kameyama, Akinori Tamai, Atsushi Kasahara, Kazuo Saito (2000) "Determination of the International Friction Index (IFI) Using the Circular Texture Meter (CTM) and the Dynamic Friction Tester (DFT). PIRAC 109.

Henry, J. J., (2000) "Evaluation of Pavement Friction Characteristics". NCHRP synthesis 291. Transportation Research Board. Washington, D.C. 66pp.

Henry, J. J., Leu, M C. (1978). "Prediction of Skid Resistance as a Function of Speed from Pavement Texture Measurements." In Transportation Research Record: Journal of the Transportation Research Board, No. 666, Transportation Research Board of the National Academies, Washington, D.C., pp. 7–13.

Jayawickrama, P.W., and Thomas, B., (1998) "Correction of Field Skid Measurements for Seasonal Variations in Texas", Transportation Research Record 1639. Transportation Research Board, National Research Council, Washington, D.C., pp. 147-154.

Li, S., Noureldin, S., and Zhu, K. (2004). "Upgrading the INDOT Pavement Friction Testing Program." Joint Transportation Research Program, Perdue Libraries: 6-9.

Mauer, G. F. (1995). "A Fuzzy logic controller for an ABS braking system", IEEE Transaction on Fuzzy Systems, **3**, 4, 381-388.

Montgomery, D.C, (2008). “Design and Analysis of Experiments”, 7th. New York: John Wiley & Sons Inc. Print.

Moore, D. F, (1975). “The Friction of Pneumatic Tyres” New York: Elsevier Scientific Pub. Co.

NCHRP, (2009) Guide for Pavement Friction Project No. 01-43. Transportation Research Board. National Research Council. February.

Roth, F.L., Driscoll, R.L., and Holt, W.L., (1942) “Frictional Properties of Rubber”, J. Res. Nat. Bur. Stds. 28, 439.

Sayers, M. (1995) “On the Calculation of International Roughness Index from Longitudinal Road Profile”, Transportation Research Record 1501, Transportation Research Board Business Office, Washington, D.C., pp. 1-12.

Schallamach, A. (1952) “The Load Dependence of Rubber Friction”, Proc. Phys. Soc., Section B, Volume 65, Issue 9, pp. 657-661.

Seneviratne, H. N. Rajapakshe, M.P. Gunaratne, M. (2009). “Field Calibration of an Analytical Model for Pavement Friction Testing Applications”, Journal of Testing and Evaluation, 37(1), pp. 1-10.

Thirion, P., (1946) “ Les coefficients d' adherence du caoutchouc., Revue Generale du. Caoutchouc 23(5), 101-6.

Tighe, S., Li, N.Y., Falls, L.C., & Haas, R. (2000) “Incorporating Road Safety into Pavement Management”. Transportation Research Record: Journal of the Transportation Research Board (1699), 1-10, Washington, D.C.

Wambold, J. C., C. E. Antle, J. J. Henry, and Z. Rado (1995) “International PIARC Experiment to Compare and Harmonize Texture and Skid Resistance Measurements”, Final Report submitted to the Permanent International Association of Road Congresses (PIARC), State College, PA.

Weather Underground, (2007) "Toledo, OH Typical Weather.”,. Website. <http://www.accuweather.com/forecast-normals.asp?partner=cnn&traveler=0&zipcode=43655&u=1 >. Last Accessed on 20 November 2007.

Weather Underground, (2007) "History for Toledo Metcalf, OH.", Website. <http://www.wunderground.com/history/airport/KTDZ/2006/1/1/CustomHistory.html?dayend=16&monthend=11&yearend=2007&req_city=NA&req_state=NA&req_statename=NA>. Last Accessed on 20 November 2007.

ABOUT THE AUTHOR

Luis Fuentes received a Bachelor's Degree in Civil Engineering from Universidad del Norte, Colombia, in 2005 and a Master in Civil Engineering (MCE) from University of South Florida in 2006. He entered the Ph.D. program at the University of South Florida in 2006, where he worked on a project sponsored by the National Aeronautics and Space Administration (NASA) to investigate the skid resistance phenomenon. He has also coauthored publications on different journals such as the ASCE Journal of Transportation Engineering and the TRR Journal of the Transportation Research Board; and made paper presentations at the annual meetings at the Transportation Research Board (TRB).